Synthesis of small-molecule HGF-Met inhibitors for use in preventing cell motility

Alexander Bunte

MSc By Research

University of Salford

School of Science, Engineering and Environment

2020

Table of Contents:

List of tables:

Acknowledgements:

I would firstly like to thank Dr Jim Wilkinson for his continuous guidance throughout the time I have been at this university, without which I would not have had the opportunity to develop myself as a chemist to the extent that I have.

I would also like to thank Dr Kirit Amin for his assistance in running and interpreting complex NMRs, in addition to keeping our temperamental NMR machine running.

My gratitude also goes to the entire technical team and my lab partners at the University, who never hesitated to give any assistance, be it with equipment, searching for chemicals or checking over the smallest of things.

Finally, I would like to thank my family, who have supported me endlessly throughout my time as a student, inspiring me to try my best, and to push though when I encountered difficulties.

Alex Bunte

List of Abbreviations:

HGF – Hepatocyte Growth Factor

ERK – Extracellular Receptor Kinase

SAR – Structure Activity Relationship

ISNR – Insulin Receptor

RTK – Receptor Tyrosine Kinase

MAPK - Mitogen-activated protein kinase

PI3K – Phosphoinositide 3-kinase

VEGFR – Vascular endothelial growth factor

VEGFR2 – Vascular endothelial growth factor 2

NSCLC – Non-small cell lung cancer

PFS – Progression-free survival

EFGR – Epidermal growth factor receptor

EMT- Epithelial mesenchymal transition

FGFR – Fibroblast growth factor receptor

IGF1R – Insulin-like growth factor 1 receptor

GAG – Glycosaminoglycan

ECM – Extracellular Matrix

PG – Proteoglycan

GlcNAc – N-acetyl-D-glucosamine

GalNAc – N-acetylgalactosamine

HexA – Hexuronic acid

GlcA – Glucuronic acid

IdoA – Iduronic acid

HS – Heparan Sulfate

HA – Hyaluronic Acid

CS – Chondroitin Sulfate

DS – Dermatan Sulfate

NMR – Nuclear magnetic resonance

DIAD – Diisopropyl azodicarboxylate

DEAD – Diethyl azodicarboxylate

TPPO – Triphenylphosphine oxide

TPP – Triphenylphosphine

Abstract:

Glycosaminoglycans are becoming more and more focused upon as a research topic due to the broad use they have in aiding wound healing and preventing cell motility through competitive inhibition of the HGF-Met pathway. This pathway is extremely important in various cellular processes including cancer development, metastasis, tissue regeneration, damage and cell motility.

This project aimed to synthesise a series of easily prepared (3 step) mono, di-, tri- and tetra-sulfated glycomimetic compounds for their use in preventing HGF-induced cell motility in cancers, prevention of Met activation and for their beneficial actions in assisting wound healing.

These compounds were prepared through 4 major synthetic routes:

1) Coupling reaction of phenols with solketal, followed by deprotection of the acetonide and reaction of hydroxyl groups with SO_3 complexes.

2) Coupling phenols with allyl bromide, followed by asymmetric dihydroxylation and reaction of hydroxyl groups with SO_3 complexes.

3) Direct sulfation / sulfonation of phenols with SO_3 complexes.

4) Directed *ortho*-lithiation followed by exchange with an electrophile.

These compounds were tested for cell motility prevention by a wound healing assay and cytotoxicity was determined through a cell viability assay.

Results showed that many of the compounds were easily synthesised in few steps and relatively high yields, with a number of the compounds demonstrating promising activity in slowing HGF-mediated cell motility at low µM concentrations, with motility being stimulated at higher concentrations. Further optimisation of the compounds with the highest activity along with further biological testing would help to ascertain a more certain SAR.

Details of the compound observed with the highest efficacy (Compound **26**) are shown in Figures **1-3**.

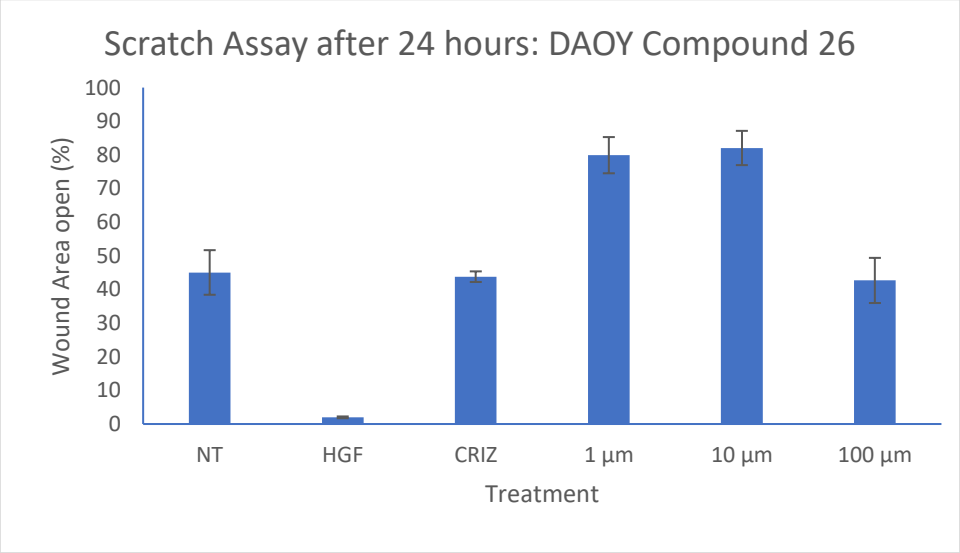

Figure 1. **Graph showing percentage of wound still open after 24 hours following treatment with control drugs and varying concentrations of compound 26.**

Table 1. **Percentage of wound still open after 24 hours**

NT	HGF	CRIZ	1	2	3
45.05%	1.98%	43.8%	79.91%	82.05%	42.67%

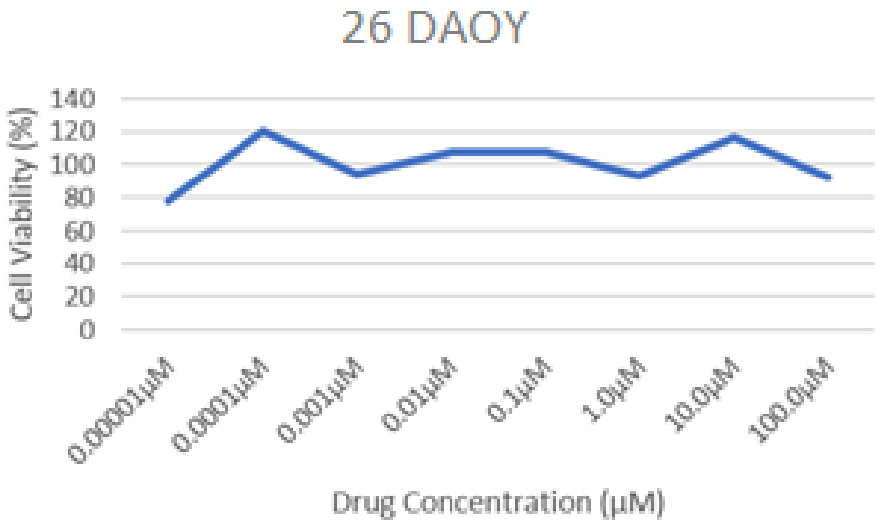

Figure 2. **Graph showing the effects of varying concentrations of compound 26 on DAOY cell viability.**

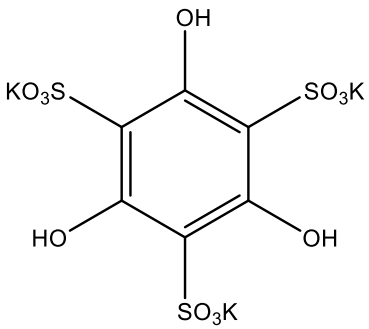

26

Figure 3. **Structure of 1,3,5-trihydroxy-2,4,6-benzenetrisulfonic acid potassium salt.**

Overall, several of the sulfated glycomimetic compounds synthesised in this project show promising activity in inhibiting the HGF/Met pathway, although more work is required to further optimise the SAR and assure effective inhibition.

1. Introduction:

1.1. Hepatocyte Growth Factor:

Hepatocyte Growth Factor (HGF) is an extremely important pleiotropic heparin-binding glycoprotein which is involved in cellular processes in virtually all multicellular organisms (Ricci, Catizone, & Galdieri, 2002; Yano, Tsuda, Ueda, & Higashio, 1998). HGF is commonly associated with the formation, repair and growth of cells and was initially purified through isolation from rat serum in 1984 (Buchstein et al., 2009; Mizuno & Nakamura, 2013). HGF has been documented as having significant roles in helping heal and repair damage, mediating various disorders with Oliveira et al., (2018) highlighting that HGF is a factor in one such disease: diabetes, more specifically in insulin resistance. They continue to explain that in individuals where insulin resistance is displayed, HGF is usually upregulated, along with other growth factor-like hepatokines which affect the way glucose reacts to several insulin sensitive cell types. Additionally, the receptor for HGF, c-Met is structurally similar to the insulin receptor, ISNR. This suggests that as the level of HGF increases, it can potentially interfere competitively with insulin, binding to ISNR and assisting insulin resistance (Fafalios et al., 2011).

Other functions of HGF include tissue repair and cellular regeneration. Firstly, in relation to the repair of nerve cells, Ko, Lee, Lee, Nho, & Kim, (2018) explain that peripheral nerve regeneration in sciatic nerve injury was promoted through the increase of HGF released in areas of injury. Furthermore, when treated with a c-Met inhibitor, axon and myelin regrowth was decreased, demonstrating involvement of HGF and c-Met in nerve repair.

HGF is widely known to be heavily involved in the process of wound healing, allowing cells to proliferate and migrate enabling wounds to close, in addition to reducing inflammation and scarring (Dally et al., 2017). Dally et al., (2017) and Nakamura & Mizuno, (2010) go on to demonstrate that HGF is found to play a significant part in embryogenesis, tissue homeostasis, repair, regeneration, organ development and protection. It was found that during various organ diseases, the level of HGF is highly upregulated, likely as an attempt to repair any damage that may have been caused to any tissues (Nakamura & Mizuno, 2010). They further state that when the level of HGF was reduced through anti-HGF antibodies, the rate of degradation in tissue was observed to increase, demonstrating the role HGF plays in the maintenance of tissue function.

HGF is secreted in its inactive form referred to as pro-HGF and activated in the body through a urokinase-type plasminogen activator (uPA) to αß-HGF through hydrolysis of an arginine-valine bond, thus becoming the ligand for the tyrosine kinase Met (Naldini et al., 1995). Buchstein et al., (2009) goes on to explain that pro-HGF has a relatively uncommon structure in comparison to other growth factors which are generally much smaller and usually only single-domain proteins, whereas HGF is relatively large (92 kDa) and is a multi-domain protein. This is further enforced by Naldini et al., (1995) and Dally et al., (2017), who explain that αß-HGF is comprised of a 55-60 kDa α domain which contains a N-terminal hairpin loop and 4 kringles (NK1-NK4), which allow binding and activation of the receptor. There is also the 32-34 kDa ß domain which contains a secondary receptor binding site linked through a disulfide bridge as a heterodimeric protein. This then exists as 3 major isoform variants: HGF-NK, NK1 and NK2, where NK1 is an agonist to c-Met and NK2 is a partial c-Met antagonist.

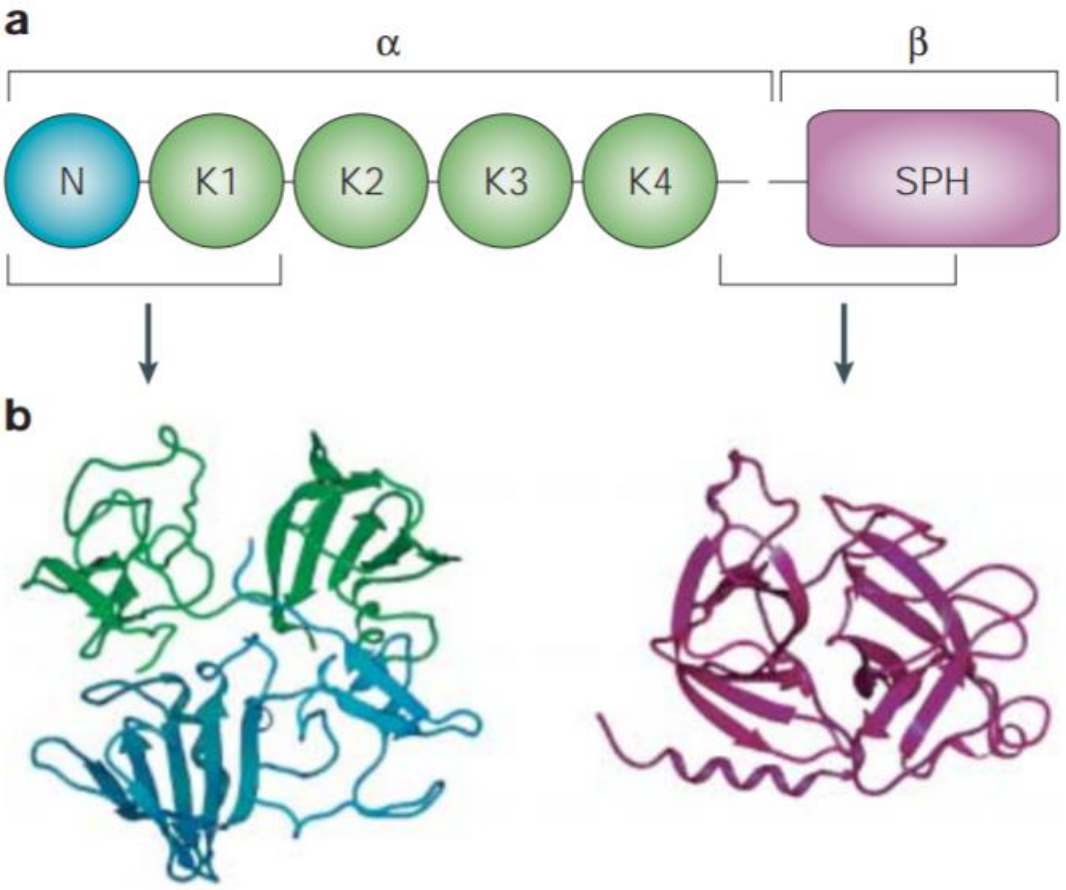

Figure 4. **Domain structures of α and ß HGF chains (a) Crystal structure of NK1 and SPH domains (b). Reprinted from "Met, metastasis, motility and more" by Birchmeier, C., Birchmeier, W., Gherardi, E., & Vande Woude, G. F. 2003. *Nature Reviews Molecular Cell Biology*, *4*(12), 915–925.**

Nakamura & Mizuno, (2010) explain that HGF is produced by stromal cells and is involved in stimulating many cellular functions such as angiogenesis, cell motility, cell proliferation, and morphogenesis. This is then a particular target for anticancer drugs as it shows activity in many human cancer pathways. This further assists the progression of tumour cells whilst aiding metastasis through increasing cell motility (Matsumoto & Nakamura, 1997). Targeting HGF, and consequently its receptor the tyrosine kinase Met, allows reduction in the activity of the HGF-Met pathway. Focussing on treating this pathway in cancer may achieve reduced

mortality rates, as the rates of tumour progression, angiogenesis, and metastasis would be minimised thus leading to potentially less aggressive and slower growing cancers (Cecchi, Rabe, & Bottaro, 2012).

1.2. Met:

Met is a Receptor Tyrosine Kinase (RTK) which are a class of cell surface receptors primarily involved in signalling pathways of most cancers. This is largely due to their ability to control cellular invasion, proliferation, cancer cell regulation and angiogenesis which have a distinct role in the manifestation of many cancers (Maroun & Rowlands, 2014). All 518 known human RTKs have similar molecular structures, which further fall into 20 subfamilies, all sharing three common features: a ligand binding region in the ECM, a singular transmembrane helix and a cytoplasmic region that contains the tyrosine kinase, in addition to the carboxy terminal and juxtamembrane regions (Lemmon & Schlessinger, 2010).

The Met pathway is initiated through the binding of HGF to Met, resulting in dimerisation followed by autophosphorylation of two tyrosine residues. This in turn activates further downstream signalling pathways, in particular MAPK and PI3K, resulting in cell morphogenesis, proliferation, apoptosis protection, cell scatter and mobility (Mo & Liu, 2017).

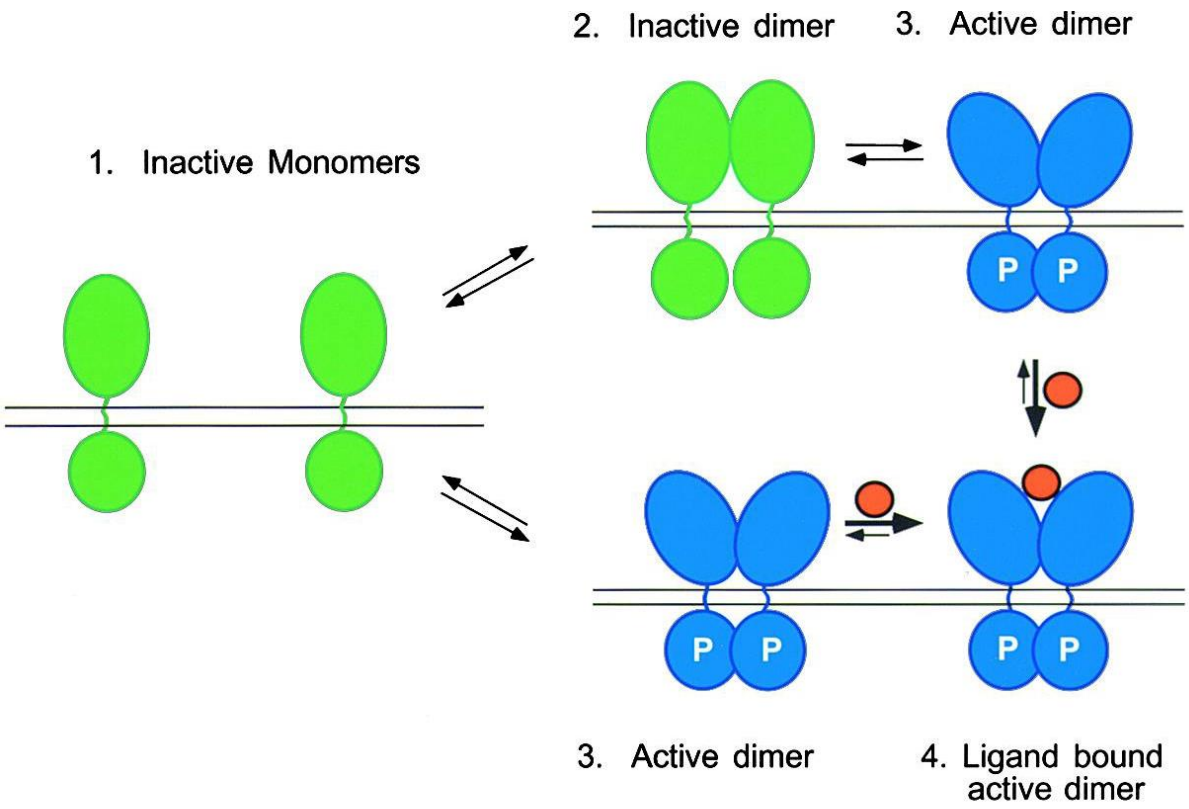

Figure 5. **Dimerisation of inactive monomers to form the active RTK dimer. Adapted from "Cell Signaling by Receptor Tyrosine Kinases" by Schlessinger, J. 2000. *Cell,* 103(2), 211-225.**

Met is a key example of this; in many cancers it is overexpressed. This is especially seen in non-small cell lung, gastrointestinal and hepatocellular carcinomas due to Met being the major pathway affecting cancer progression rate as suggested by Maroun & Rowlands, (2014). They suggest that its ability to communicate with the vascular endothelial growth factor receptor (VEGFR), results in upregulated angiogenesis and endothelial cell growth. This is reinforced by Cecchi et al., (2012) and Maroun & Rowlands, (2014) who explain that elevated Met and HGF levels as a result of mutations to Met generally lead to a poor prognosis for the sufferer due to the increased activity allowing primary cancer effecting pathways to function unchecked. Organ & Tsao, (2011) further support this by explaining

that some cancers can be “addicted” to Met expression (oncogene addiction) and require it to support tumour growth and survival of the cancer itself.

In terms of selecting Met as a target for anticancer drugs and therapies, there are 3 main routes: a) preventing the combination of HGF and Met extracellularly, b) preventing phosphorylation of the tyrosine domain, and c) inhibiting Met kinase-dependent signalling (Maroun & Rowlands, 2014). When targeting Met, HGF is found to be the sole co-factor ligand. This allows us to select Met as an effective target for anticancer drugs due to both Met’s activation of a large range of its own and other receptors’ oncogenic processes in addition to the fact that there is only one known ligand in which anticancer drugs would be competing, in order to inhibit the pathway effectively (Dua, Zhang, Parry, & Penuel, 2011).

Met possesses a very complex structure due to it being a transmembrane bound receptor with several extracellular (Sema, PSI, IPT) and intracellular domains (Juxtamembrane, Kinase) and a multifunctional docking site (Organ & Tsao, 2011). Met is initially secreted as an inactive single-chain molecule that is then cleaved between residues 307-308, resulting in the production of a disulfide-bridged heterodimer (Birchmeier, Birchmeier, Gherardi, & Vande Woude, 2003). Cleavage of an inactive form of Met to give the active form is similar to the way active HGF is produced, as discussed earlier, pro-HGF is cleaved to form active HGF. Structurally, Met is comprised of a cysteine domain attached to four immunoglobulin domains which are suggested to hold the ß chain of the protein in such a way that it allows binding of its ligand, HGF resulting in the activation of the HGF-Met pathway (Birchmeier et al., 2003).

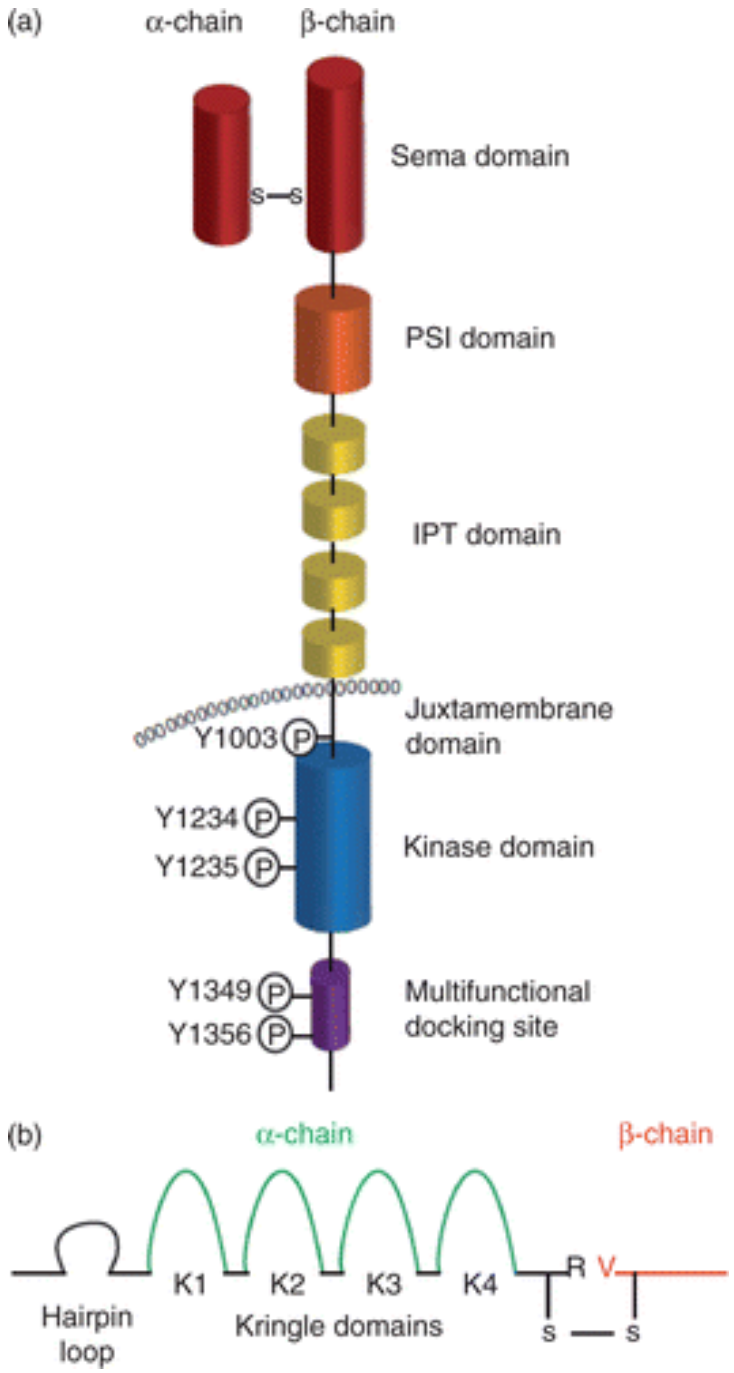

Figure 6. **Transmembrane domain structure of Met. Reprinted from "An overview of the c-MET signaling pathway" by Organ, S. L., & Tsao, M. S. 2011.** ***Therapeutic Advances in Medical Oncology*****, *3*(1), S7–S19.**

Other RTKs are able to be targeted through the use of drugs such as cabozantinib, an inhibitor for Met, VEGFR2, AXL, KIT, KIE2, FLT3 and RET kinases. This targets multiple RTK

pathways at the same time, allowing increased survival rates due to the level of kinase inhibition when compared to other drugs like erlotinib (Maroun & Rowlands, 2014). They report that in a phase II randomised and controlled clinical trial investigating the efficacy of cabozantinib and erlotinib alone, versus a combination of the two, was found that in patients with advanced NSCLC, erlotinib alone gave 1.8 months of progression free survival (PFS) whereas cabozantinib gave 4.3 months. This demonstrates the effectiveness of a multi-kinase inhibitor (cabozantinib) versus a single EGFR inhibitor (erlotinib). However, a combination of the two gave 4.7 months of PFS, an increase over drug monotherapy showing that inhibiting many RTK pathways will generally increase the level of PFS.

1.3. Cell Motility:

Cell motility is a process which is involved in various critical bodily processes and diseases, namely wound repair, tissue growth and cell invasion in metastatic cancers. In cancer it is rarely the primary tumour that is the cause of death, rather the formation of various metastases throughout the body as a result of malignant cells moving and uncontrollably growing in remote tissues (Yilmaz & Christofori, 2010). They continue to explain that cells can migrate both as a group, or as single cells with several processes being undertaken during the migration. During this the cell itself changes at the molecular level through modification to its cell-cell and cell-matrix adhesion and the actin cytoskeleton. However, as of yet the understanding of how cells physically migrate out of tissues, survive immune detection and response, and begin metastasis in distant tissues is not fully known.

Jiang et al., (2015) describe that cell adhesion and inter-cellular structures are the primary factors in maintaining a single tumorous mass, and failures of these structures may lead to cells spreading out from the tumour and forming metastases. Jiang et al., (2015) and Stuelten, Parent, & Montell, (2018) both introduce the role of the E-cadherin "switch" which in most epithelial cell mediated cancers show loss of functionality. They clarify that loss of the "switch" in cancers leads to reduced cellular adhesion, increasing the chance of cancer cells detaching from the primary tumour and migrating. In addition to this, loss of contact inhibition allows these cells to have unchecked cellular growth and therefore support the process of secondary tumour growth (Cavallaro & Christofori, 2004).

Another process which leads to similar effects to that of the E-cadherin "switch" is EMT (epithelial-mesenchymal transition). This is a differentiation which epithelial cells undergo in order to morph into a mesenchymal phenotype. This is achieved through a series of biochemical modifications to the cell (Kalluri & Weinberg, 2009). Completion of this modification enables the cells to have an increased level of motility, invasiveness and the ability to resist apoptotic signals that are characterised by the deterioration of the basement membrane. Subsequent formation of mesenchymal cells enables them to migrate away from the source and form metastases.

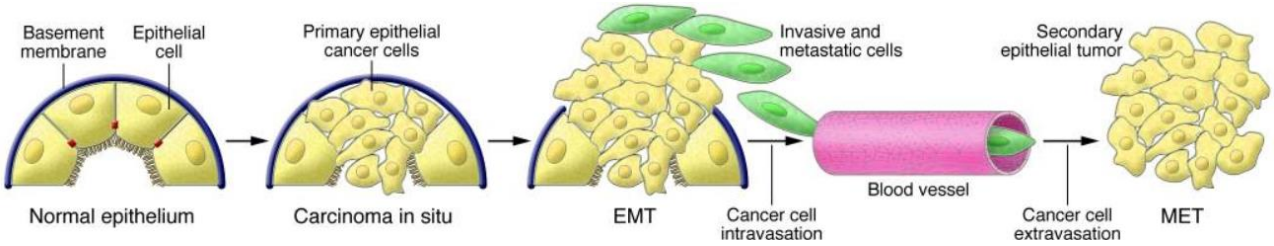

Figure 7. **Role of EMT in cancer metastasis. Reprinted from "The basics of epithelial-mesenchymal transition" by Kalluri, R., & Weinberg, R. A. 2009. *Journal of Clinical Investigation*, *119*(6), 1420–1428.**

Normal and malignant cells are said to generally migrate through amoeboid, mesenchymal or individual pathways (Stuelten et al., 2018), or collective cell migration in cellular sheets, strands, clusters and tubes (Jiang, Li, He, & Zhao, 2013). The format of cell migration is dependent on the cell type; epithelial cells usually migrate in sheets, whereas colorectal cancer cells disseminate as single, solitary cells (Yilmaz & Christofori, 2010).

As tumour metastasis is the primary death factor in 90% of cancer related deaths, selecting this as a target for anticancer drugs would be a credible choice, as the inhibition of signalling pathways such as EGFR, HGF-Met, FGFR and IGF1R which are involved with cell movement, proliferation, differentiation and survival could reduce the level of both primary tumour size and metastasis formation, making treatment a much more streamlined, specific, less toxic and more successful approach (Leber & Efferth, 2009; Yilmaz & Christofori, 2010).

Cell motility is also essential to wound healing, utilising various processes such as EMT and scatter factor mediated collective cell migration to close up wounds through the directional migration of a cell sheet, in addition to increased epithelial cell proliferation and the following migration of cells to the centre of the wound, allowing wound closure and therefore repair (Jiang et al., 2013).

1.4. Glycosaminoglycans:

Glycosaminoglycans or GAGs are one of the most complex of the four major sulfated polysaccharide biopolymers found generally on cell surfaces and in the extracellular matrix (ECM) within mammals, and have been found to be a very worthwhile target for the development of new drugs, nanoparticles and imaging agents for use in cancers and healing medicines through the mimicry of GAGs and proteoglycans (PGs) (Yamada, Sugahara, & Özbek, 2011).

These are found primarily as glycolipids or PGs in the body, bound to cell membrane protein and lipids respectively, and are usually comprised of alternating units of N-acetyl-D-glucosamine (GlcNAc), or N-acetylgalactosamine (GalNAc) and a hexuronic acid (HexA), being either glucuronic acid (GlcA) or iduronic acid (IdoA) (Scott & Panitch, 2013; Yamada et al., 2011). It has been also discovered that some PGs are substituted with multiple GAG chains, for example syndecan-1 (heparan sulfate, chondroitin sulfate) and aggrecan (keratan sulfate, chondroitin sulfate). This increases the level of structural diversity of the GAG family, as PGs are usually classed by their location, basement membrane, ECM and GAG substitution pattern (Yip, Smollich, & Götte, 2006). Scott & Panitch, (2013) continue to explain that the monomer units of GAGs and PGs have sulfation patterns that vary across the monomer units, with GlcA being sulfated on carbon 2 and/or 3, whereas GalNAc is usually sulfated on carbons 4 and/or 6.

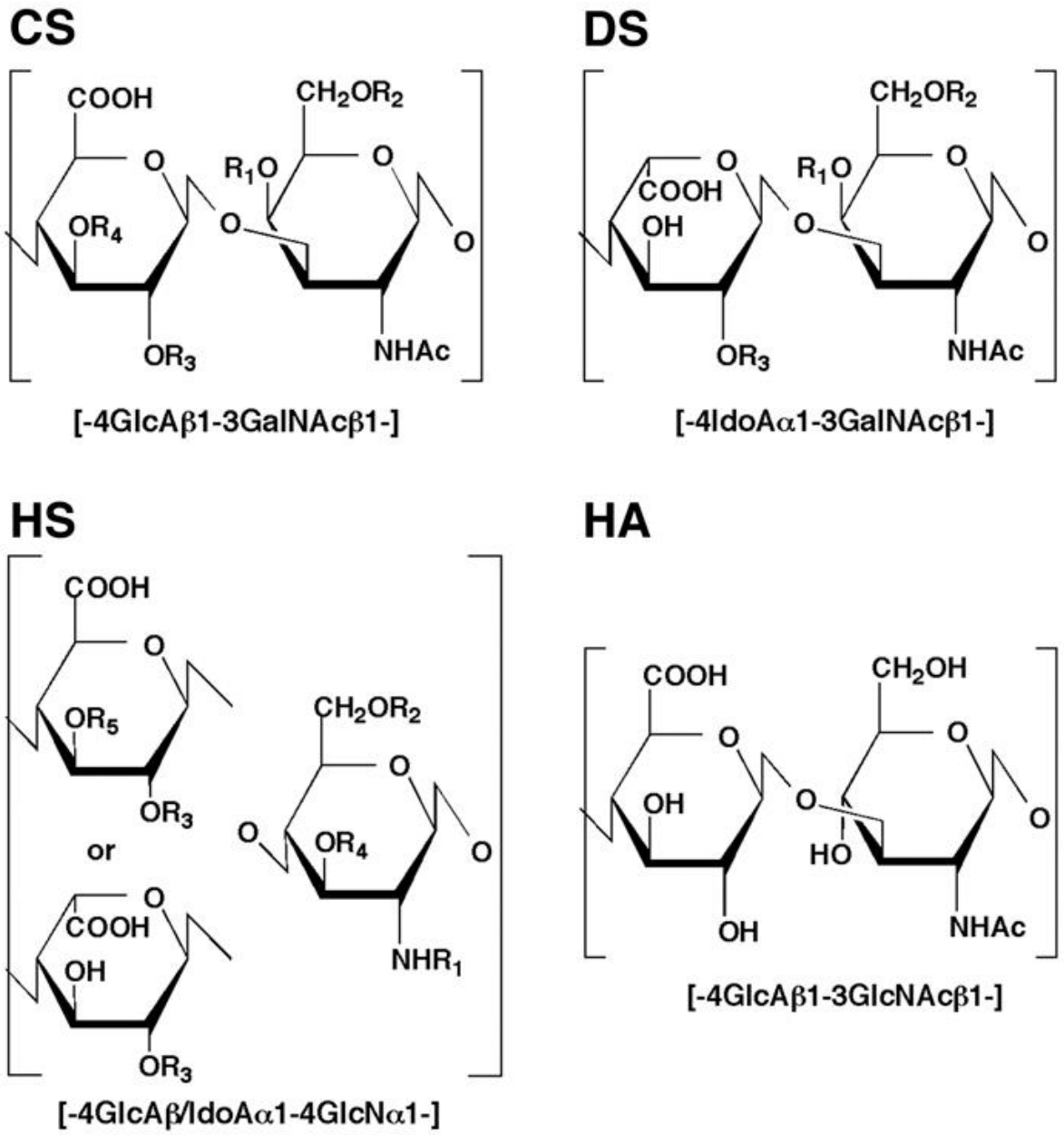

***Figure 8*. Structures of Chondroitin Sulfate (CS), Dermatan Sulfate (DS), Heparan Sulfate (HS) and Hyaluronic Acid (HA). Reprinted from "Evolution of glycosaminoglycans: Comparative biochemical study" by Yamada, S., Sugahara, K., & Özbek, S. 2011. *Communicative and Integrative Biology*, *4*(2), 150–158.**

Sulfation in these molecules is a key feature, as the presence of multiple -SO_3 groups each providing a negative charge allows for a high level of anionic charge density, therefore giving

GAGs the ability to increase osmotic pressure around areas which are highly saturated with GAGs (Scott & Panitch, 2013). Scott & Panitch, (2013) further explain that the anionic quality of these molecules facilitates their ability to interact as several growth factors, cytokines and proteases.

Yamada et al., (2011) and (Yip et al., 2006) explain that GAGs are involved in a range of important roles throughout the body, the focus being on cell growth and differentiation, morphogenesis, angiogenesis, cell adhesion, cell signalling, inflammation, cell migration and wound healing. This gives GAGs a strong foundation in many physiological processes which may facilitate the development of new drugs and treatments for a wide range of diseases in the form of anticancer, anticoagulant, antithrombotic and wound healing drugs (Volpi, 2006). Cancer is a key example, as GAGs and PGs are known to be dysregulated in various cancer pathways, generally correlating to the severity of the prognosis (Yip et al., 2006). They continue to illustrate that cancer cell GAGs and PGs can influence several factors of the cancer itself in the way of reduced cell adhesion, increased cell invasion, motility and angiogenesis, this being a major factor in determining the cancer's invasiveness and growth rate.

One such example of this is Heparan Sulfate (HS) which in transformation from colon adenoma to carcinoma is seen to have a reduction in the level of sulfated sites when compared to normality. This strongly influences the function of the molecule, resulting in increased cancer progression and is also observed across ovarian, squamous cell and hepatocellular carcinomas (Yip et al., 2006). Afratis et al., (2012) and Belting, (2014) suggest that an oversulfated HS mimic would have strong anti-tumour effects, as this inhibits various tumour cell functions through promotion of phenotype transformation. This results in

suppression of processes involved in further progression of the cancer as well as inhibiting interactions with growth factors and cytokines such as the HGF-Met pathway through their HS chains. These are largely responsible for cell motility and proliferation. Furthermore, HS has uses outside of cancer treatment as suggested by Yamada et al., (2011) who explain that oversulfated HS could have a role in the protection of tissues in direct environmental contact from pathogens without use of any active immune system.

1.5. Aims:

This project aimed to synthesise a series of mono, di, tri and tetra-sulfated glycosaminoglycan mimics and investigate their functionality in both reducing the level of HGF-induced cell motility and their ability to inhibit the activation of the Met pathway through HGF.

Synthesis of these glycomimetic compounds was the major focus of this project and was achieved in 1-4 steps depending upon the molecule being synthesised. Three major categories of compounds were synthesised during this project:

a) Enantioenriched benzonitrile glycomimetics – through coupling with allyl bromide, followed by asymmetric dihydroxylation and sulfation (Compounds **12** + **13**).

b) racemic benzonitrile glycomimetics – through coupling with solketal, deprotection of the acetonide, and sulfation of the vicinal diol (Compounds **6, 8 + 17**).

c) aryl sulfated and sulfonated glycomimetics – through direct sulfation and sulfonation of OH groups on substituted phenols (Compounds **24 – 30**).

Following synthesis of glycomimetic compounds, subsequent testing on DAOY medulloblastoma cells was performed to investigate firstly, their ability to reduce cell motility in wound healing assays and secondly, to ascertain whether the compound has any effect on cell viability, as we are aiming to prevent cell mobility while having little to no effect on cell viability. These tests would show us if the compounds synthesised here would have any effect on cell proliferation, motility or Met inhibition. Successful results in slowing wound healing and high cell viability counts would suggest effective inhibition of HGF-Met, with little cytotoxicity, and would therefore lend itself as a good candidate for use as an anti-cancer drug. Conversely, should the compound show increased cell proliferation and motility on the wound healing assay, this would suggest its suitability for use as a wound healing drug.

2. Results and discussion:

2.1. Synthetic Overview:

This project addresses 6 major synthetic pathways (A – F) in preparation of a series of novel glycomimetic compounds for testing on DAOY cells in order to determine efficacy.

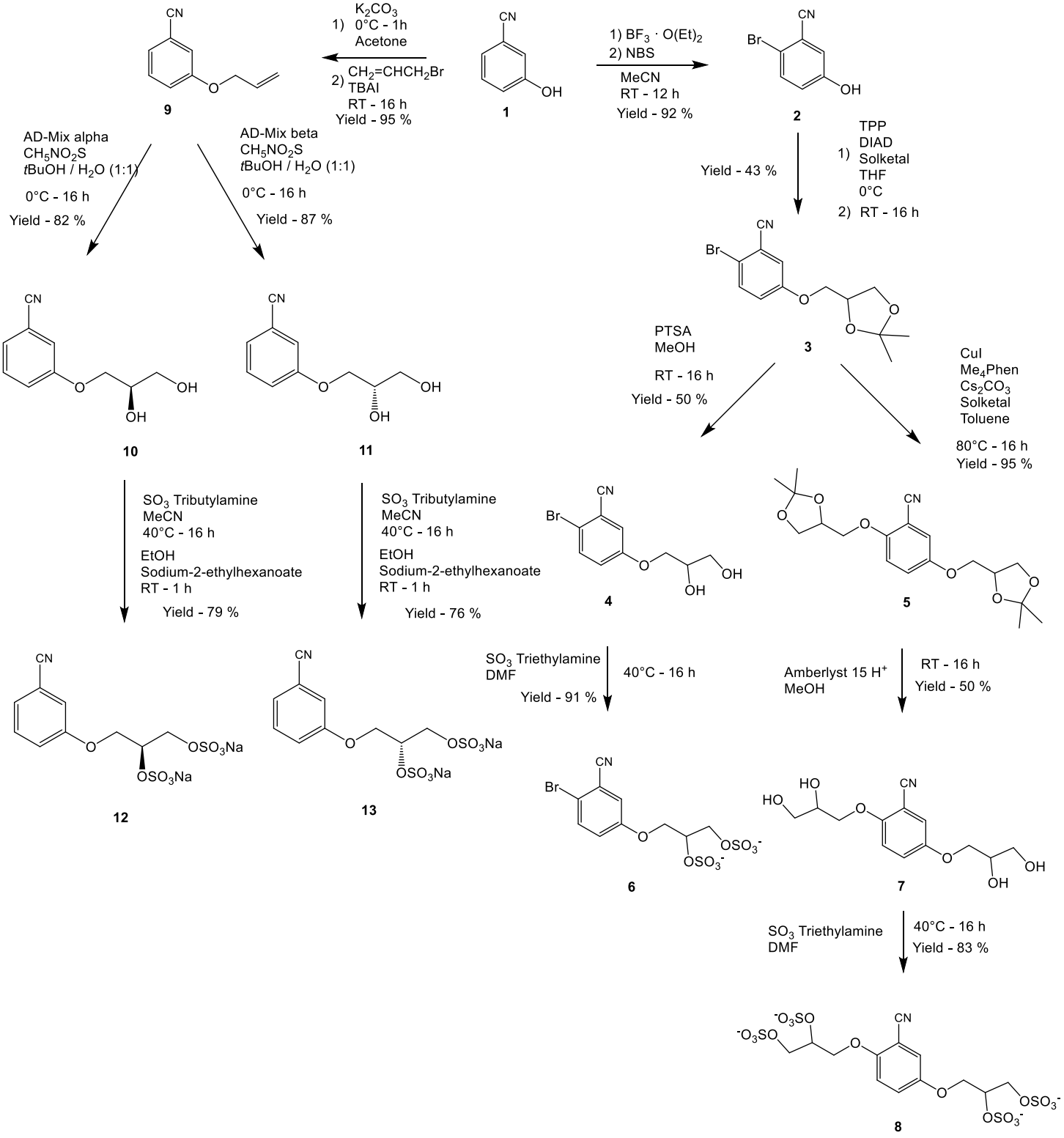

Figure 9. **Synthetic pathway A - Preparation of 3-cyano substituted glycomimetics.**

Compounds **2 - 13** were derived from 3-cyanophenol, and the reaction pathway split into 3 distinct sub routes:

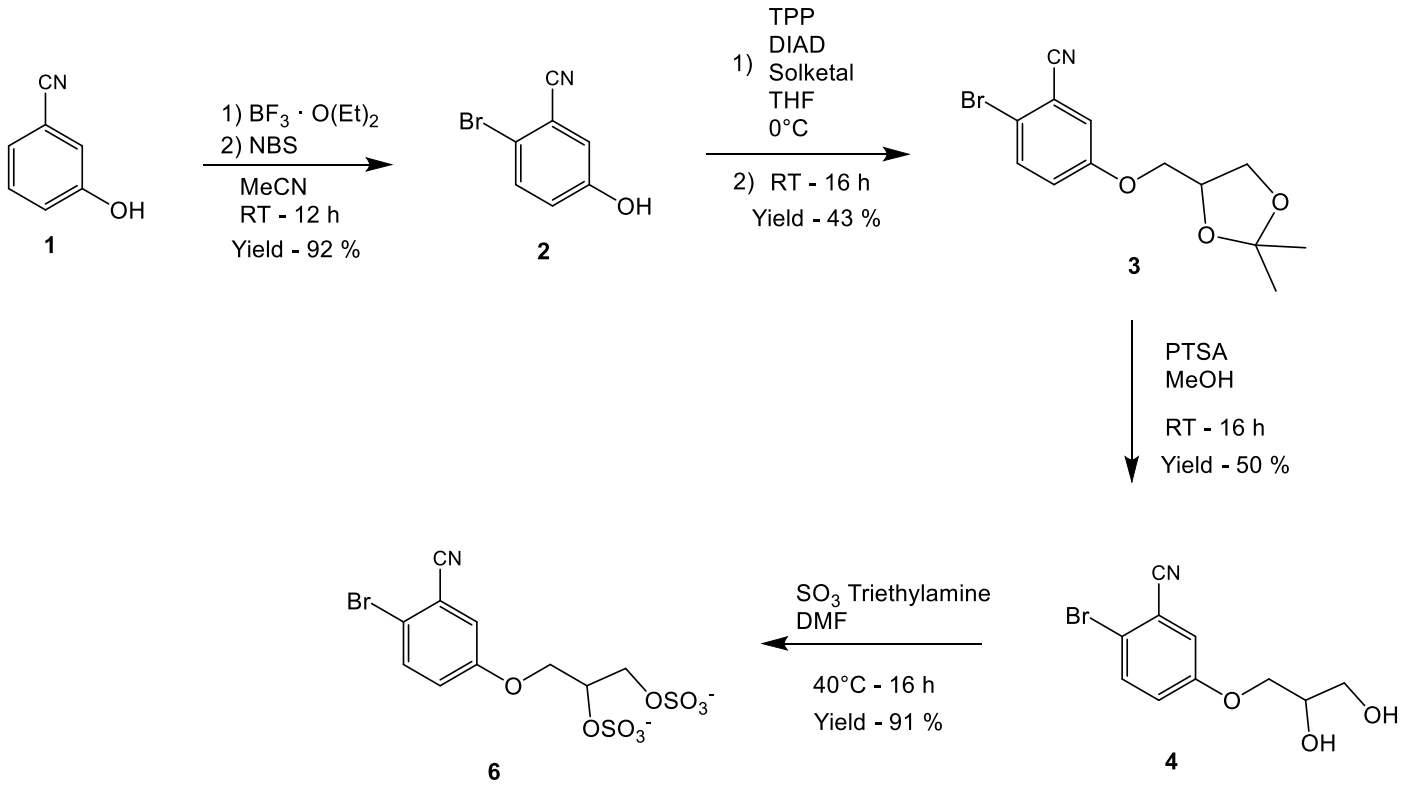

Figure 10. **Sub-route A-1 - Preparation of 5-substituted racemic sulfates.**

These compounds were formed by firstly reacting *N*-bromosuccinimide with 3-cyanophenol by electrophilic aromatic substitution to give compound **2** in high yield (92%). This was then coupled with solketal through the Mitsunobu reaction which exhibited some difficulty in purification and isolation of the compound to yield 43% of compound **3**. This low yield is likely due to loss of product through the multiple purification steps undertaken required to remove contaminants. Additionally, some cleavage of the acetonide may have occurred during column chromatography due to the acidic nature of silica resulting in a portion of the product eluting as the diol at a different point, resulting in loss of yield.

Subsequently, the acetonide was cleaved using *p*-toluenesulfonic acid to give the vicinal diol, compound **4** in a moderate yield (50%). This low yield is attributed to having worked on a very small scale, as considerable amounts of product can be lost in various simple steps such as transfer of the compound between glassware, with some quantity of product becoming unrecoverable both from traces left on glassware used and in the aqueous waste left over following the workup. Furthermore, we have seen that small-scale workups are usually relatively inefficient, firstly due to the issues discussed earlier, and secondly to the fact that comparatively large amounts of solvent and water are required to allow for ease of handling, therefore facilitating successful isolation of product.

Once successful deprotection of the acetonide was achieved, the diol was then sulfated to give the glycomimetic, compound **6** in high yield (91%). Sulfation of these 2,3-diols is facile and requires low temperatures over an extended reaction period. Purification poses some challenges, as aqueous extraction is not viable due to the solubility of the sulfate. Therefore, solvent must be removed under high vacuum, followed by column chromatography in methanol to yield the pure sulfate. Ways to mitigate this have been achieved and is discussed further in section 2.4.

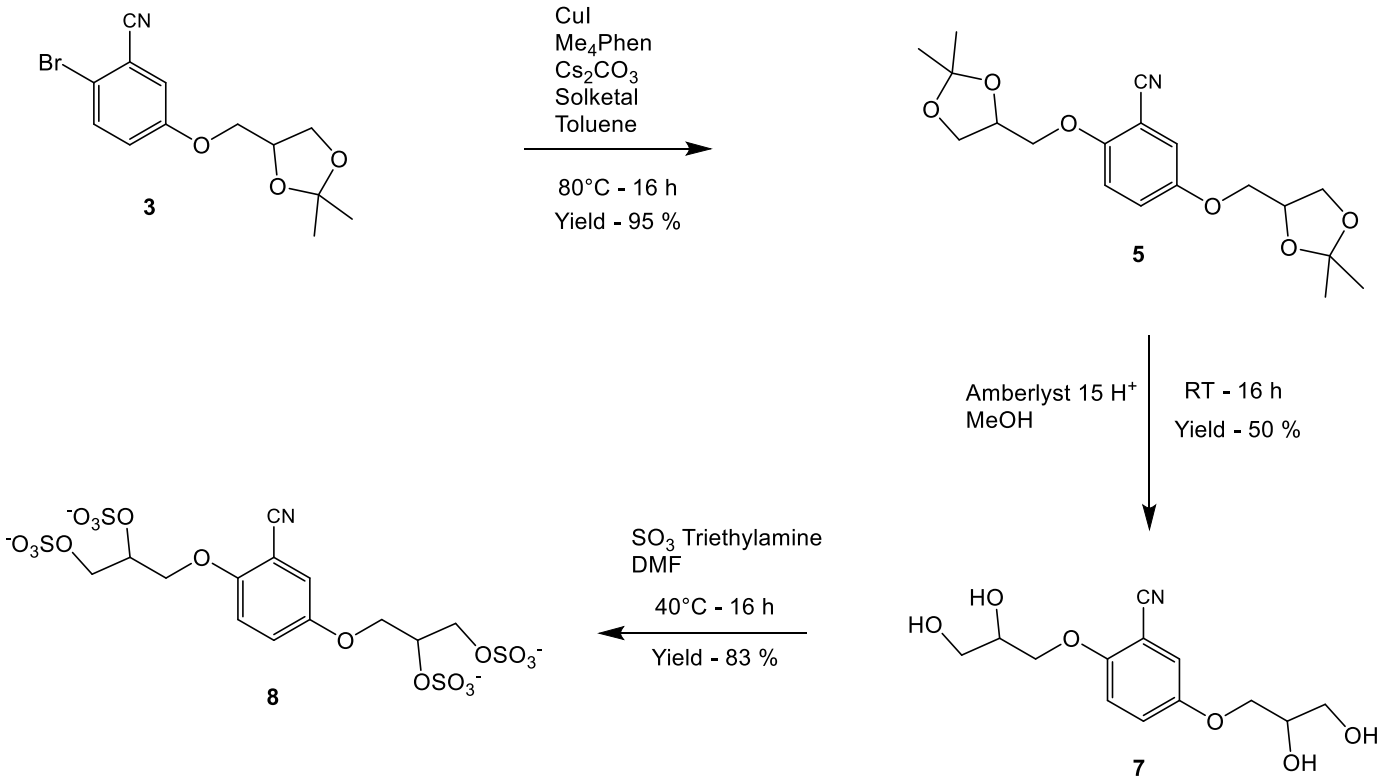

Figure 11. **Sub-route A-2 - Preparation of 2,5-substituted stereorandom sulfates.**

Following synthesis of 5-substituted sulfates, compound **3** was utilised to produce a 2,5-substituted sulfate **8** which was achieved through coupling a second molecule of solketal to compound **3** through an Ullmann-type reaction to give compound **5** (95%). This reaction functioned extremely well, and a further series of bis substituted sulfates with varying positions should be investigated using this method as chlorine-substituted arenes are relatively common and easy to obtain from chemical suppliers.

Compound **5** was deprotected with use of Amberlyst 15 H+ resin as an acidic source to give the bis diol compound **7** (50%), resulting in a moderate yield. This again may have been due to loss through transfer and workup, although some of this loss may have been due to degradation of the molecule from the acidic conditions resulting in loss through in the

workup. There is also the potential for the product to bind to the ion exchange resin, ultimately being lost upon discarding the used resin, this should be investigated in order to mitigate losses.

Sulfation of the bis diol was then completed to give the final glycomimetic compound **8** (83%). As with compound **6**, solvent needed to be removed through high vacuum followed by methanol column chromatography to give the pure sulfate.

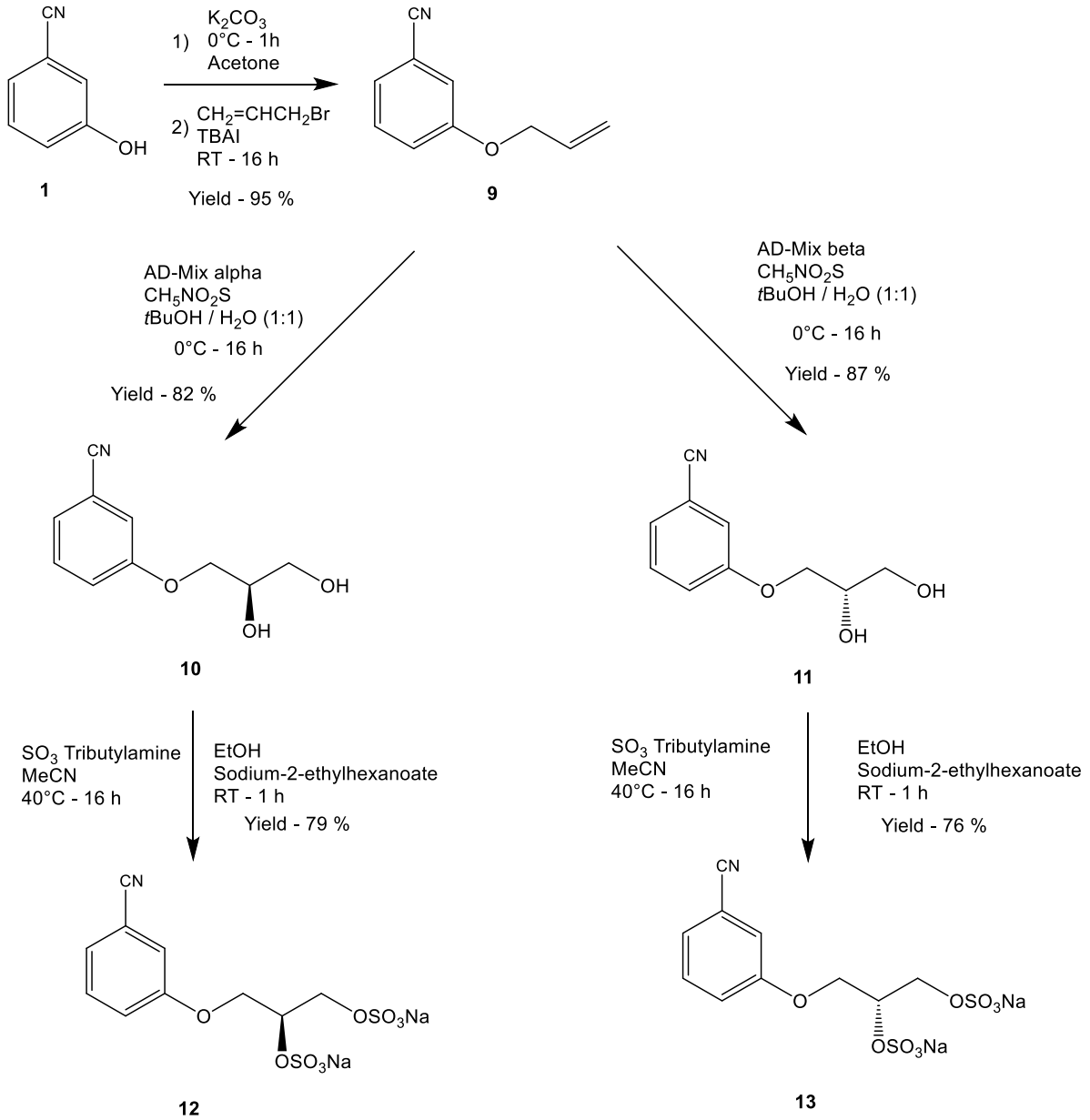

Figure 12. **Sub-route A-3 - Preparation of 2,5-substituted enantio-enriched sulfates.**

Preparation of compound **9** was accomplished through allylation of compound 1 and gave the product in good yield (95%).

Subsequent Sharpless asymmetric dihydroxylation was undertaken to give the enantioenriched *S* (compound **11**) and *R* (compound **10**) 2,3-diols in 82% and 87% yields respectively. Asymmetric dihydroxylation of simple alkenes is very easy but has some drawbacks in the form of extended reaction times and low temperatures (>12 h, 0 °C) which can require specialist equipment. High yields and success rates are almost always observed from this reaction, making it an effective way to form enantiomeric diols (Hentges & Sharpless, 1980). Due to our inability to measure the e.e of these enantioenriched compounds, it was assumed to be successful due to preceding literature demonstrating success with similar substrates and conditions.

Following this, compounds **10** and **11** were then sulfated to give the enantioenriched *S* and *R* sulfates (compounds **12** and **13**) in good yields of 79% and 76%. In this case a different sulfation method was utilised, using sulfur trioxide tributylamine complex, which allows for an aqueous workup, making purification much easier (Gill, Male, & Jones, 2019). Furthermore, this method introduced an integral sodium salt exchange step, allowing simple removal of the product – tributylamine salt and giving an easy to handle, pure sulfate.

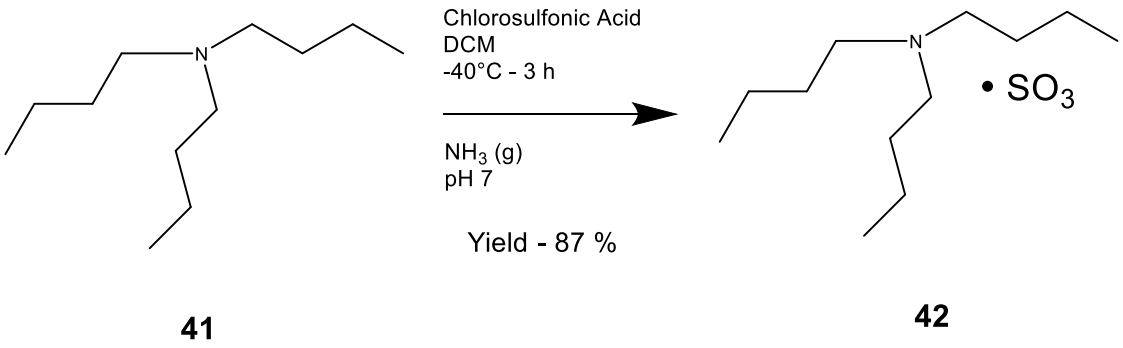

Figure 13. **Synthesis of sulfur trioxide tributylammonium complex.**

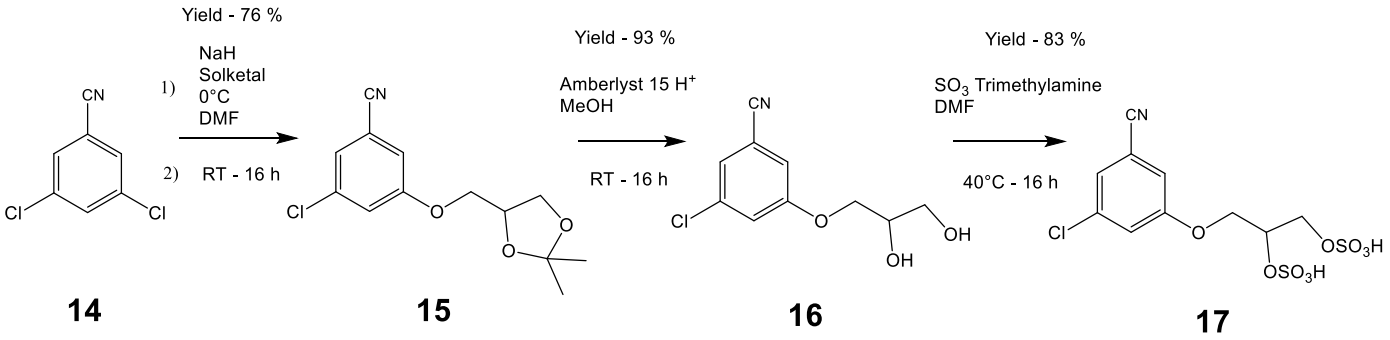

Figure 14. **Synthetic pathway B - Preparation of 5-chloro substituted sulfates.**

Synthesis of compound **15** was attained by nucleophilic aromatic substitution of compound **14** with solketal and gave a good yield of 76%. A disubstituted variant of this molecule was attempted, compound **43** (Figure **15**), however the electron donating effect from the acetonide and the loss of a chlorine electron withdrawing group, greatly deactivates the ring preventing further substitution. This reaction proceeds with relative ease and efficiency and it would be worthwhile investigating its use in other syntheses, where chlorine is in a different position on the aromatic ring.

Following nucleophilic substitution, compound **15** was then deprotected using Amberlyst 15 H+, utilising the same method used in previous deprotections to give compound **16** at a high yield of 0.166 g, 93%. As with previous deprotections, this proceeds without issue, giving the vicinal diol.

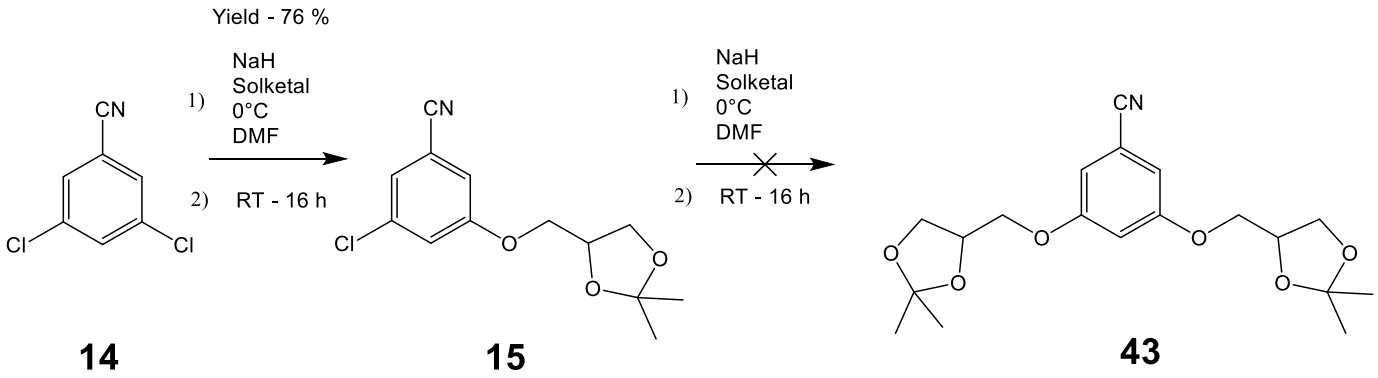

Figure 15. **Failed synthesis of compound 43.**

Compound **16** was sulfated using the basic sulfation method (sulfur trioxide trimethylamine complex, DMF, 40 °C, 16 h), to give the glycomimetic compound **17** in high yield (83%). This sulfate was subjected to the same isolation and purification methods as described earlier to give the pure sulfated compound.

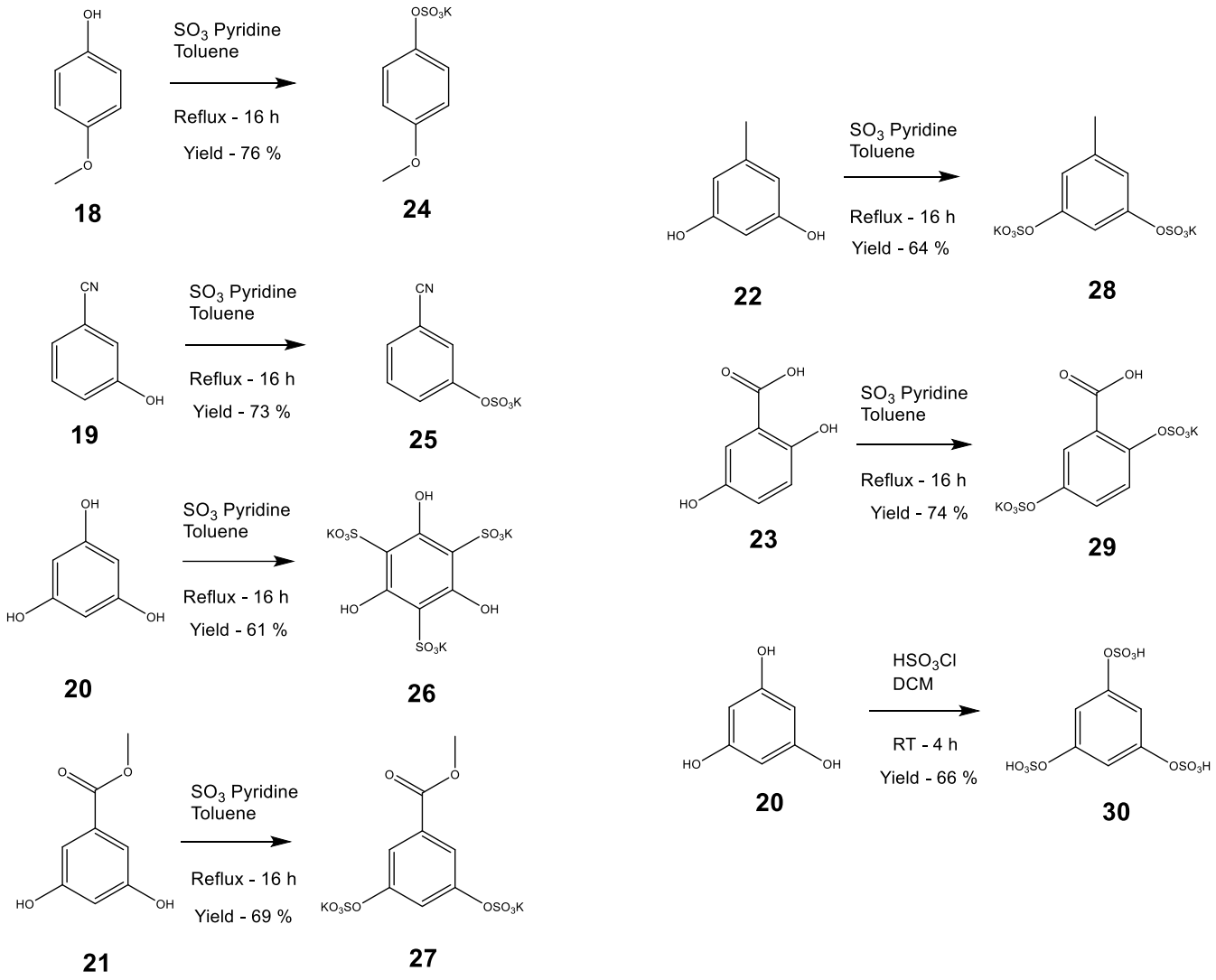

Figure 16. **Synthetic pathway C - Synthesis of compounds 24 – 30.**

Compounds **24-30** were prepared by reaction of the chosen substituted phenol with SO_3 pyridine complex at reflux in toluene to give the corresponding aryl glycomimetic. Potassium salts were obtained through treatment of the sulfate with 0.2M KOH. Synthesis of these simple glycomimetics was sustained at high yields throughout the series of compounds, likely due to the simplicity of the reaction and purification steps.

Compound **30** is an exception to the general conditions, requiring a different set of reaction conditions (chlorosulfonic acid, dichloromethane, room temperature, 16 h), to yield the

trisulfate rather than the trisulfonic acid **26**, which is produced when the general procedure is used.

Table 2. **Yields of compounds 24 - 30.**

Compound Number	Yield
24	76%
25	73%
26	61%
27	69%
28	64%
29	74%
30	66%

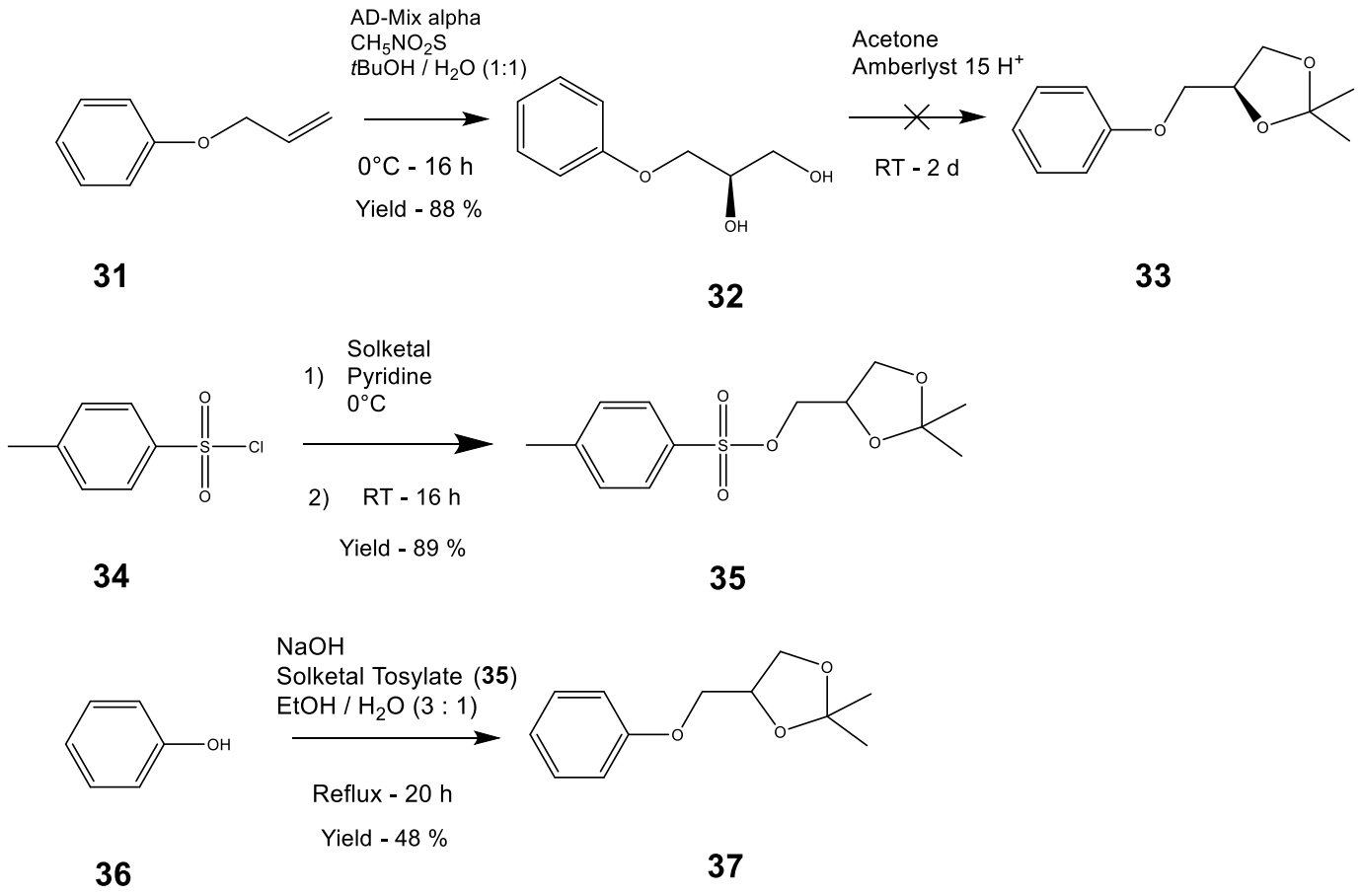

Figure 17. **Synthetic pathway D - Preparation of 2,2-dimethyl-4-(phenoxy)methyl-1,3-dioxolane.**

Compound **37** was investigated as we were attempting to determine a synthetic step which would allow us to couple substituted phenols with solketal, without the use of the Mitsunobu reaction, which had proved somewhat unsuccessful for us. However, this was found to be even more labour intensive as the formation of compound **37** was not achieved in good yield without the use of a tosylate intermediate which required prior preparation.

Synthesis of compound **33** was attempted through asymmetric dihydroxylation of compound **31**, and then protection of the diol (compound **32**) to form the acetonide, compound **33**. However, this was found to be inviable as only a small percentage of

acetonide was formed in the protection step even with considerably extended reaction times.

We therefore synthesised the protected diol (compound **37**) through a more involved route utilising solketal tosylate (compound **35**) formed through coupling of solketal with tosyl chloride (compound **34**). This tosylate intermediate allowed us to prepare compound **37** easily in one step. This route was also not without its difficulties however, as the initial attempt at the synthesis was met with failure, yielding compound **35** in a low amount of product. This was due to contamination of the tosyl chloride with *p*-toluenesulfonic acid resulting in subsequent deprotection of the acetonide *in situ*. We resolved this through purification of the tosyl chloride by Soxhlet extraction with petroleum ether to exclude any *p*-toluenesulfonic acid.

The reaction was repeated with the purified tosyl chloride, and yielded compound **35** in a high yield of 89% which was then used to synthesise compound **37** in a moderate yield of 48%.

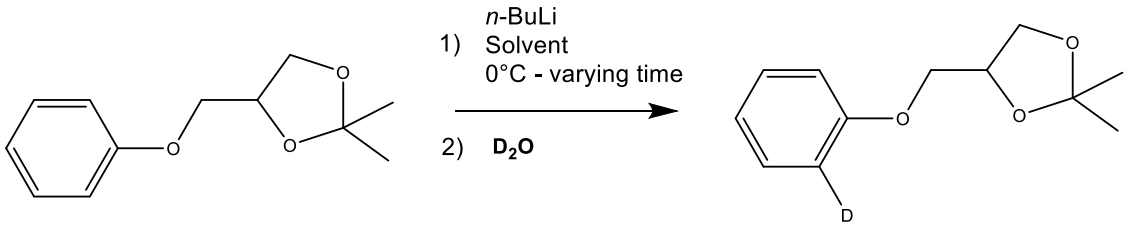

37 **38**

Figure 18. **Synthetic pathway E - Determination of lithiation conditions.**

Lithiation of this compound was investigated in order to determine whether *ortho* lithiation was attainable on substrates similar to compound **37**. In order to determine the correct

conditions for *ortho* lithiation, it was decided to run several trial reactions utilising the same materials with varying conditions, as shown in table 3. in section 3.2.16. Reactions were quenched with D_2O, to achieve lithium - deuterium exchange. This was followed by ^1H NMR spectroscopy, allowing us to determine reaction success quantitatively. Loss of 1 aromatic proton in the spectrum signifies reaction success, as deuterium is not observed in NMR spectra.

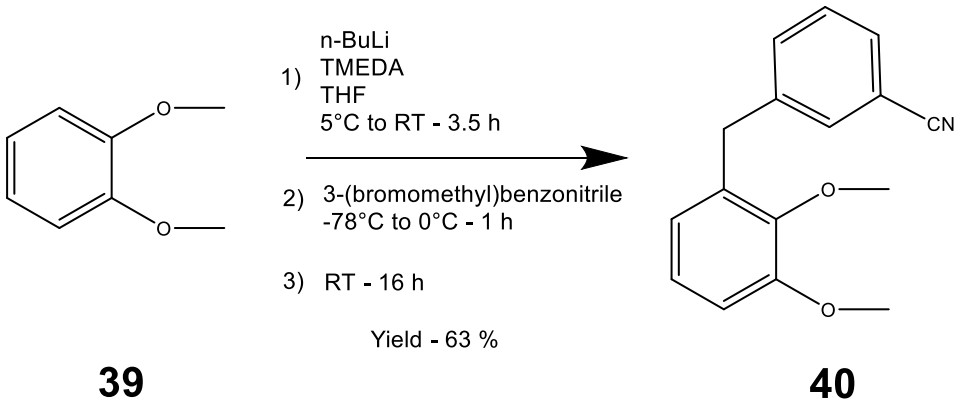

Figure 19. **Synthetic pathway F - Preparation of substituted diarylmethanes.**

Substituted diarylmethanes were selected for synthesis and subsequent investigation, due to the lack of data available for more complex multi-ringed sulfates. A diarylmethane species was selected, as the coupling of the phenyl rings were able to be both easily joined through a simple lithium cross coupling reaction in one step while directing the coupling to the desired *ortho* position on compound **39**.

The synthesis of these was attempted through reaction of compound **39** with 3-(bromomethyl)benzonitrile by directed *ortho* lithiation to give the substituted diarylmethane, compound **40** at a yield of 63%.

Due to time constraints, this synthesis was never completed. However, given more time, this would be a worthwhile area to continue research, as diarylmethane-based glycomimetics have not been investigated thoroughly as of yet.

2.2. Synthesis of enantio-enriched diols:

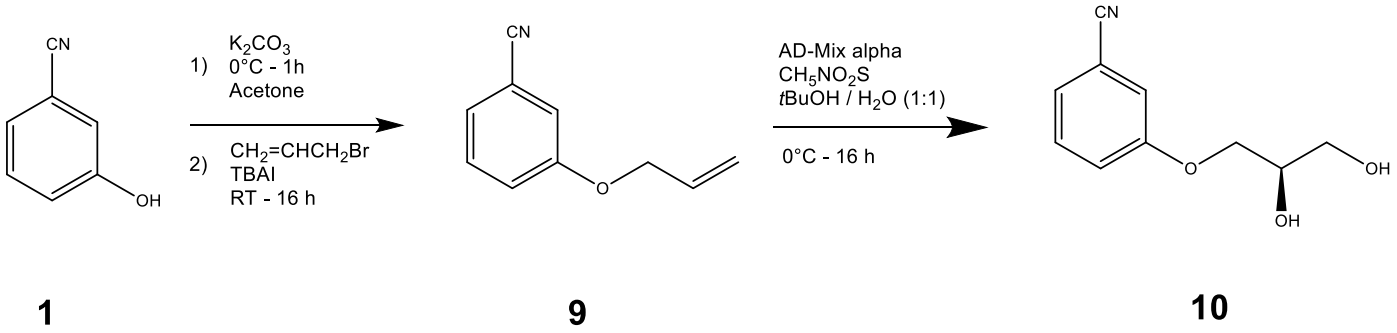

Figure 20. **Synthesis of (*R*)-3-(2,3-dihydroxypropoxy)benzonitrile.**

Synthesis of enantiomeric vicinal diols such as (*R*)- and (*S*)-3-(2,3-dihydroxypropoxy)benzonitrile by Sharpless asymmetric dihydroxylation have been documented in literature to a large extent (Elsevier, 2019). Synthesis of these compounds was achieved through preparation according to the route taken by Raiber et al., (2007) in which, a substituted phenol was reacted with allyl bromide to give the O-allyl species, an example of which can be seen in Figure **20** as compound **9**, 3-allyloxybenzonitrile. Coupling of allyl groups generally shows a very specific set of peaks in the product, 6.05 ppm (m, 1H), 5.48 ppm (dd, 1H), 5.40 ppm (dd, 1H) and 4.55 ppm (d, 2H). Aromatic peaks integrate to 1 :

1 : 2 at 7.45 – 7.1 ppm, signifying 4 aromatic protons, as expected . These are easily observed in Figure **21**, signifying a successful reaction.

This was followed by Sharpless asymmetric dihydroxylation to give the vicinal diol enantiomer. Both the allylation and asymmetric dihydroxylation (AD) reactions always seem to proceed with yields above 80% and require little to no purification, even on large scales. These procedures were repeated to give both (*R*)- and (*S*)- 3-(2,3-dihydroxypropoxy)benzonitrile which were then subjected to sulfation outlined in section 2.5.

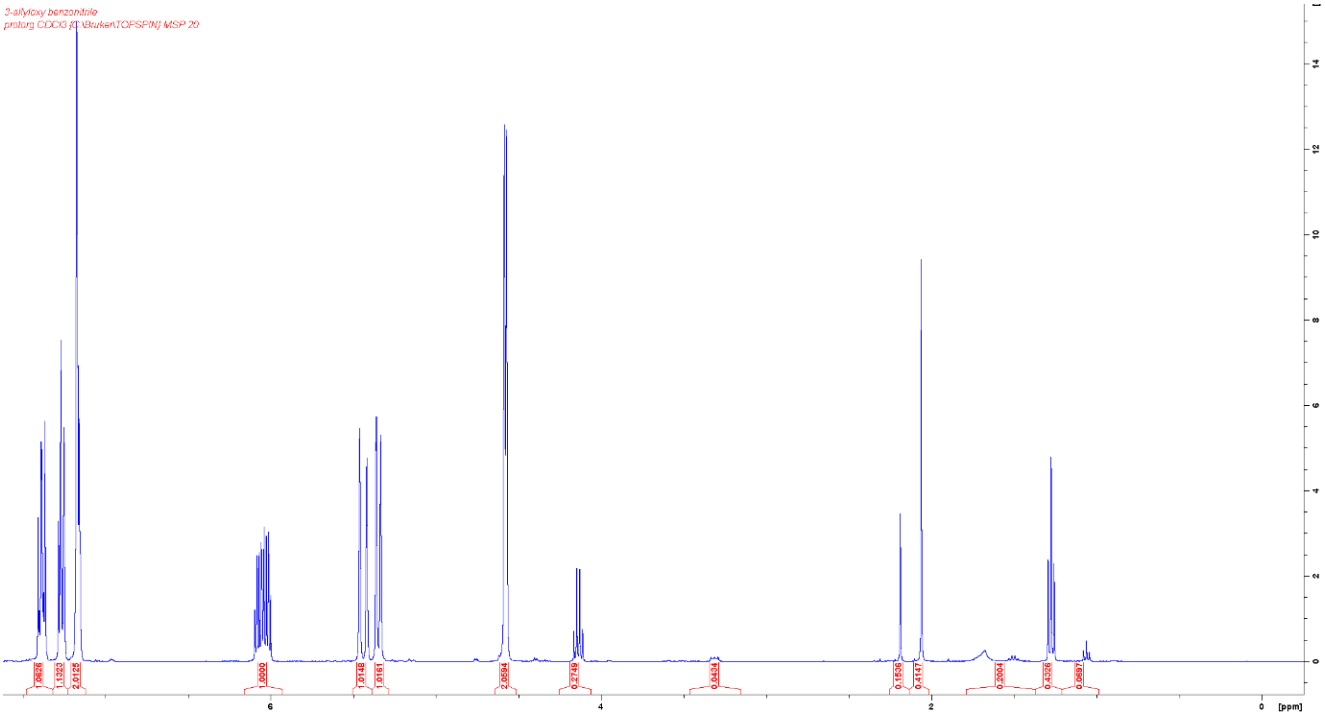

Figure 21. **^{1}H NMR of 3-allyloxybenzonitrile.**

Although AD reactions are very simple to carry out, due to commercial AD reagents being readily available for use from various suppliers, they do however require a relatively long reaction time (>12 h) in addition to maintaining constant cooling at 0 °C throughout the whole duration of the reaction. Maintaining the low temperature can prove to be somewhat

challenging without available specialist equipment to hand. Given that we do not have a way to monitor our e.e, we can assume that a good e.e would be achieved due to preceding literature reporting that low temperatures, and high pH in asymmetric dihydroxylation, yield a good e.e, and as temperature increases and pH decreases, e.e tends to suffer (Mehltretter, Dobler, Sundermeier, & Beller, 2000).

A way to overcome this could be to utilise the Mitsunobu reaction, as discussed in section 2.2, using pre-purchased optically pure (*R*)-(-) and (*S*)-(+)-solketal and then coupling it with the desired phenol to give a product with a definite high e.e.

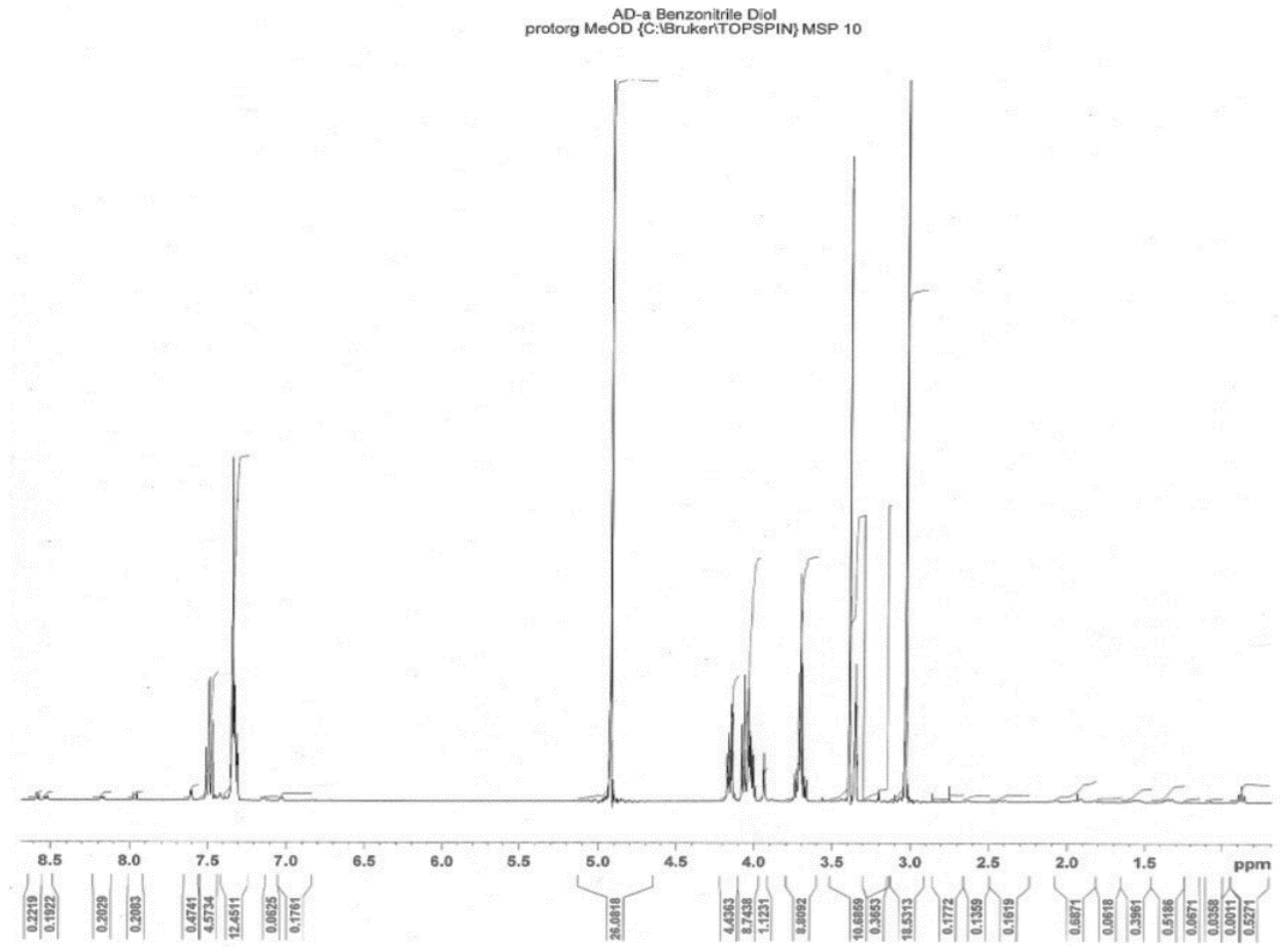
AD-a Benzonitrile Diol
protorg MeOD {C:\Bruker\TOPSPIN} MSP 10
8.5
8.0
7.5
7.0
6.5
6.0
5.5
5.0
4.5
4.0
3.5
3.0
2.5
2.0
1.5
ppm
0.2219
0.1922
0.2029
0.2003
0.4741
4.5734
12.4511
0.0625
0.1761
26.0816
4.4363
8.7438
1.1231
8.8092
10.6859
0.3853
18.5313
0.1772
0.1359
0.1619
0.6871
0.0618
0.3961
0.5186
0.0671
0.0358
0.0011
0.5271

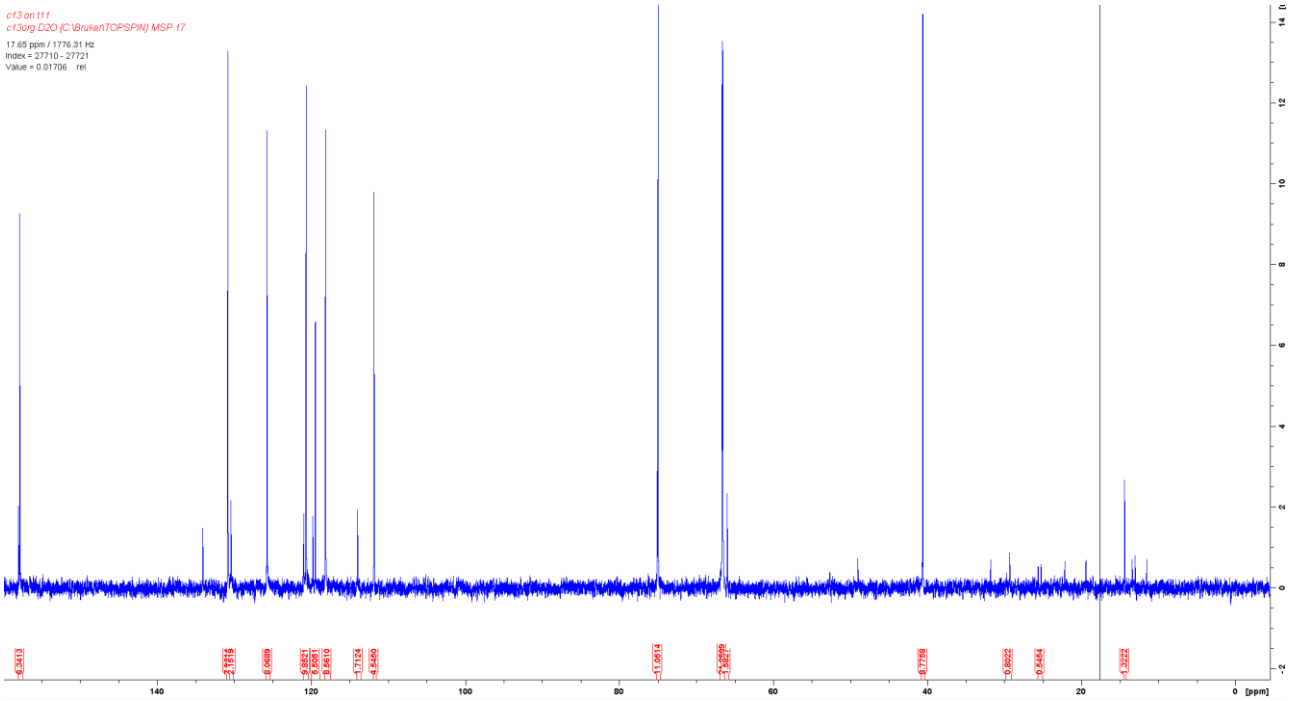
c13 on f11
c13org D2O {C:\Bruker\TOPSPIN} MSP 17
17.65 ppm / 1776.31 Hz
Index = 27710 - 27721
Value = 0.01706 rel
140
120
100
80
60
40
20
0 [ppm]

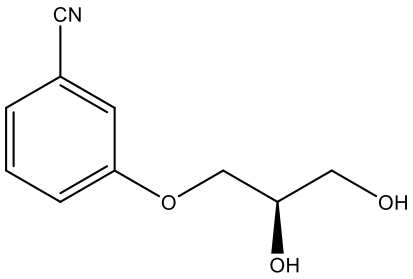

10

***Figure 22*. ^{1}H NMR, ^{13}C NMR and structure of (*R*)-3-(2,3-dihydroxypropoxy)benzonitrile.**

Figure **22** shows successful formation of the vicinal diol through asymmetric dihydroxylation, as peaks at 4.19 ppm (d, 1H), 4.05 ppm (m, 1H) and 3.2 ppm (d, 1H) in the ^{1}H NMR spectrum assign to the 5 protons present on the alkyl chain, in addition to aromatic protons integrating to a total of 4 (1 : 3) at 7.53 – 7.25 ppm. The shift upfield indicates the presence of oxygen, which combined with peak assignment, demonstrate successful synthesis. The ^{13}C spectrum helps confirm this, as the peaks at 64.96, 65.02 and 75 ppm confirm the presence of the alkyl chain with a slight amount of impurities upfield.

2.3. Synthesis of racemic diols through coupling with solketal:

Solketal was chosen as the primary reagent in this synthesis for preparing a series of nitrile-substituted arenes with 1-2 (2,3-dihydroxypropoxy) chains per molecule. Solketal seemed to be the most logical choice, as it enabled us to easily couple substituted benzonitriles with itself. This was followed by deprotection of the acetonide to give the vicinal diol with little difficulty. Solketal benefits from the 2,3 diol being by an acetonide. This allows further reactions to be carried out following the initial solketal coupling, as the acetonide may be

left untouched, subsequent reactions can then be carried out without modification of the initial chain, followed by deprotection of the acetonide in one step.

One such example of this can be seen in our preparation of compound **3** from its starting material, 2-bromo-5-hydroxybenzonitrile (Figure **23**). In this case, the Mitsunobu reaction was used to couple the first solketal molecule with the hydroxyl group, yielding compound **3**.

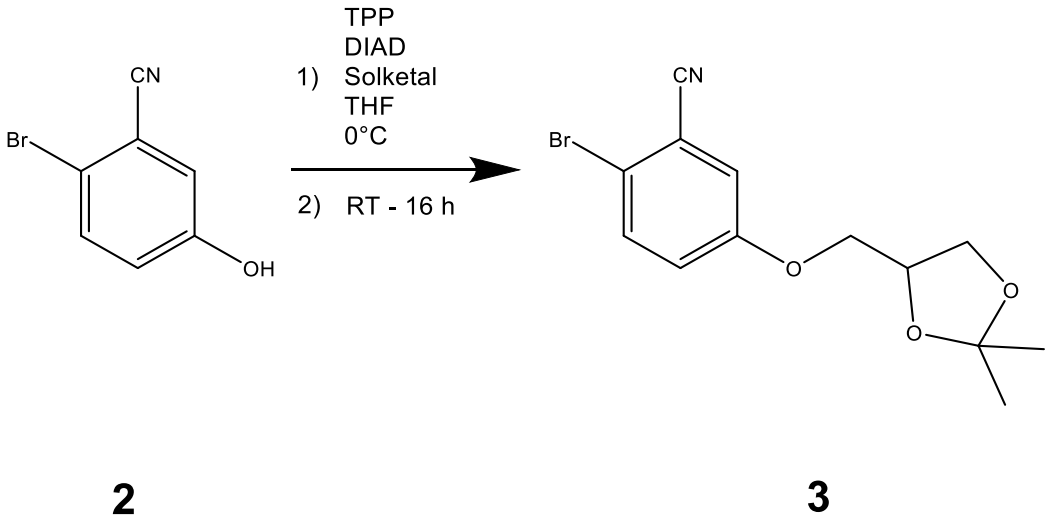

Figure 23. **Synthesis of 2-bromo-5-[(2,2-dimethyl-1,3-dioxolan-4-yl)methoxy]benzonitrile.**

While leaving the diol protected, an additional solketal molecule was added to 2-bromo-5-[(2,2-dimethyl-1,3-dioxolan-4-yl)methoxy]benzonitrile though an Ullmann-type reaction, in which the aryl bromine was substituted by solketal. Both acetonides could then be cleaved in one step using Amberlyst 15 H^+ resin, leaving the 2,5-bis diol for use in further synthesis.

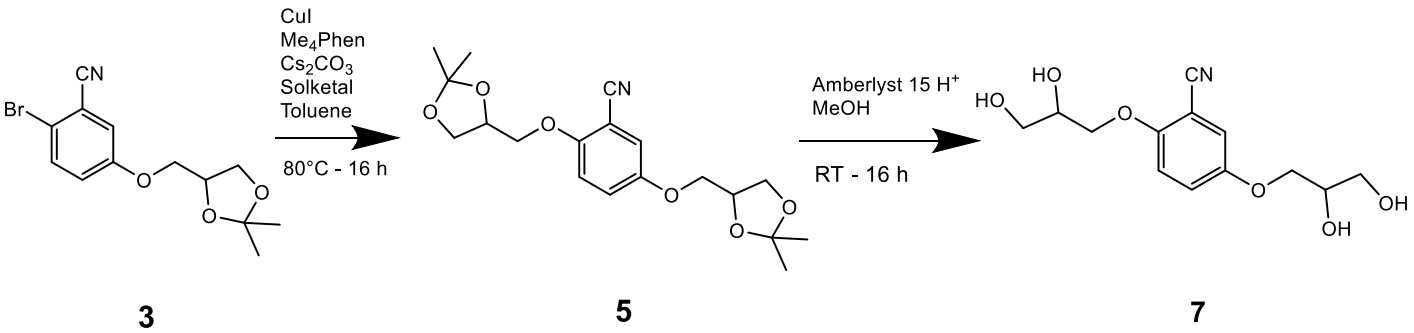

Figure 24. **Synthesis of 2,5-bis-[(2,2-dimethyl-1,3-dioxolan-4-yl)methoxy]benzonitrile and 2,5-bis-(2,3-dihydroxypropoxy)benzonitrile from 2-bromo-5-[(2,2-dimethyl-1,3-dioxolan-4-yl)methoxy]benzonitrile using sub-route A – 2.**

The reactions used in these couplings are as follows:

1) Mitsunobu Reaction:

In our aim to prepare a phenyl ether, the Mitsunobu reaction was selected due to its proven history of being predictable and successful, while using relatively cheap and readily available laboratory reagents. While we were initially successful in coupling solketal to 2-bromo-5-hydroxybenzonitrile using standard conditions as seen in Figure **10**, subsequent attempts to prepare further quantities met with failure. There may be several explanations for this, as the Mitsunobu reaction can prove to be difficult for a number of reasons.

Firstly, one of the reagents necessary for successful ether formation within the Mitsunobu reaction is an azo-reagent such as diisopropyl azodicarboxylate (DIAD) or diethyl azodicarboxylate (DEAD). This is required to form the triphenylphosphine adduct

(Mitsunobu, 1981). Unfortunately, Azo-reagents such as DIAD and DEAD are extremely sensitive both to light, moisture and heat and when given enough exposure, breaks down leading to reaction failure (Yang, Dai, Wang, & Chen, 2011). There is concern about using these reagents in terms of their safety, as when subjected to heating above 100 °C, explosive decomposition occurs and can pose a significant safety hazard in the laboratory (Sigma Aldrich, 2019).

This can be easily remedied by purchasing small quantities of the reagent and using them on a single use basis, although this can result in high per-reaction costs. Upon completion of the reaction, 2 major by-products are formed, reduced DIAD and TPPO (triphenylphosphine oxide), which can be seen in Figure **25** at 5 ppm and 1.3 ppm (DIAD), and 7.4 – 7.75 ppm (TPPO) in large quantities. Both of these by-products can prove difficult to remove using standard purification techniques, such as flash column chromatography, with reduced DIAD generally co-eluting with product (Yang et al., 2011). TPPO can also be problematic, as large quantities of it remain following reaction completion and can cause issues such as precipitation in the column, in addition to sharing the problem of co-elution as with reduced DIAD (Falconer, Jablonkai, & Toth, 1999). Ways to mitigate this have been developed, such as the method suggested by Batesky, Goldfogel, & Weix, (2017) where TPPO is reacted with zinc chloride, and precipitated out as a zinc complex, therefore avoiding the need for difficult and lengthy columns.

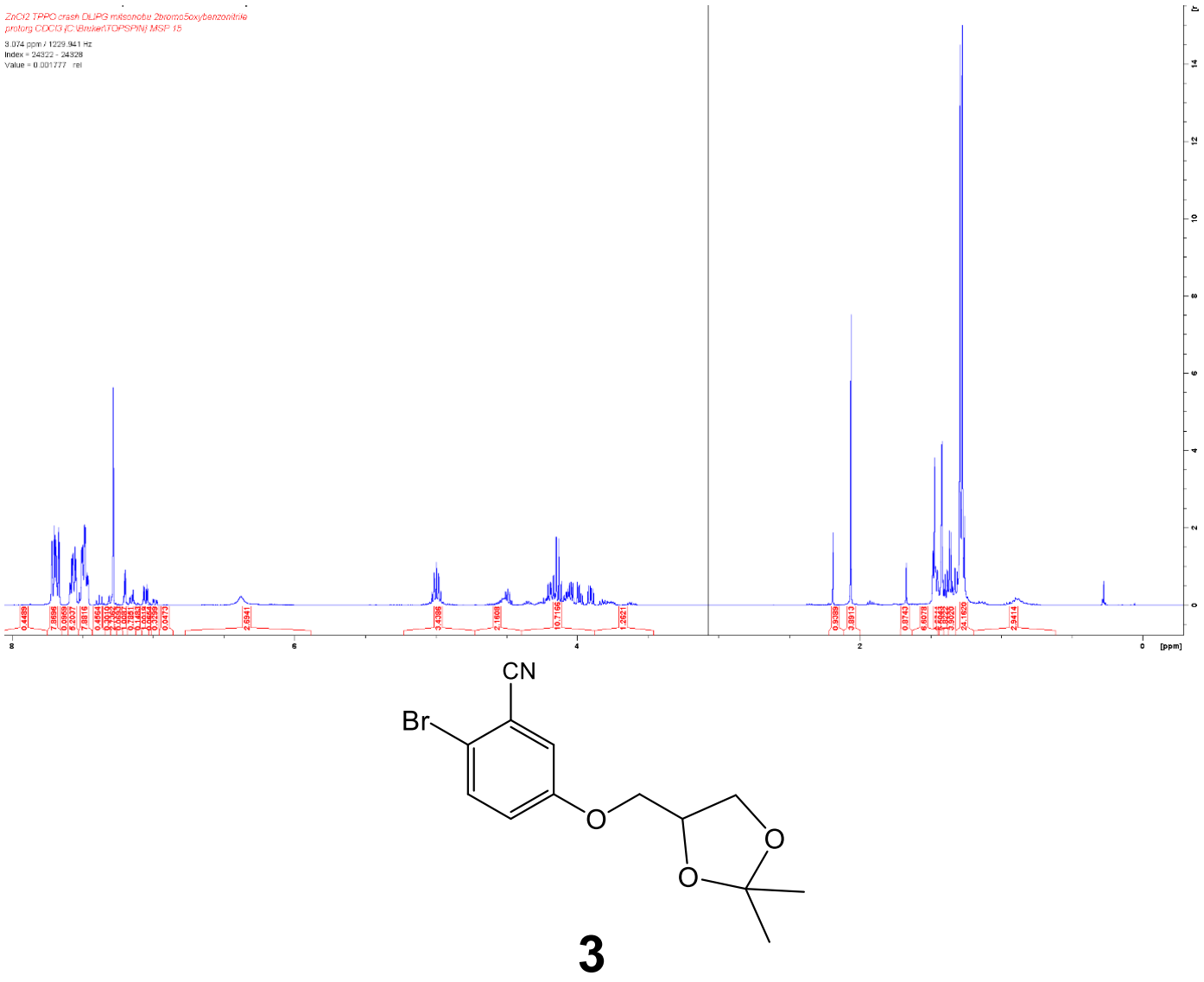

Figure 25. **^{1}H NMR showing 2-bromo-5-[(2,2-dimethyl-1,3-dioxolan-4-yl)methoxy]benzonitrile contaminated with TPPO and reduced DIAD.**

Secondly, this reaction proceeds more successfully when moisture is excluded, this significantly increases the difficulty in setting up and maintaining conditions throughout the reaction, due to the sensitivity of the azo-reagent with moisture, as described earlier. Reagent addition order is also important here, as the phosphonium – azo adduct must first be prepared at 0 °C, to prevent heating and decomposition of the azo-reagent. This is

followed by addition of the substrate, then nucleophile (Varasi, Walker, & Maddox, 1987). Deviation from this can result in reaction failure.

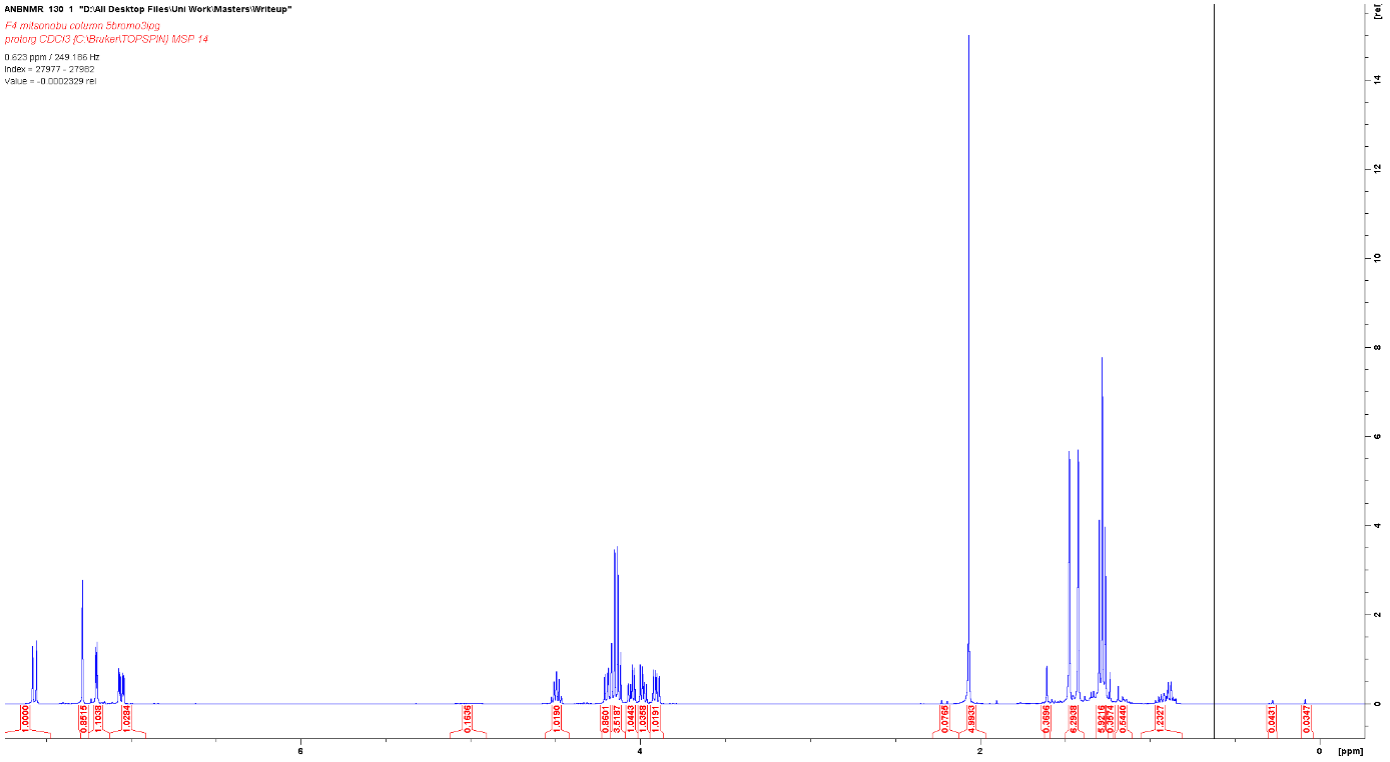
ANBNMR 130 1 "D:\All Desktop Files\Uni Work\Masters\Writeup"
P4 mitsonobu column 5bromo3log
proton CDCl3 [C:\Bruker\TOPSPIN] MSP 14
0.623 ppm / 249.186 Hz
Index = 27977 - 27982
value = -0.0002329 rel
[rel]
[ppm]

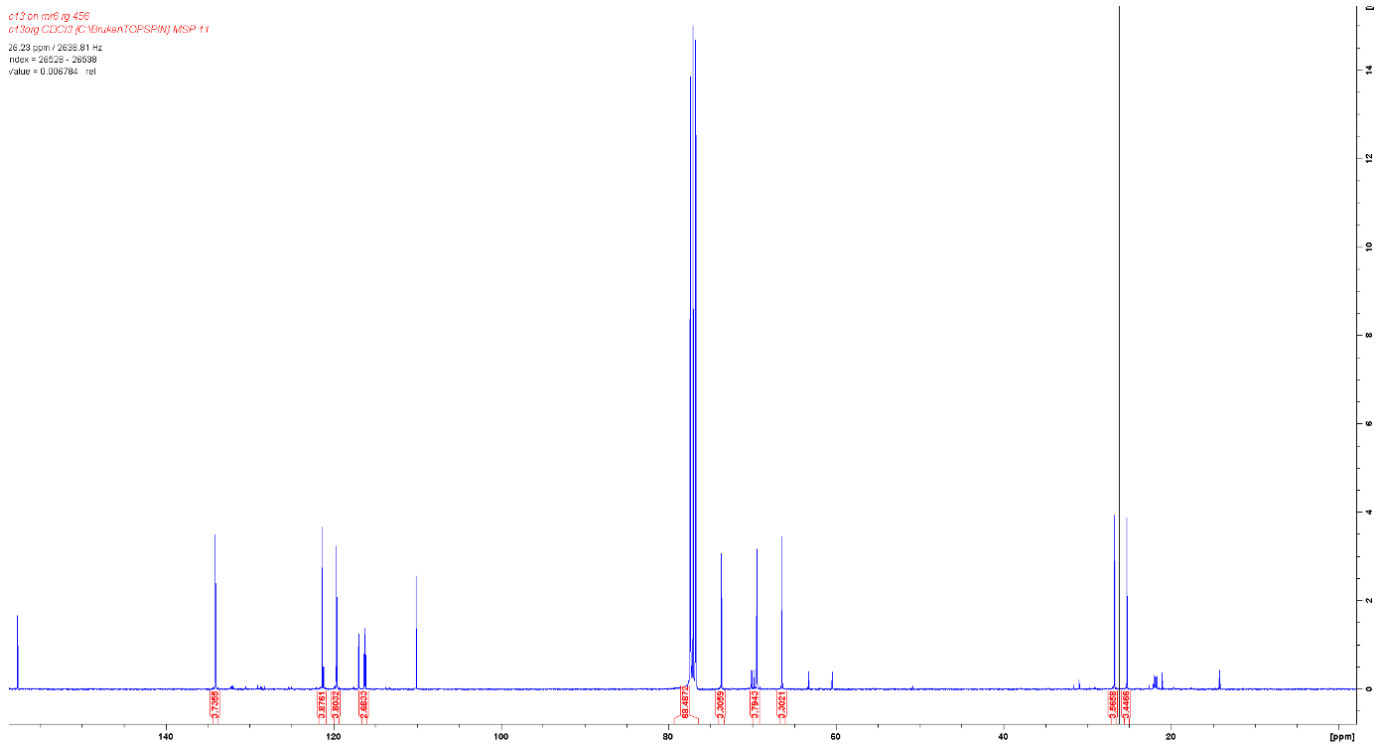
c13 on nmr6 rg 456
c13org CDCl3 [C:\Bruker\TOPSPIN] MSP 11
26.23 ppm / 2638.81 Hz
index = 26528 - 26538
value = 0.006784 rel
[ppm]

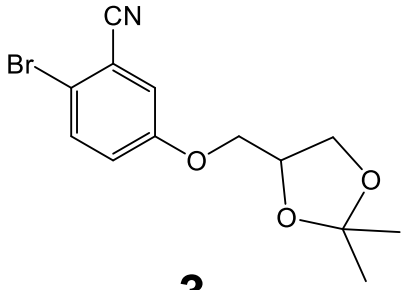

3

Figure 26. **^{1}H NMR, ^{13}C NMR and structure of 2-bromo-5-[(2,2-dimethyl-1,3-dioxolan-4-yl)methoxy]benzonitrile.**

Following purification, it is able to clearly see the peaks in both spectra for the presence of the solketal chain, shown below.

^{1}H NMR - 4.36 - 4.40 ppm (m, 1H), 4.10 ppm (dd, 1H) 3.86 – 4.00 ppm (m, 2H) 3.81 ppm (dd, 1H), 1.38 ppm (s, 3H) and 1.33 ppm (s, 3H).

^{13}C NMR - 110.10, 73.66, 69.42, 66.41, 26.75 and 25.26 ppm.

Additionally, aromatic protons can be seen integrating to 1 : 1 : 1 at 7.0 – 7.6 ppm, for a total of 3, which together demonstrate reaction success.

Ways to mitigate purification problems in the Mitsunobu reaction have been developed in the form of new, more advanced reagents and variations in the reaction itself. Replacements for both DIAD and TPP in the forms of Di-*p*-chlorobenzyl azodicarboxylate (Lipshutz, Chung, Rich, & Corral, 2006) and polymer-supported TPP (Tunoori, Dutta, & Georg, 1998) have been discovered and function identically to the original reagents, however once consumed, the by-products are then easily filtered off and disposed of or recycled.

Furthermore, Beddoe et al., (2019) recently developed a vastly improved version of the Mitsunobu reaction which uses a phenol containing phosphine oxide in the +5 oxidation state that catalytically drives the reaction as a dual purpose oxidant and reductant, releasing only water as by product (Figure **27**). Furthermore, they state that the number of substrates compatible with the reaction is increased compared to the “traditional” Mitsunobu. This both increases the reaction’s scope in future syntheses and removes several of the problems commonly associated with the Mitsunobu reaction.

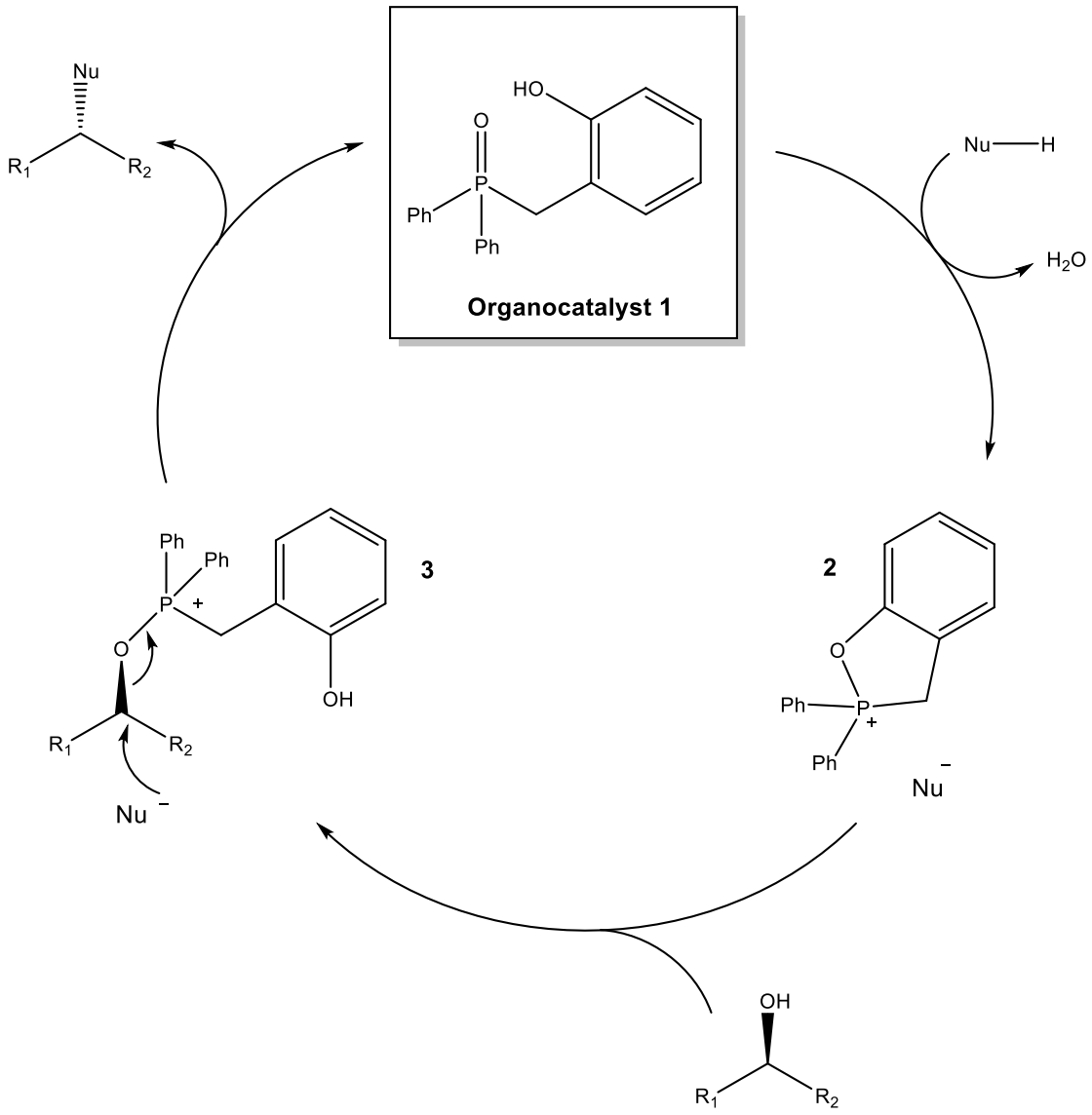

Figure 27. **Mechanism for catalytic Mitsunobu. Reprinted from "Redox-neutral organocatalytic Mitsunobu reactions." By Beddoe, R. H., Andrews, K. G., Magné, V., Cuthbertson, J. D., Saska, J., Shannon-Little, A. L., … Denton, R. M. 2019. *Science*, *365*(6456), 910–914.**

2) Ullmann Reaction:

Our aim was to add a second solketal molecule at the 2-position to one of our compounds. We investigated a number of substitution reactions that may be used and found there are a few reactions that can be successful in this, such as Chan-Lam coupling (aryl NH_2/OH as substrate, substituted boronic acid as reactant with Cu (II) as catalyst) (Munir et al., 2019).

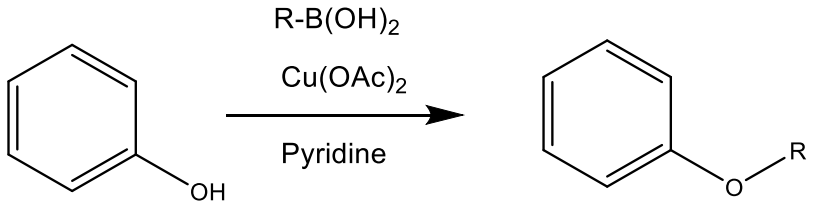

Figure 28. **Chan-Lam Coupling.**

Or the Ullmann-type reaction (aryl bromide/iodide as substrate, substituted nucleophile as reagent with Cu (I) as catalyst) (Sambiagio, Marsden, Blacker, & McGowan, 2014).

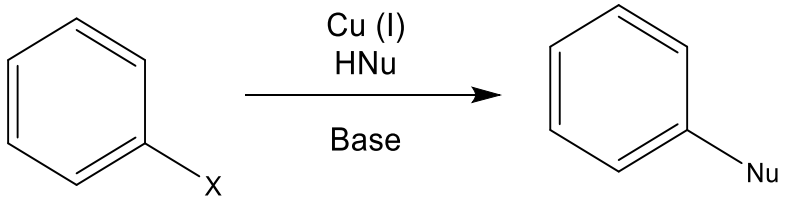

Figure 29. **Ullman-Type Reaction.**

Ultimately, we selected the Ullmann reaction as preparation of the aryl bromide reaction substrate through the reaction of *N*-bromosuccinimide with 3-cyanophenol by electrophilic aromatic substitution was far easier than preparation of the required substituted boronic acid for Chan-Lam coupling. The Ullmann reaction we used is not a “true” Ullman coupling, as the classic reaction is generally used to prepare biaryl systems. We used a variation of

this which is essentially a copper-catalysed nucleophilic aromatic substitution of an aryl bromide with solketal as the nucleophile.

Initially, we attempted this coupling with conditions as stated by Ma & Cai, (2003) (CuI, Cs_2CO_3, *N,N*-dimethylglycine, 1,4-dioxane). However, this resulted in no notable product formation. The reaction was re-attempted using conditions from Altman, Shafir, Choi, Lichtor, & Buchwald, (2008) (CuI, Cs_2CO_3, 3,4,7,8-tetramethyl-1,10-phenanthroline, toluene), which yielded complete conversion of starting material to product. This second procedure utilises commercially available 3,4,7,8-tetramethyl-1,10-phenanthroline as a ligand, which improves copper catalysed coupling reactions of aryl halides with a range of hydroxyl containing reactants while maintaining relatively mild conditions as stated in Figure **11**.

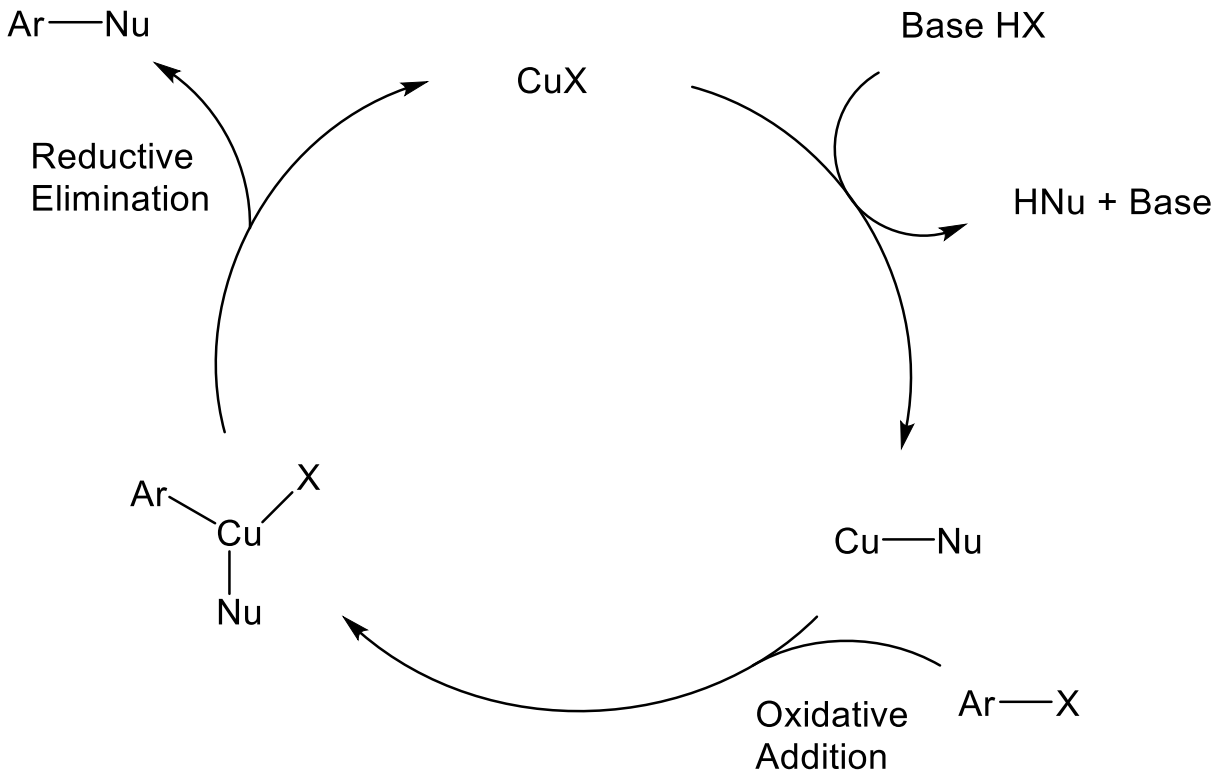

Figure 30. **Mechanism for the Ullmann reaction. Reprinted from "Ullmann Reaction" by Organic Chemistry Portal, n.d, Retrieved from https://www.organic-chemistry.org/namedreactions/ullmann-reaction.shtm**

3) Nucleophilic Substitution:

In searching for a good replacement for the Mitsunobu reaction to synthesise substituted benzonitriles, we considered the use of nucleophilic substitution. Investigation of literature gave several worthwhile methods, and we selected a reaction described in a patent by Smithkline Beecham (World Patent No. WO 2008/157273 A1, 2008), which involved nucleophilic substitution of a chlorine on 3,5-dichlorobenzonitrile with solketal sodium salt to give the substituted product. This was then able to be taken, deprotected and sulfated to give our final glycomimetic.

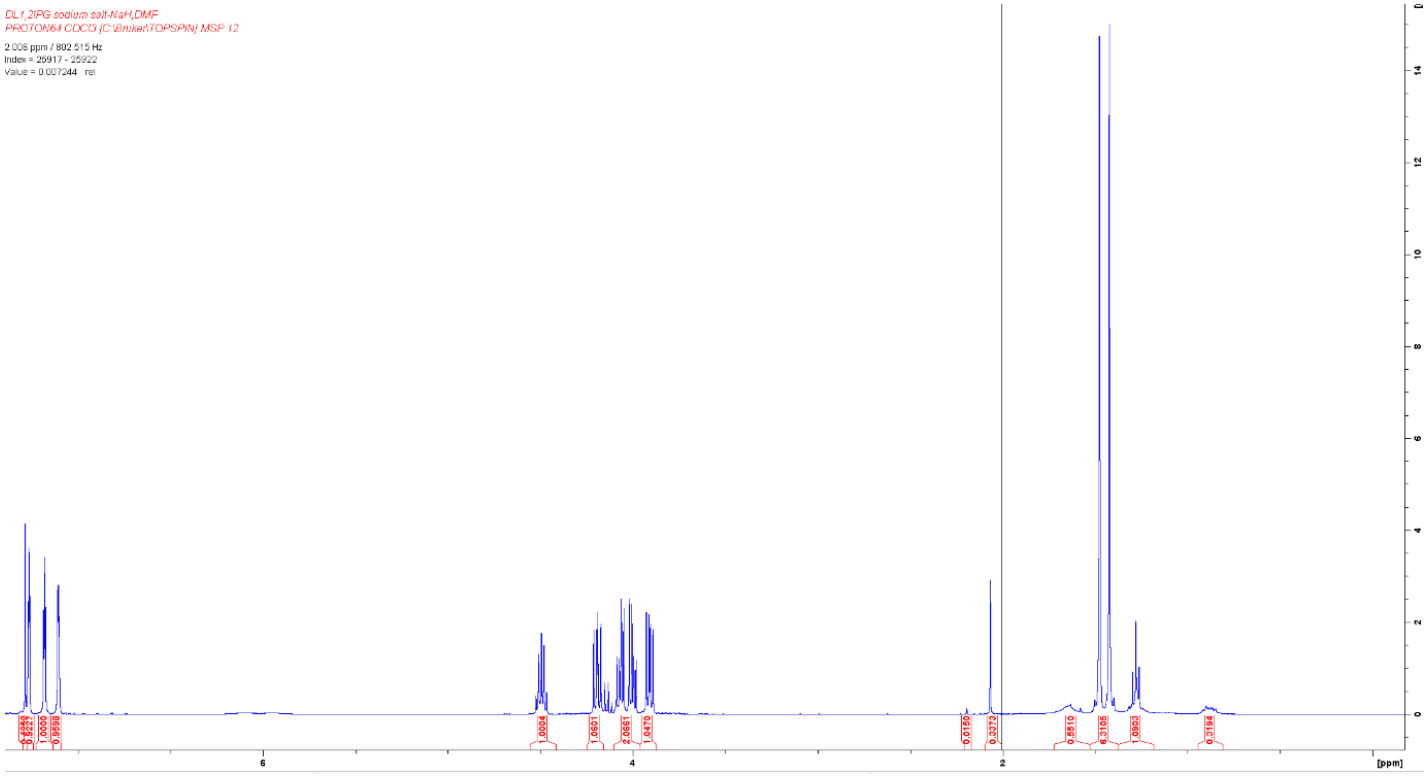
DL1,2IPG sodium salt-NaH,DMF
PROTON64 CDCl3 {C:\Bruker\TOPSPIN} MSP 12
2.006 ppm / 802.515 Hz
Index = 25917 - 25922
Value = 0.007244 rel
[ppm]

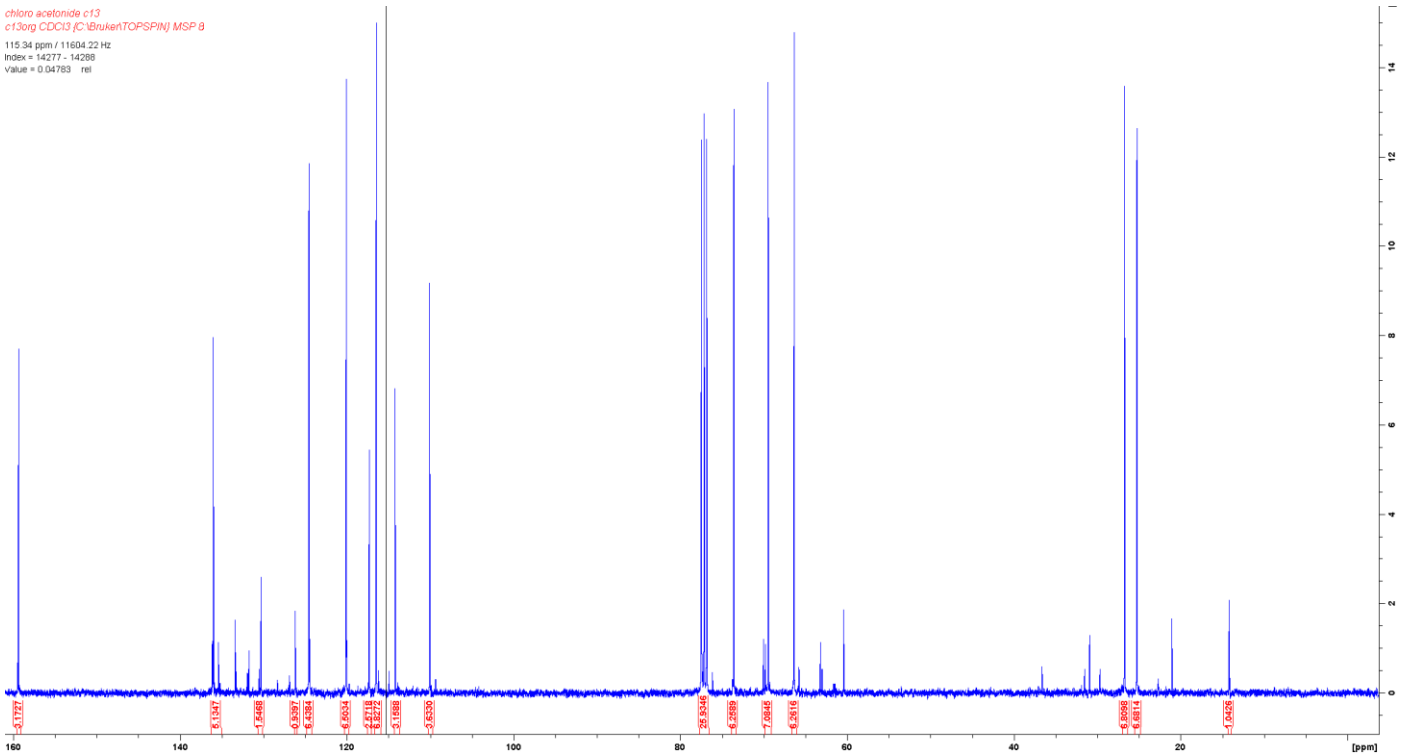
chloro acetonide c13
c13org CDCl3 {C:\Bruker\TOPSPIN} MSP 8
115.34 ppm / 11604.22 Hz
Index = 14277 - 14288
Value = 0.04783 rel
[ppm]

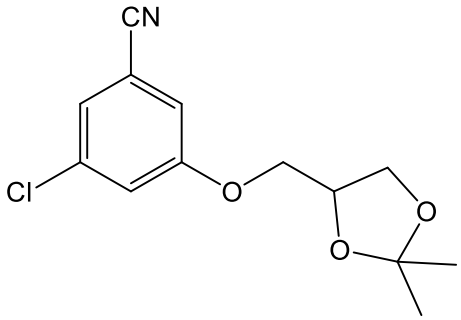

15

Figure 31. **^{1}H NMR,^{13}C NMR and structure of 3-chloro-5-([2,2-dimethyl-1,3-dioxolan-4-yl]methoxy)benzonitrile.**

This reaction was extremely effective and gave product in high purity with good yield, as shown by the spectra in Figure **31** signified by only small peaks not corresponding to product. These spectra are quite similar to those in Figure **26** for compound **3**, as they differ only in the position of the halogen and its substitution. Presence of product was confirmed through identification of the peaks which correspond to the solketal sidechain. The presence of aromatic protons was confirmed by the peaks shown at 7.1 – 7.4 ppm, integrating to 1 : 1 : 1 for a total of 3, as expected for a trisubstituted product. Peaks assigned to the solketal sidechain are as follows:

^{1}H NMR - 4.53 – 4.45 ppm (m, 1H), 4.19 ppm (dd, 1H), 4.09 – 3.97 ppm (m, 2H), 3.90 ppm (dd, 1H), 1.47 ppm (s, 3H) and 1.42 ppm (s, 3H).

^{13}C NMR - 110.00, 73.80, 69.41, 66.43, 26.80 and 25.22 ppm.

Given the success of the initial substitution, we attempted to devise a procedure for a one-pot synthesis of the 3,5-disubstituted species. Unfortunately, attempts at substituting positions 3 and 5 both together, and sequentially, gave only the 3-substituted product. This is likely due to changes in ring electronics, as loss of one chlorine electron withdrawing

group would deactivate the aromatic ring somewhat. Additionally, the substituted group is electron donating, further contributing to deactivating the ring, giving a deactivated species resistant to further nucleophilic attack.

Furthermore, conditions for this reaction were somewhat tedious to maintain effectively, as the nucleophile is prepared in dry solvent with extremely water sensitive reagents (sodium hydride) and therefore must be done under completely dry conditions in order to get a good yield and success in the reaction.

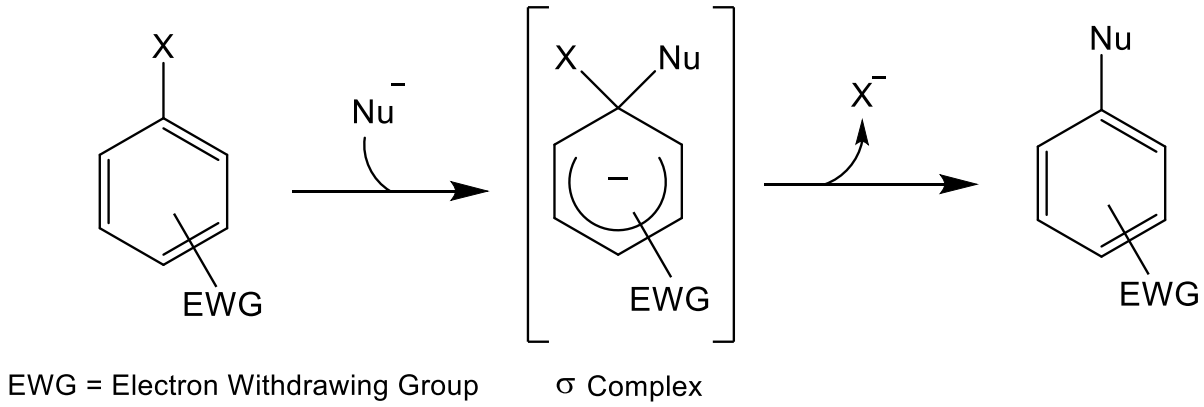

***Figure* 32. Mechanism for nucleophilic aromatic substitution.**

2.4. Synthesis of final glycomimetics by sulfation/sulfonation:

We aimed to prepare 3 categories of sulfates during these syntheses; Aryl sulfated and sulfonated glycomimetics, homochiral benzonitrile glycomimetics and racemic benzonitrile glycomimetics. Benzonitrile glycomimetics were selected for further investigation as, from our previous research (Bunte, 2017), have been shown to demonstrate good efficacy in inhibiting the HGF-Met pathway.

Aryl glycomimetics were selected for investigation as there has been limited research into this class of molecules. We therefore synthesised a series of novel aryl sulfates and sulfonates, with an aim to effectively prevent cell mobility, and inhibit the HGF-Met pathway.

Formation of the final compounds was achieved through sulfation of hydroxyl groups through 4 major routes, utilising SO_3-amine complexes and chlorosulfonic acid as sources of sulfate. These routes and reagents were selected due to considerable research showing *O*-sulfation under relatively mild conditions with generally high yields (Gill et al., 2019). Basic sulfations generally only required mild conditions, but reactions where sulfonation and aryl *O*-sulfation were required used harsher conditions with higher temperatures and more aggressive reagents. An exception to this is formation of phloroglucinol trisulfate, which required a different set of conditions to prevent formation of the sulfonate.

Purification of the final compounds were carried out in a number of ways:

1) Silica gel column chromatography utilising a highly polar solvent system (methanol or 2:1 methanol : dichloromethane) due to the high polarity of the sulfated compounds. This had

its limitations and on occasion, the compound would elute containing a portion of the sulfate-amine salt due to lack of exchange of the amine with H^+ on the silica gel.

2) Preparation of the sulfate-potassium salt through the workup. This was generally the easiest to achieve, as purification, product isolation and formation of the alkali metal salt was easily completed in one workup step, then lyophilised to give the final dried product.

3) Ion exchange with a sodium ion containing resin. If it was not possible to prepare the alkali metal salt in the workup, ion exchange was chosen for purification. Amberlite IR120 Na was selected for use, and the compound passed though the resin in water, giving the pure sulfate sodium salt as product, which was then lyophilised to give the final dried sulfate.

4) Isolation of the sulfate-tributylamine salt through aqueous workup, followed by reaction of the amine salt with sodium 2-ethylhexanoate to form the sulfate-sodium salt as final product, which was then lyophilised to give the final dried sulfate.

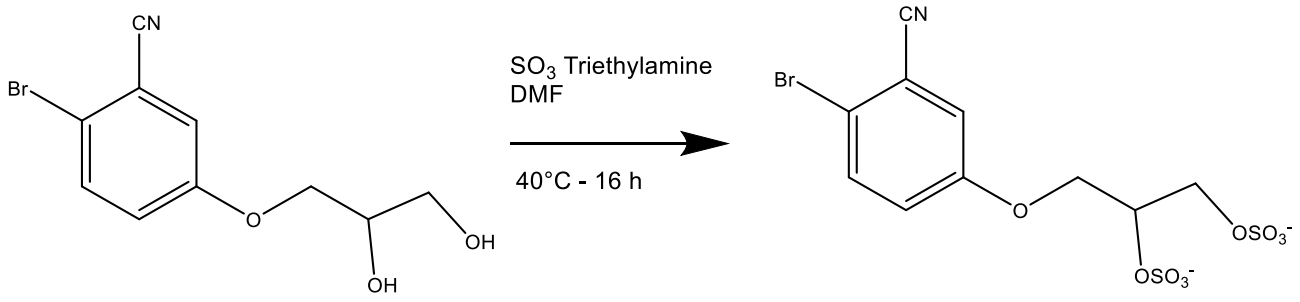

4 **6**

Figure 33. **Synthesis of 2-bromo-5-(2,3-dihydroxypropoxy)benzonitrile using sub-route A - 1.**

Initially, SO_3-trimethylamine complex was used as the primary route for sulfation of alkyl hydroxyl groups and while effective, produced some considerable drawbacks. These consist of:

1) using a high-boiling solvent which decomposes when heated aggressively, creating difficulties in evaporation.

2) Extreme solubility of product in water, removing possibilities for aqueous workup, resulting in difficulties in purification.

3) Formation of product-trimethylammonium salts which must be thoroughly removed through either ion exchange or column chromatography prior to cell testing due to the amine's biological effect, which would affect test results.

This sulfation was carried out according to Raiber et al., (2007) and utilised 2-3 equivalents of SO_3-trimethylamine per OH group in N,N-dimethylformamide at 40 °C for 12 hours to fully sulfate the desired molecule.

Furthermore, sulfation using sulfur trioxide trimethylamine complex is fast, easy and effective but generates a considerable quantity of impurities, which can be visualised in Figure **34** by the many small peaks distributed throughout the spectrum. While it is possible to identify the product from these spectra, it shows the necessity of thorough purification.

Identification was achieved through assignment of the peaks to the propoxy sidechain, in addition to the upfield shift induced by the addition of several $-OSO_3$ groups. Peaks assigned to the propoxy chain are as follows:

^{1}H NMR - 2.86 – 2.74 ppm (m, 2H), 2.69 – 2.56 ppm (m, 2H) and 2.56– 2.41 ppm (m, 1H).

^{13}C NMR - 71.55, 69.35 and 63.90 ppm

Further confirmation of reaction success was demonstrated by the aromatic protons integrating to 1 : 1 : 1 at 5.65 – 6.16 ppm for a total of 3, as expected from this product.

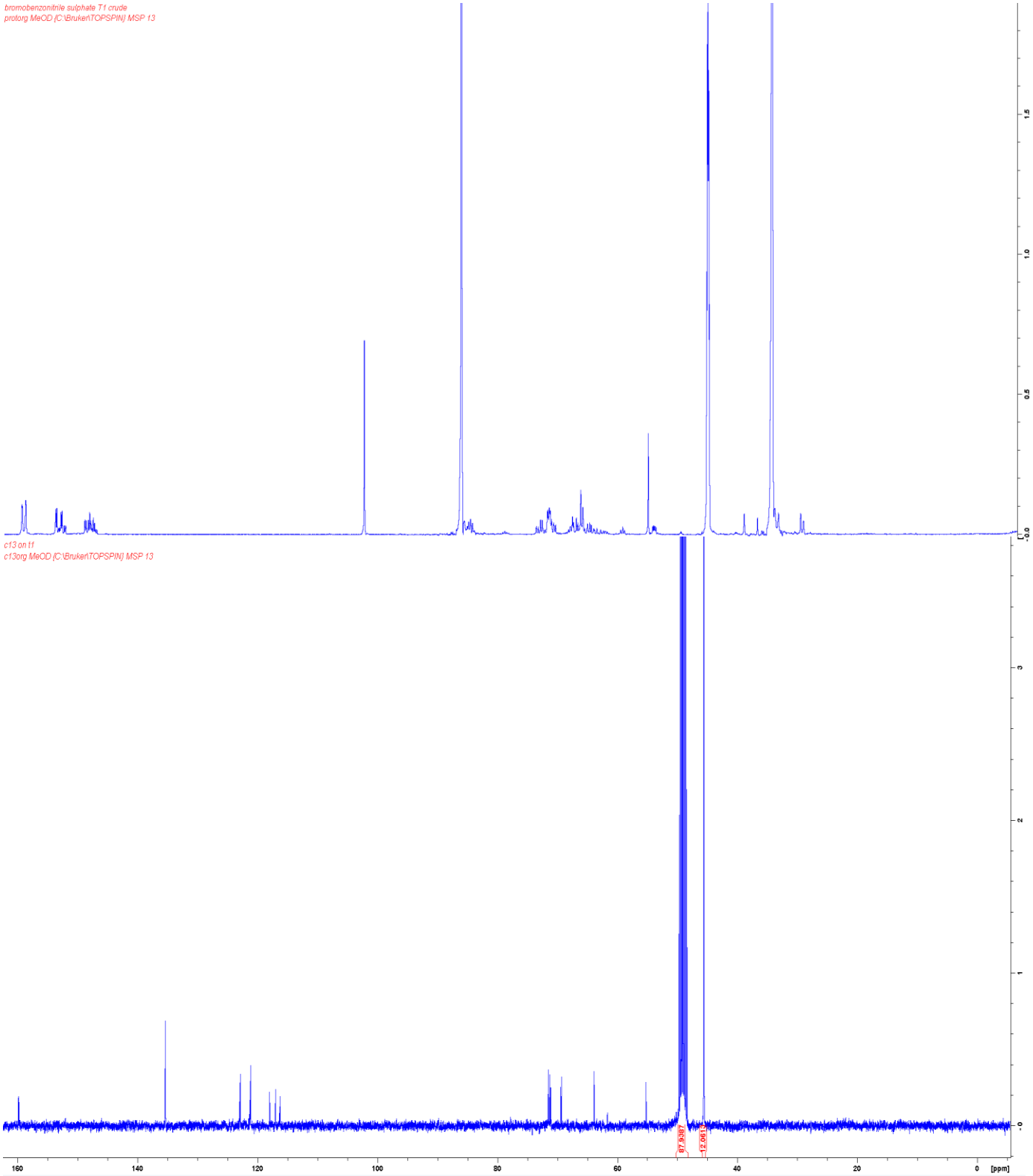

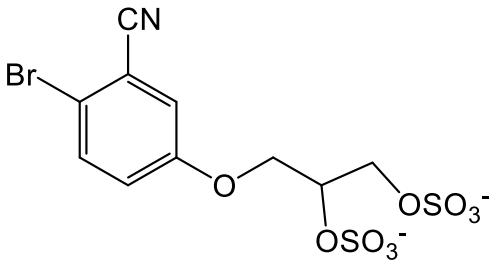

6

***Figure 34*. ^{1}H NMR, ^{13}C NMR and structure of 2-bromo-5-(2,3-bis(sulfooxy)propoxy)benzonitrile.**

Synthesis of compound 24 by synthetic pathway C:

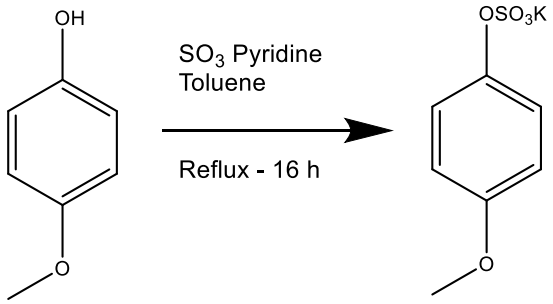

18 **24**

***Figure 35.* Synthesis of potassium-4-methoxyphenyl sulfate using synthetic pathway C.**

Another route was used to prepare the aryl sulfates and sulfonates and was carried out according to the procedure by Burkhardt and Lapworth, with minor modifications, as suggested by Denehy, White, & Williams, (2006). This procedure required 1 equivalent of SO_3-pyridine per OH group in toluene at reflux overnight to form the required aryl sulfate/sulfonate.

This procedure utilised much harsher conditions than previous routes, due to the relatively high temperature and long reaction times. This procedure also resulted in some drawbacks, namely the length of workup that was required to give a relatively pure product free from pyridine, it was however free from all the major drawbacks outlined from Route: 1, as workups for this procedure addressed the problems of solubility, amine salts and solvent removal due to conversion to the potassium salt being achieved in the workup. This was done through basification of the compound with dilute KOH, washing with ethyl acetate at each step to exclude any pyridine or other impurities, followed by lyophilisation of the aqueous layer to yield the dried product. Yields of these aryl sulfates were generally moderate and preparation of the compounds was achieved quickly and easily.

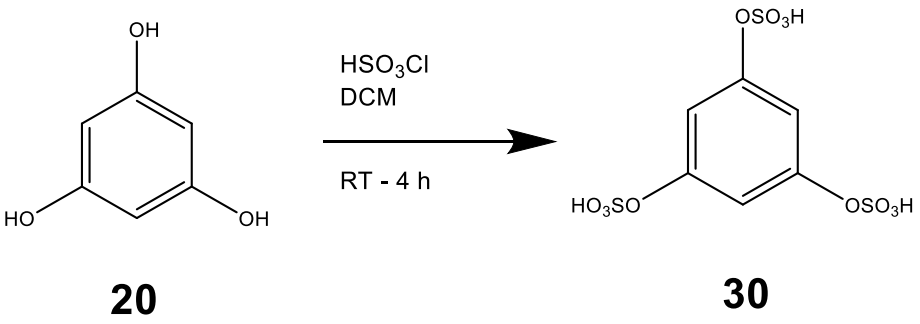

Figure 36. **Synthesis of phloroglucinol trisulfate using synthetic pathway C.**

It was necessary to use a slightly different method, as suggested by Karimi-Jaberi, Pooladian, Moradi, & Ghasemi, (2012) in Route: 3 when preparing the phloroglucinol trisulfate, as using the harsher set of conditions outlined in the previous route gave 1,3,5-trihydroxy-2,4,6-benzenetrisulfonic acid potassium salt as product.

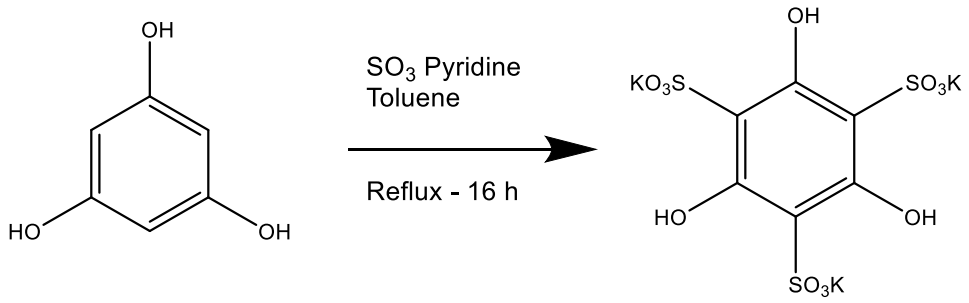

20 **26**

Figure 37. **Synthesis of 1,3,5-trihydroxy-2,4,6-benzenetrisulfonic acid potassium salt using synthetic pathway C.**

Therefore, another sulfation procedure was devised, using 1 equivalent of chlorosulfonic acid per OH group in dichloromethane at room temperature for a total of 4 hours to give phloroglucinol trisulfate as the final product. This route led to merely minor drawbacks, as no usage of SO_3-amine complexes was necessary in addition to an easy workup being available. These were likely side reactions due to the high reactivity of chlorosulfonic acid, resulting in a lowered yield of 66%.

This product was confirmed by investigation of the NMR spectra. Lack of peaks belonging to product in the ^{1}H spectrum indicates the product having no C-H bonding, as expected for this product. The peak at 1.8 ppm is assigned to sodium acetate contamination, produced during the workup. The peak at 4.7 ppm is assigned to water contamination in D_2O.

The single peak at 181.50 ppm in the ^{13}C spectrum indicates the 6 aromatic carbons present in this compound, allowing us to confirm product presence. The peak at 24 ppm is assigned to sodium acetate contamination.

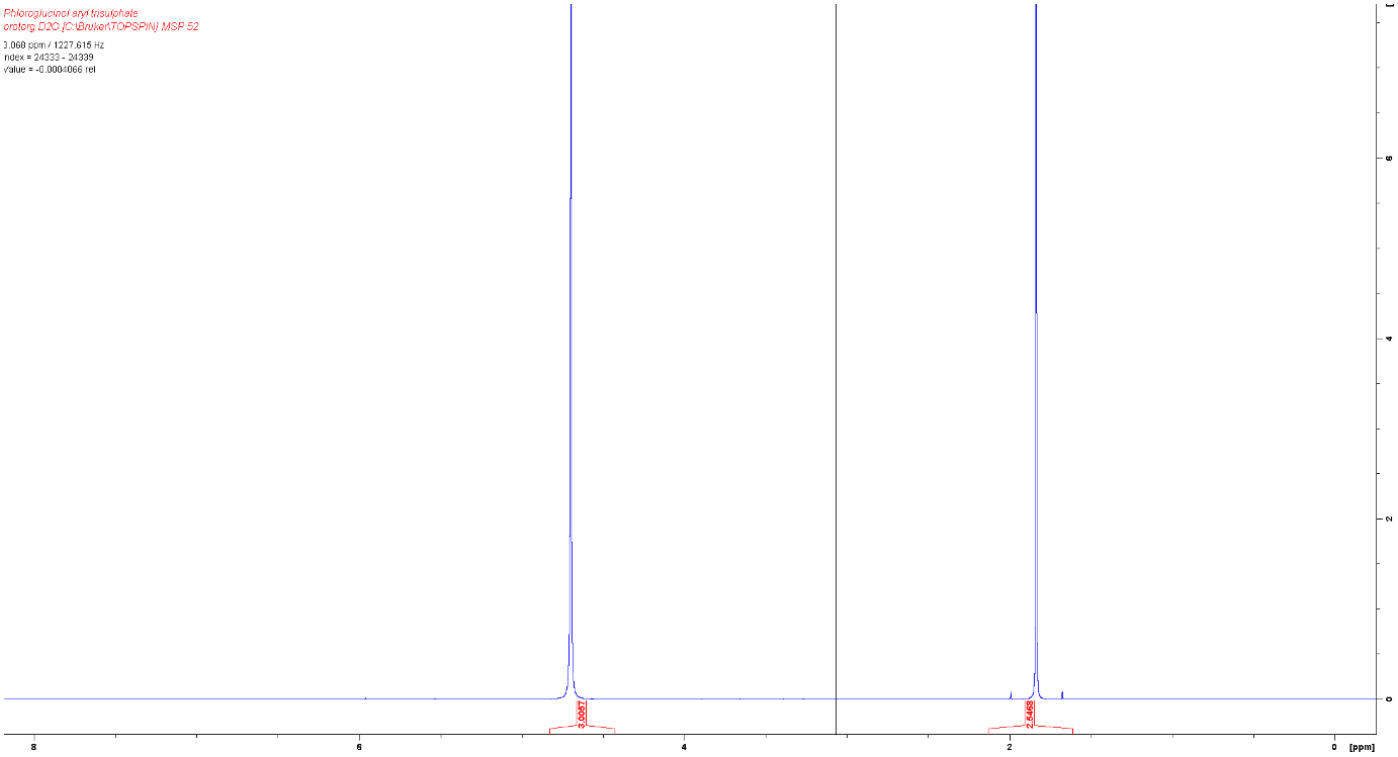
Phloroglucinol aryl trisulphate
orotorg D2O {C:\Bruker\TOPSPIN} MSP 52
3.068 ppm / 1227.615 Hz
index = 24333 - 24339
value = -0.0004066 rel
8
6
4
2
0
[ppm]

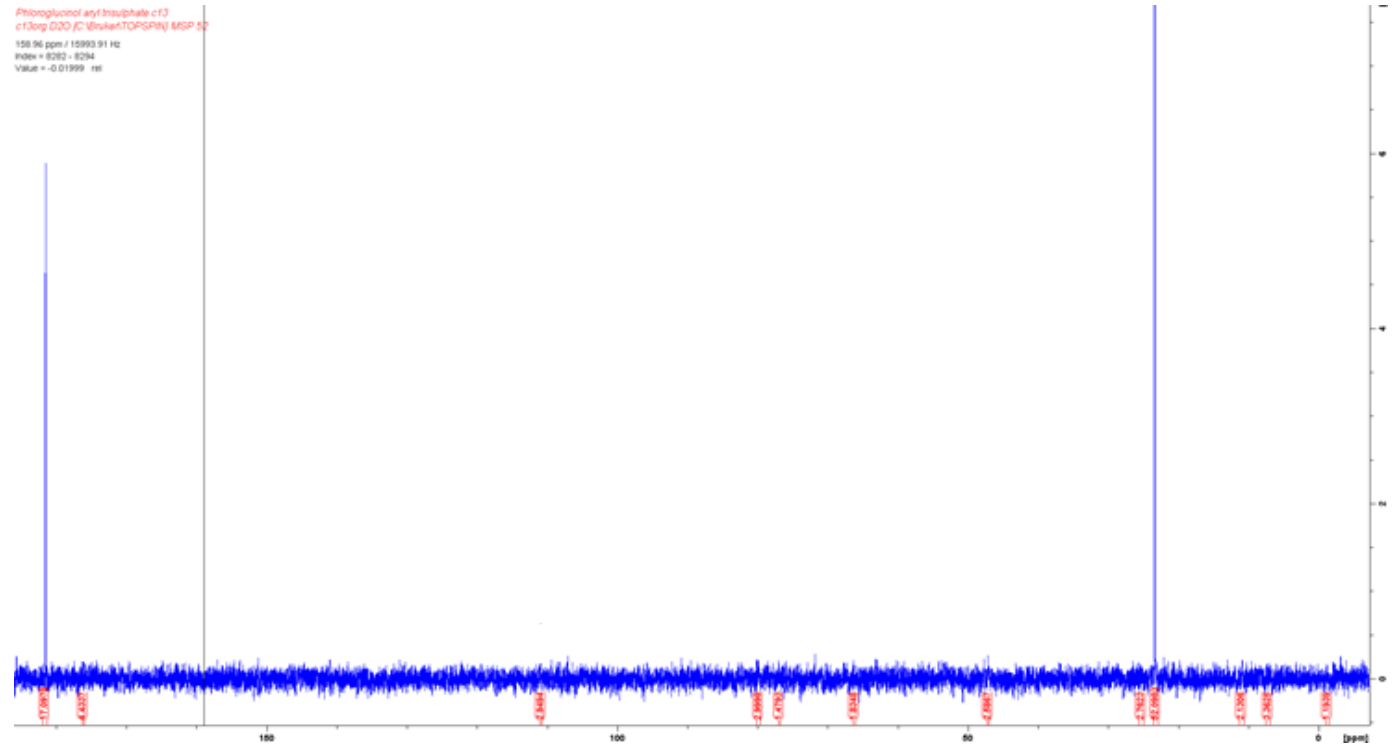
Phloroglucinol aryl trisulphate c13
c13org D2O {C:\Bruker\TOPSPIN} MSP 52
158.96 ppm / 15993.91 Hz
index = 8282 - 8294
Value = -0.01999 rel
150
100
50
0
[ppm]

Figure 38. **^{1}H NMR and ^{13}C NMR of 1,3,5-trihydroxy-2,4,6-benzenetrisulfonic acid potassium salt.**

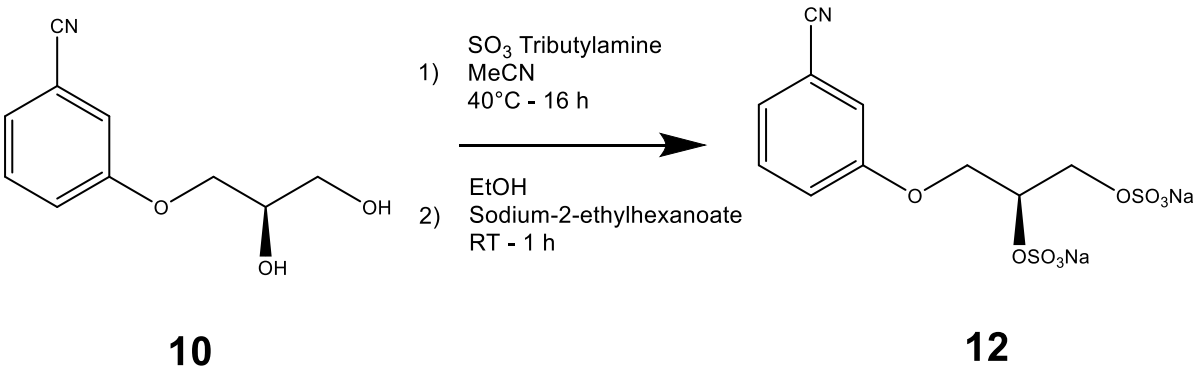

10 **12**

Figure 39. **Synthesis of (*S*)-3-(2,3-bis(sulfooxy)propoxy)benzonitrile using sub-route A - 3.**

Upon further investigation of literature regarding *O*-sulfation of hydroxyl containing alkyl chains, a procedure which negated all major drawbacks was discovered by Gill, Male, & Jones (2019), who devised a synthesis of a novel SO_3-amine complex which, with some preparation allows molecules to be sulfated in a similar way as outlined in Sub-route A-1. This procedure addresses the major issues of product isolation, purification and sulfate-amine salt contamination by facilitating an aqueous workup to be undertaken, followed by preparation of its sodium salt through ion exchange. This gave us the ability to easily isolate our product, while simultaneously removing most of the major impurities in one step, as the tributylamine complex allowed the product to be soluble in organic solvents, and therefore easily extracted. Previously, this had not been possible as the sulfated compounds were highly soluble in water, leading to loss of product in the aqueous layer, which in turn, forced us to utilise much more labour-intensive purification techniques. Our synthesis using this procedure is outlined in Figure **39**, and as mentioned, proceeds directly to the sodium salt without any labour-intensive purifications.

Unfortunately, this sulfating agent is not commercially available as yet and must be prepared though a relatively involved and time-consuming synthesis. This adds time and steps to an otherwise one-step reaction, however the benefits obtained from using this reagent far outweigh any negatives that may arise from the preparation of the reagent.

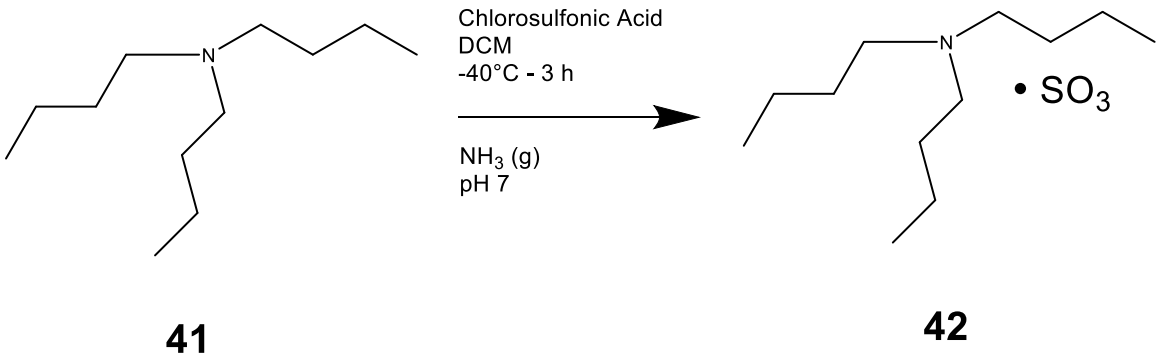

Figure 40. **Synthesis of sulfur trioxide tributylamine complex.**

The SO_3-tributylamine reagent was prepared though the reaction of tributylamine with chlorosulfonic acid at -40 °C in dichloromethane, followed by pH adjustment with gaseous ammonia, isolation and lyophilisation to give the desired sulfating agent which was used directly in future sulfations to great success. The NMR of which can be seen in Figure **41**, and corresponds directly to the NMR spectrum referenced in literature, allowing confirmation of product synthesis.

Following sulfation of the target molecule, the sulfate-tributylammonium salt was subjected to ion exchange using sodium-2-ethylhexanoate in order to prepare the sulfate sodium salt, completing purification of the product in one fast and easy step.

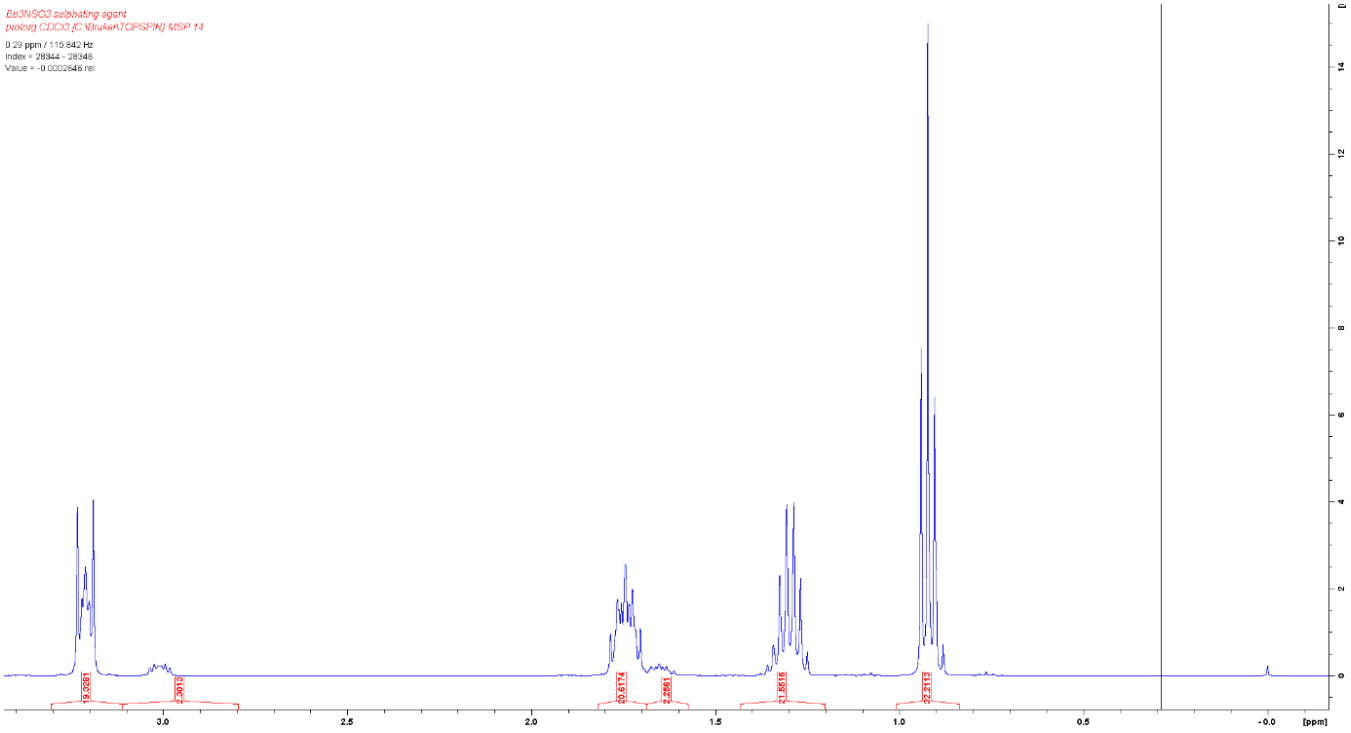

Figure 41. **^{1}H NMR of SO_3 tributylamine complex.**

In general, sulfation of these compounds is relatively facile and discovery of improved reagents and methods have all but negated the drawbacks from earlier methods used in terms of product isolation, handling and purification, allowing us to not only make the preparation easier, but also much faster, increasing the throughput of sulfates.

Purity is seen to be much higher as a result of this sulfation – ion exchange method as there is much less impurity present in the final product, shown in the spectra in Figure **42**, when compared to Figure **34**. which utilised the basic sulfation method using SO_3 trimethylamine complex. However, purification is still necessary.

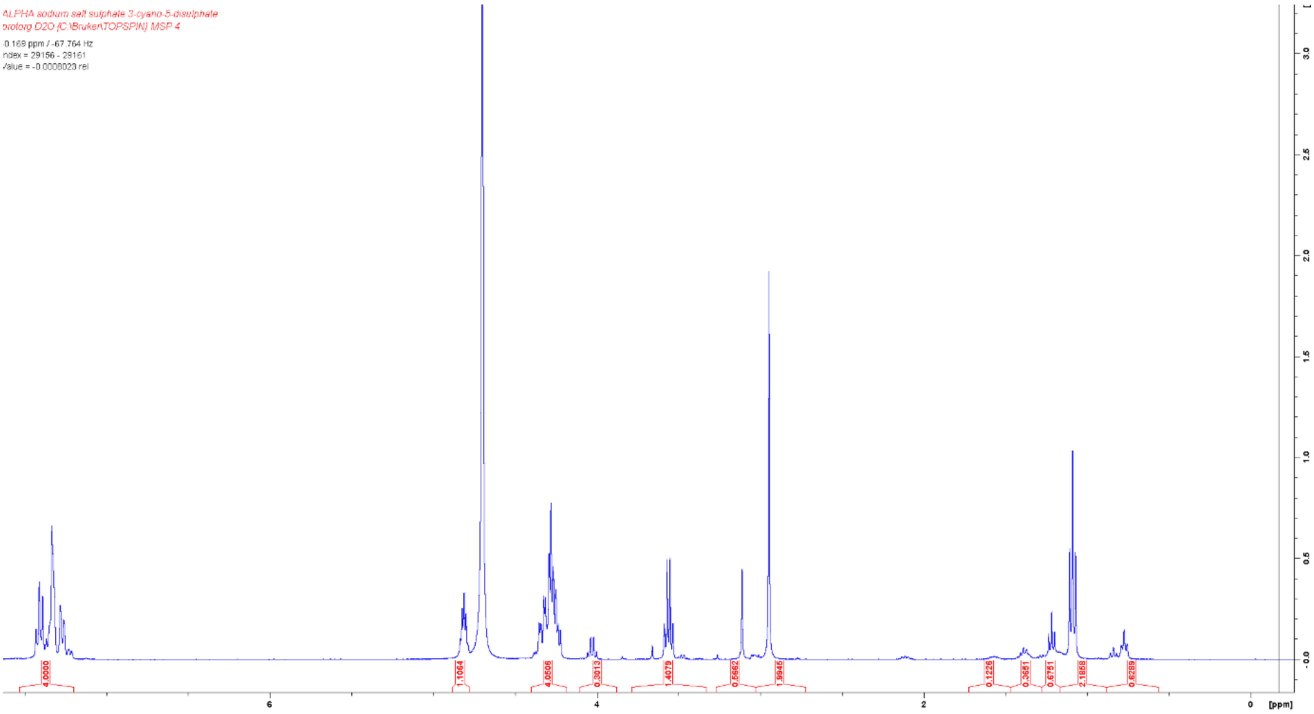
ALPHA sodium salt sulphate 3-cyano-5-disulphate
protorg D2O {C:\Bruker\TOPSPIN} MSP 4
-0.169 ppm / -67.764 Hz
Index = 29156 - 29161
Value = -0.0008023 rel
6
4
2
0
[ppm]

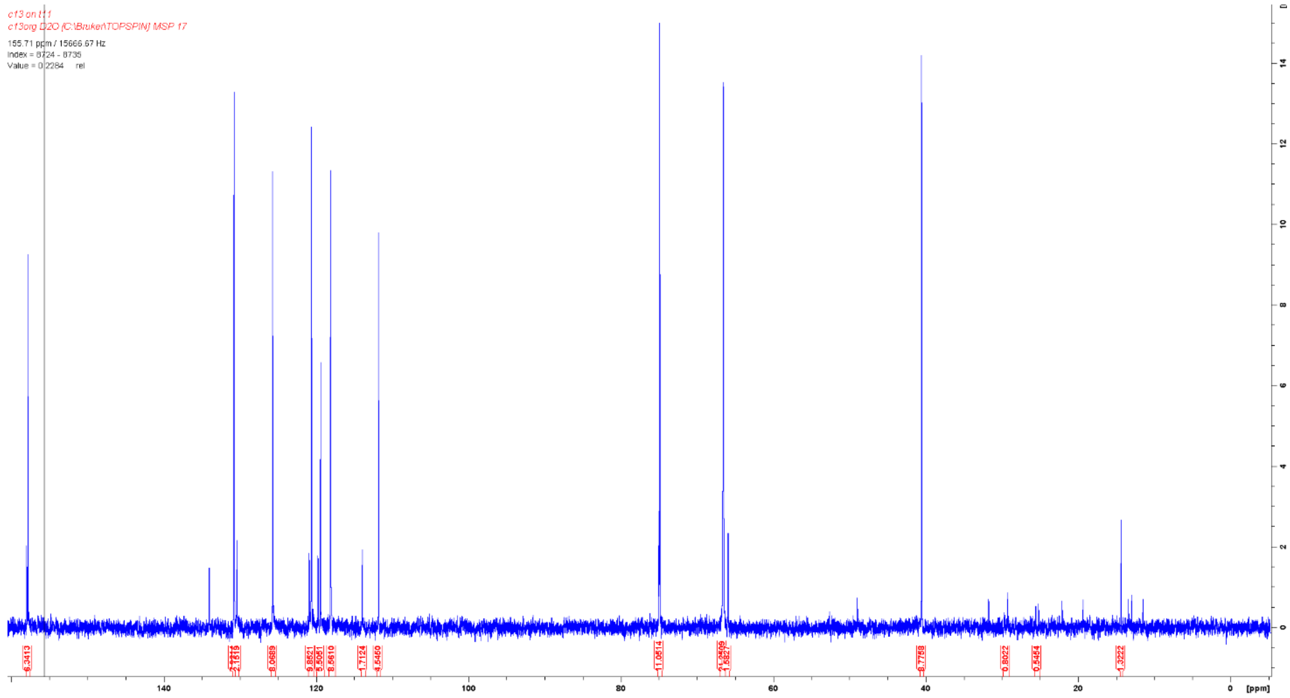
c13 on t11
c13org D2O {C:\Bruker\TOPSPIN} MSP 17
155.71 ppm / 15666.67 Hz
Index = 8724 - 8735
Value = 0.2284 rel
140
120
100
80
60
40
20
0
[ppm]

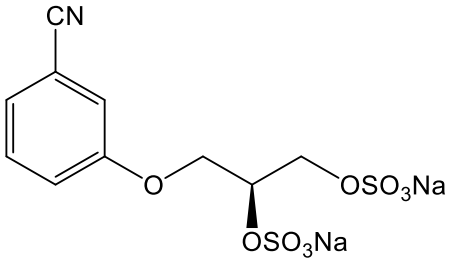

12

Figure 42. **^{1}H NMR, ^{13}C NMR and structure of (*S*)-3-(2,3-bis(sulfooxy)propoxy)benzonitrile sodium salt.**

2.5. Synthesis of substituted diarylmethanes by *ortho* lithiation:

Ortho lithiation was selected for use in preparing more complex, substituted diarylmethane glycomimetic compounds, although this was found to be somewhat limited in scope, due to several difficulties faced in preparing the aryllithium species.

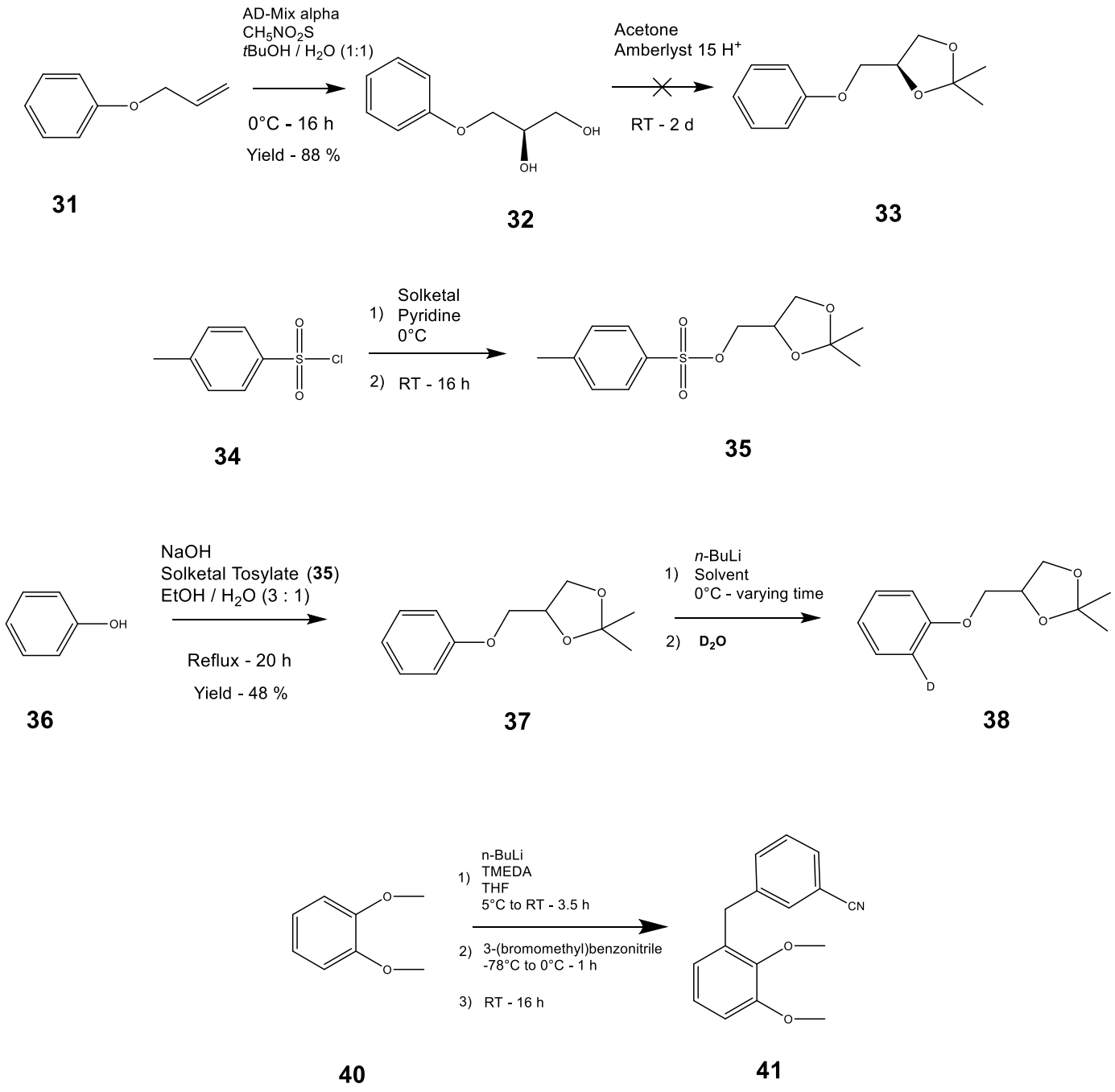

Figure 43. **Overall reaction pathway for *ortho* lithiation.**

Firstly, we selected a simple substrate for determination of optimal conditions required for successful lithiation, compound **33**. Synthesis of this was not, however, without difficulty.

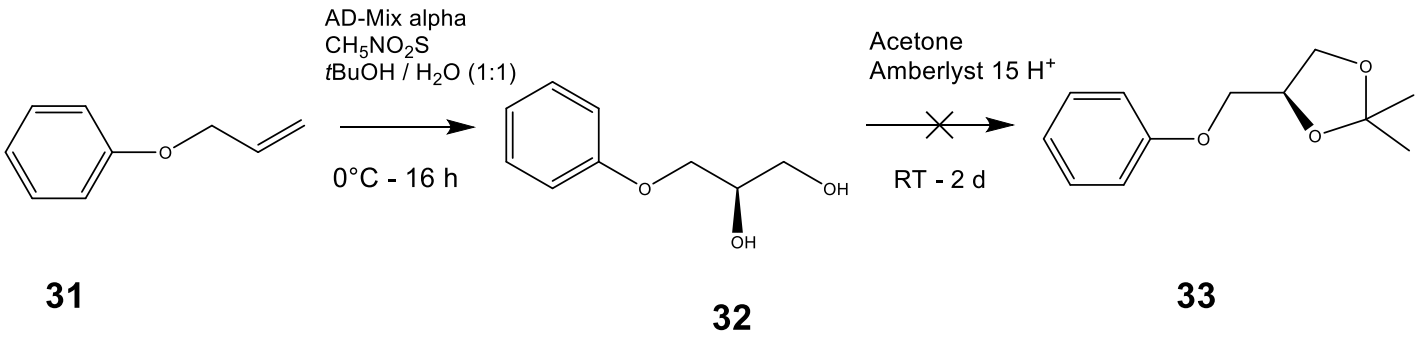

Figure 44. **Failed synthesis of 2,2-dimethyl-4-(phenoxy)methyl-1,3-dioxolane via asymmetric dihydroxylation using synthetic pathway D.**

Initially, we attempted asymmetric dihydroxylation of allyl phenyl ether to form compound **32**, then protection of the 2,3-diol by reaction with acetone catalysed by Amberlyst 15 H^+ resin to give the acetonide. This reaction was unsuccessful as can be seen in Figure **45** at 1.45 ppm, as the two methyl singlets for the acetonide dimethyl are very small and only integrate to around 0.6. This is further confirmed by the small aromatic peaks at 7.05 – 7.4 ppm integrating to 0.1 which suggests that only 10% of compound **32** was converted to product, and therefore this reaction was deemed inviable.

This is likely due to the fact that acetonide groups can both be formed (Yadav et al., 2014) and cleaved (Jumina et al., 2018) under acidic conditions, leading to an equilibrium which only allows a small of acetonide protected product to exist, resulting in very low product yield and therefore, reaction failure.

***Figure 45*. Unsuccessful formation of 2,2-dimethyl-4-(phenoxy)methyl-1,3-dioxolane.**

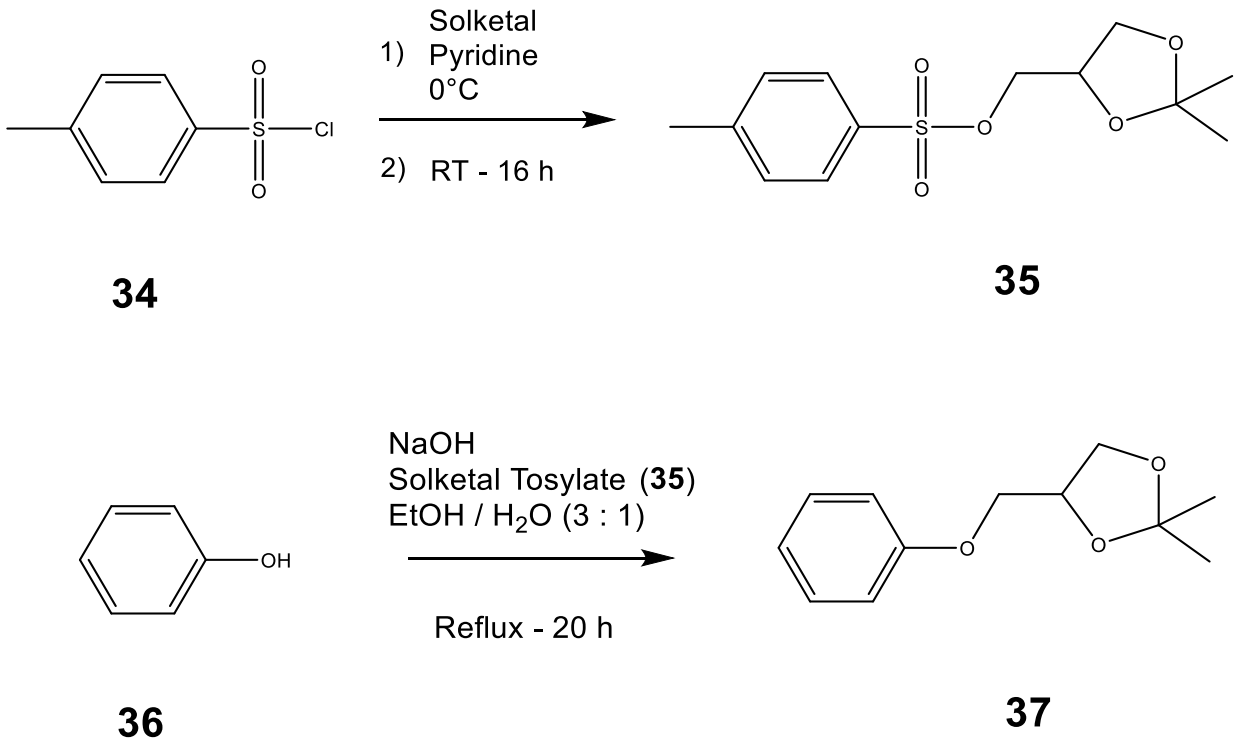

Figure 46. **Synthesis of 2,2-dimethyl-4-(phenoxy)methyl-1,3-dioxolane through 2,2-dimethyl-4-(tosyloxy)methyl-1,3-dioxolane using synthetic pathway D.**

Therefore, this synthesis was approached another way. Successful synthesis of a non-enantiomeric version, compound **37** was attained through use of a tosylate intermediate (compound **35**), prepared through the reaction of *p*-toluenesulfonyl chloride (*p*-TsCl) with solketal as shown in Figure **46**, followed by coupling with phenol to give our desired product. Upon ^{1}H NMR analysis, a portion of the acetonide had shown to have deprotected. This was due to the usage of impure *p*-TsCl containing an amount of *p*-toluenesulfonic acid in the preparation of the tosylate causing catalytic removal of the acetonide during coupling. This was remedied through purification of the *p*-TsCl through Soxhlet extraction in petroleum ether followed by reattempt at coupling with phenol.

This gave the product in good purity and high yield, as shown in Figure **47**. The 2 methyl singlets at 1.4 ppm which integrate to 3 : 3 for a total of 6 indicated the presence of the

acetonide dimethyl. The group of peaks at 3.75 – 4.55 ppm which integrate to a total of 5 are assigned to the propoxy sidechain. Aromatic protons at 6.9 - 7.4 ppm which integrate to 5 show monosubstitution on the aromatic ring. Together, these demonstrate successful synthesis of compound **37.** Spectral data corresponded to that reported by Sugata, Tsubogo, Kino, & Uchiro, (2017)

Data Obtained: ^{1}H NMR (400 MHz, $CDCl_3$) δ = 7.31 (2H, dd, *J* = 9.0, 7.2 Hz), 7.00 (1H, t, *J* = 7.2 Hz), 6.94 (2H, d, *J* = 9.0 Hz), 4.51 (1H, m), 4.19 (1H, dd, *J* = 8.4, 6.6 Hz), 4.08 (1H, dd, *J* = 9.6, 5.4 Hz), 3.96 (1H, dd, *J* = 9.6, 6.0 Hz), 3.93 (1H, dd, *J* = 8.4, 6.0 Hz), 1.50 (3H, s), 1.44 (3H, s)

Data in Literature: ^{1}H NMR (600 MHz, $CDCl_3$) δ = 7.28 (2H, dd, *J* = 9.0, 7.2 Hz), 6.96 (1H, t, *J* = 7.2 Hz), 6.91 (2H, d, *J* = 9.0 Hz), 4.48 (1H, m), 4.17 (1H, dd, *J* = 8.4, 6.6 Hz), 4.07 (1H, dd, *J* = 9.6, 5.4 Hz), 3.94 (1H, dd, *J* = 9.6, 6.0 Hz), 3.91 (1H, dd, *J* = 8.4, 6.0 Hz), 1.47 (3H, s), 1.41 (3H, s)

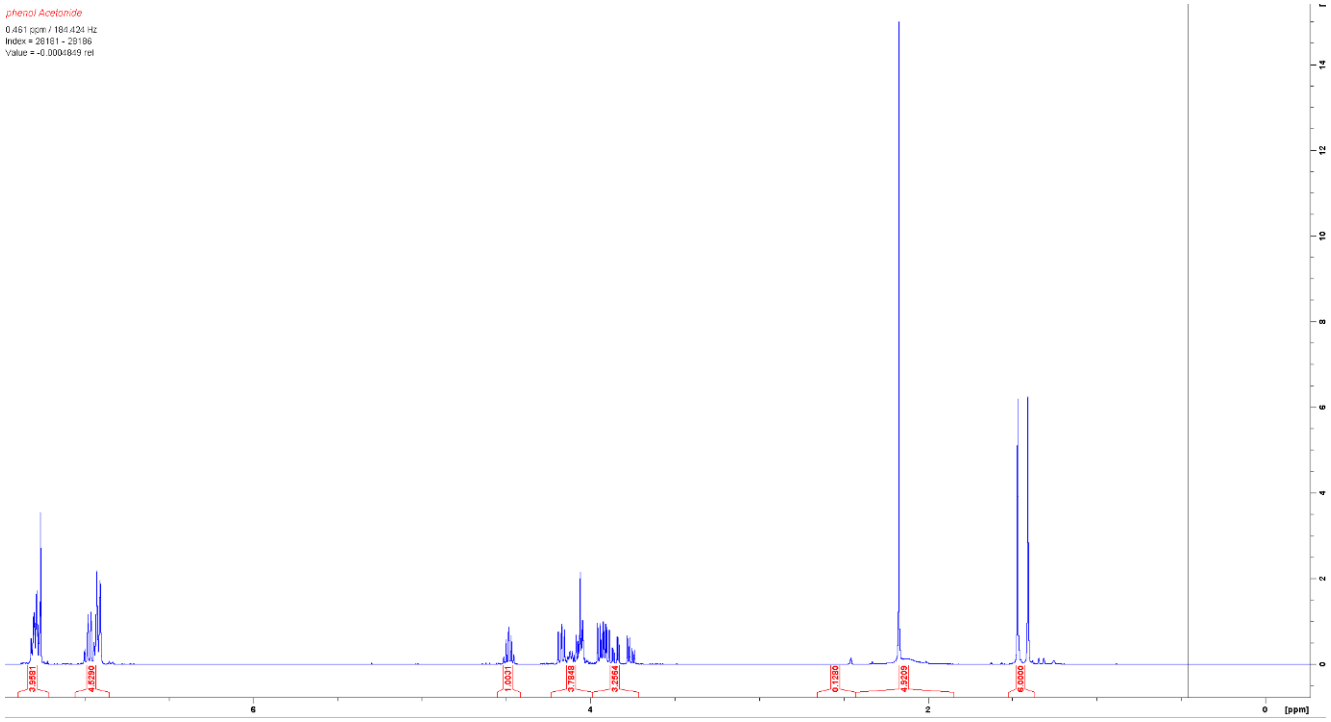

Figure 47. **^{1}H NMR of 2,2-dimethyl-4-(phenoxy)methyl-1,3-dioxolane.**

Conditions for lithiation at the *ortho* position were determined through several small-scale reactions using 2,2-dimethyl-4-(phenoxy)methyl-1,3-dioxolane. In determining these conditions, we trialled different reaction times, temperatures, solvents, additives and concentrations with various effects on yield and side-reactions.

It was found that a relatively large excess of *n*-butyllithium (2.2 - 4 equivalents), TMEDA (equal quantity to *n*-BuLi), a relatively long reaction time (>3 h) and a comparatively high reaction temperature (0 °C) was required to efficiently form the aryllithium, evidence of which was determined by quenching all reactions with D_2O, exchanging lithium with deuterium and indicating how much product had been formed, shown quantitively in the ^{1}H NMR spectrum by removal of one proton from the *ortho* hydrogen peak at 7.27 ppm. The rest of the molecule remained unchanged, which can be seen when comparing Figure **47** to Figure **48**.

Table 3. **Reaction conditions against deuteration percentage.**

Reaction Number	Solvent	Reaction Time and temperature	Equivalents of *n*-butyllithium and additives	Percentage of Deuteration
1	THF	0°C – 2 hours	1.1	9%
2	THF	0°C – 2 hours	2.2	12%
3	THF	0°C – 2 hours	2.2 + TMEDA	34%
4	Ether	0°C – 2 hours	2.2	29%
5	Ether	0°C – 4 hours	2.2	21%
6	Ether	0°C – 3 hours	2.2 + TMEDA	95%

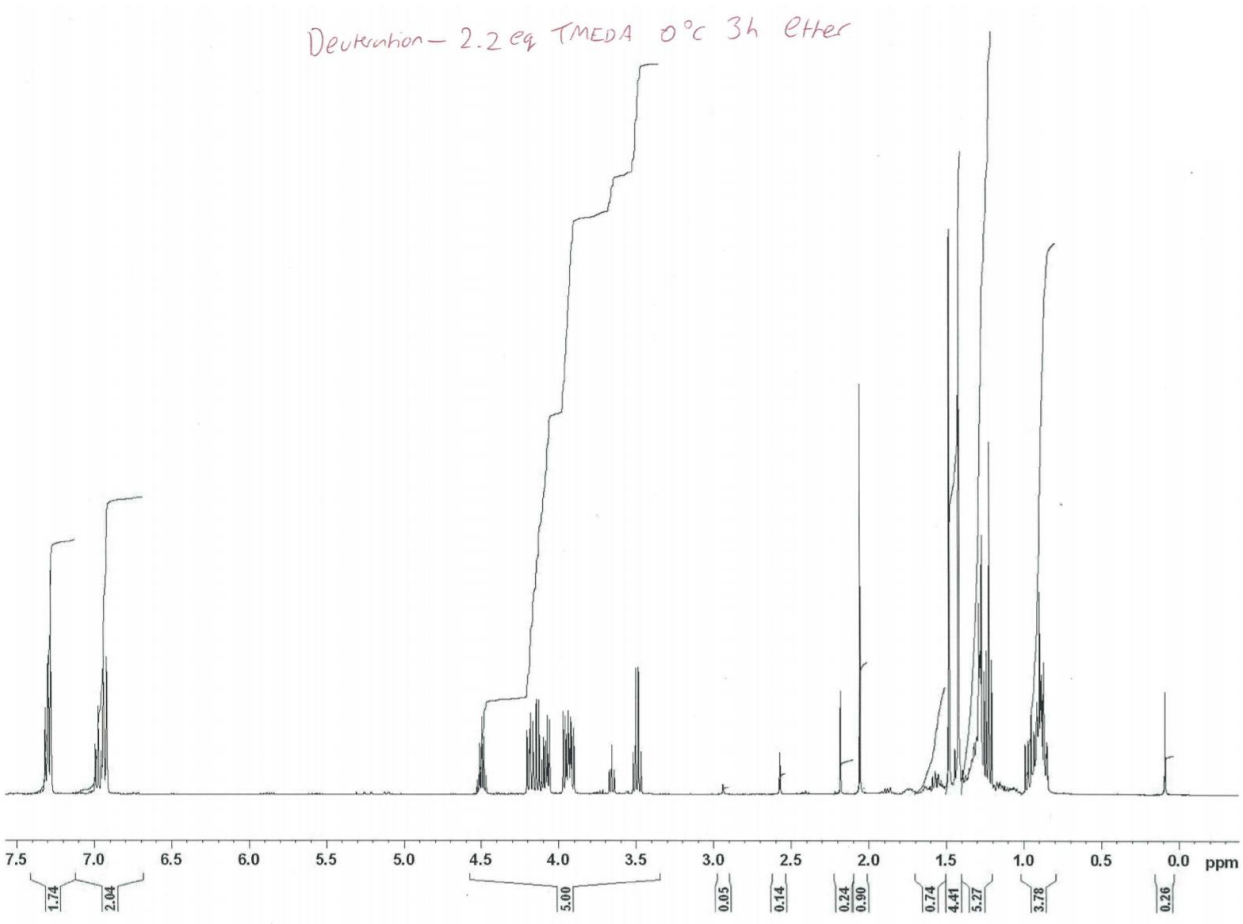

Figure 48. **^{1}H NMR of 2,2-dimethyl-4-(2-deuterophenoxy)methyl-1,3-dioxolane.**

Despite investigation of optimal reaction conditions, these trial reactions suffered from occasional failures. This may have been due to a number of factors, such as: insufficient reaction time, reaction temperature too low, old *n*-BuLi, incompatible reactant and substrate, inclusion of air and water, poor isolation of product on workup and choice of a too unreactive lithiating agent. In future, it may be worth testing other lithiating agents such as *sec* or *tert*-butyllithium as a more aggressive way to form the aryllithium species, in addition to longer reaction times and higher temperatures.

Additionally, the substrate we used in these trials may not be comparable to that used in the synthesis of the diarylmethane. This could potentially affect how the reaction behaves

when introduced to a lithiating agent, therefore the conditions used in these trials are not representative of the reaction used to synthesise the diarylmethane. Future trial reactions utilising a substrate with a likeness closer to that of the reaction should be investigated, therefore giving us a better insight into how the reaction may proceed.

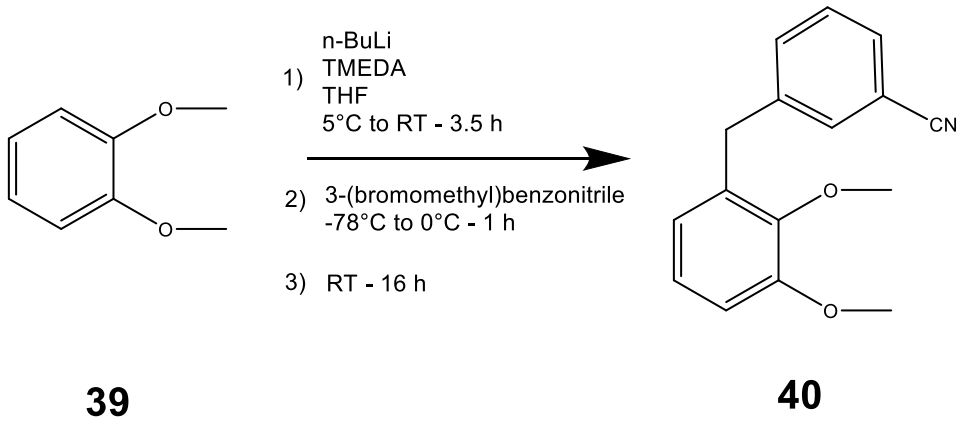

39 **40**

Figure 49. **Synthesis of 3-(2,3-dimethoxyphenylmethyl)benzonitrile using synthetic pathway F.**

Preparation of 3-(2,3-dimethoxyphenylmethyl)benzonitrile **40** was carried out according to methodology by Werle, Fey, Neudörfl, & Schmalz (2007). This reaction used 1.2 equivalents of *n*-butyllithium and 1.4 equivalents of TMEDA. Temperature was varied from 5 °C upon addition of *n*-butyllithium and increased to room temperature for 3.5 hours. Temperature was then decreased to -78 °C upon addition of the electrophile and slowly raised to 0 °C, then room temperature and allowed to stir overnight. This yielded the desired diarylmethane in moderate yield (63%).

Synthesis of compound **40** was confirmed through interpretation of NMR spectra. Presence of the nitrile-substituted ring was indicated by peaks in the ^{1}H NMR spectrum at 7.51 – 7.45 ppm (m, 1H), 7.43 – 7.38 ppm (m, 1H) and 7.36 – 7.33 ppm (m, 2H) ppm for a total of 4 protons, indicating a disubstituted ring. The second aromatic ring's presence was confirmed

by peaks at 7.11 ppm (dd, 1H), 6.92 – 6.89 ppm (m, 1H) and 6.85 ppm (dd, 1H), integrating to a total of 3 protons, indicating a trisubstituted ring.

The peak at 3.87 ppm (s, 2H) is assigned to the 2 protons linking both arenes together. The two peaks at 3.854 ppm (s, 3H) and 3.85 ppm (s, 3H) show the 2 methoxy groups integrating to a total of 6 protons.

This is further reinforced by the ^{13}C spectrum indicating 12 aromatic carbons at 153.99, 148.90, 146.55, 141.96, 133.04, 131.99, 130.13, 129.38, 125.06, 124.80, 111.70 and 111.42 ppm. The peak at 120.93 ppm is assigned to the nitrile and the two peaks at 60.56 and 55.83 ppm correspond to the two methoxy groups. The final peak at 36.77 ppm is the carbon linking the two arenes together.

This allows us to confirm the synthesis of compound **40**. A moderate amount of impurities are present, signified by the large number of small peaks across the spectrum. To rectify this, chromatography would need to be undertaken.

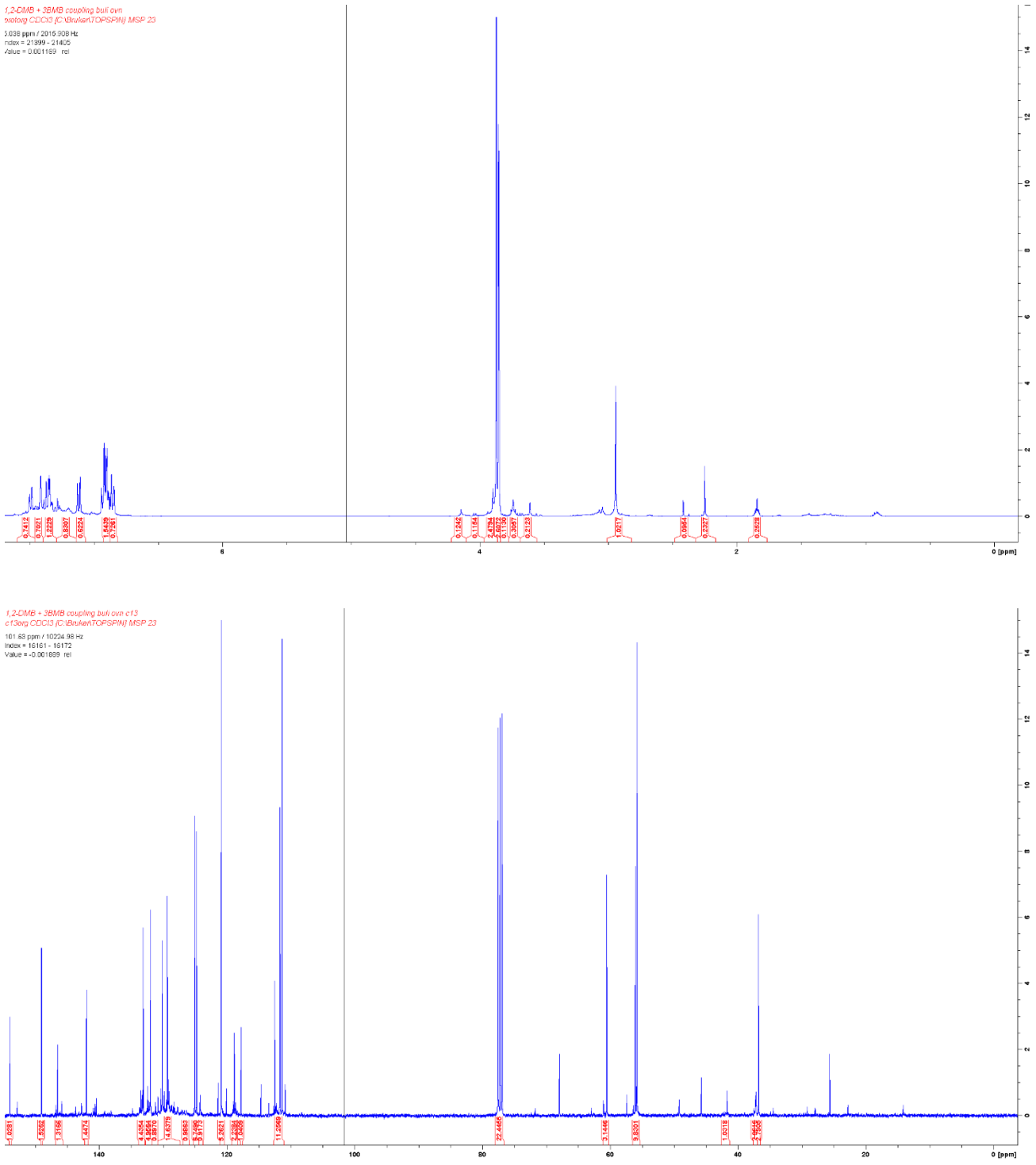

***Figure 50*. ^{1}H NMR and ^{13}C NMR of 3-(2,3-dimethoxyphenylmethyl)benzonitrile.**

Unfortunately, due to time constraints, we were unable to finish this synthetic route.

However, given more time, a series of substituted diarylmethane glycomimetic compounds may be synthesised, and tested for efficacy against the HGF-Met pathway.

2.6. Testing of synthesised compounds in cell viability and wound healing assays:

Testing on DAOY cells was performed by Sonia Morlando at the University of Salford.

1) Scratch wound healing assay:

The Scratch assay was performed by seeding cells at density of 8000 cell/s per well in a 96 well plate. After 24 h, RPMI 10% FBS media was replaced by RPMI 0% FBS and cells were under starvation for a day. Then, cells were pre-treated for 2 h with different concentrations of drug (specifically 1 mM-10 mM-100 mM) in triplicates and a scratch introduced in the well. Following MET activation with HGF 10 ng/ml, cells were incubated for 21 h in the BioTek Cytation 3 and pictures were taken every 30 minutes to evaluate wound closure.

Conditions that the cells were monitored under are as follows:

+HGF, -HGF, Crizotinib 1 µM, Drug 1 µM, Drug 10 µM, Drug 100 µM.

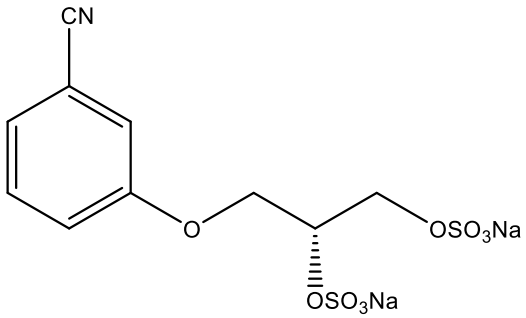

12

JW008

***Figure 51. Structure of* (*R*)-3-(2,3-bis(sulfooxy)propoxy)benzonitrile sodium salt.**

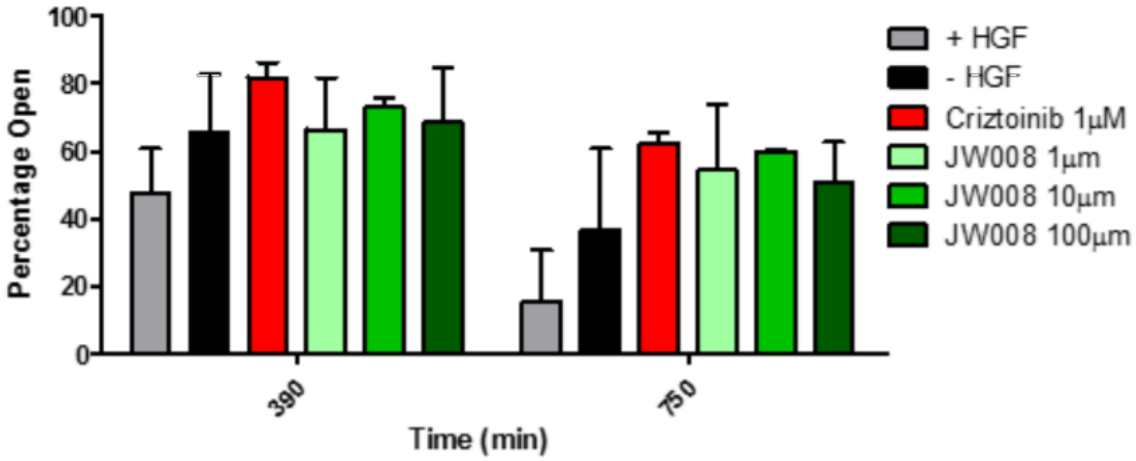

***Figure 52.* Graph showing the effects of HGF, crizotinib and (*R*)-3-(2,3-bis(sulfooxy)propoxy)benzonitrile sodium salt against wound size percent at 6- and 12-hour intervals.**

At the both 6- and 12-hour marks, the HGF stimulated cells are showing rapid closure of the wound, as expected. Crizotinib is used as a benchmark, as it is an effective and proven kinase inhibitor, shown at both the 6- and 12-hour marks as being the best at inhibiting cell mobility.

The drug shows relatively good activity at 1 µM concentration, improving slightly at 10 µM and falling slightly at the highest concentration of 100 µM. By the 12-hour mark, both HGF stimulated and unstimulated have closed the wound considerably, whereas drug treated cells are all showing the wound being mostly open. This suggests that this drug may have some activity and is worth further investigation.

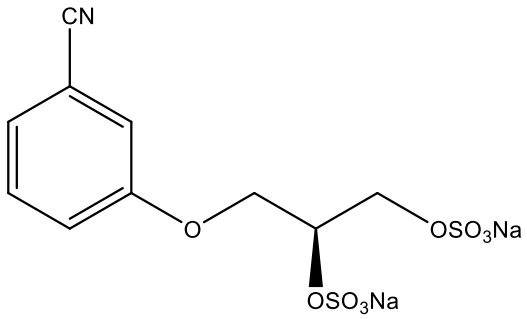

13

JW001

***Figure 53. Structure of* (*S*)-3-(2,3-bis(sulfooxy)propoxy)benzonitrile sodium salt.**

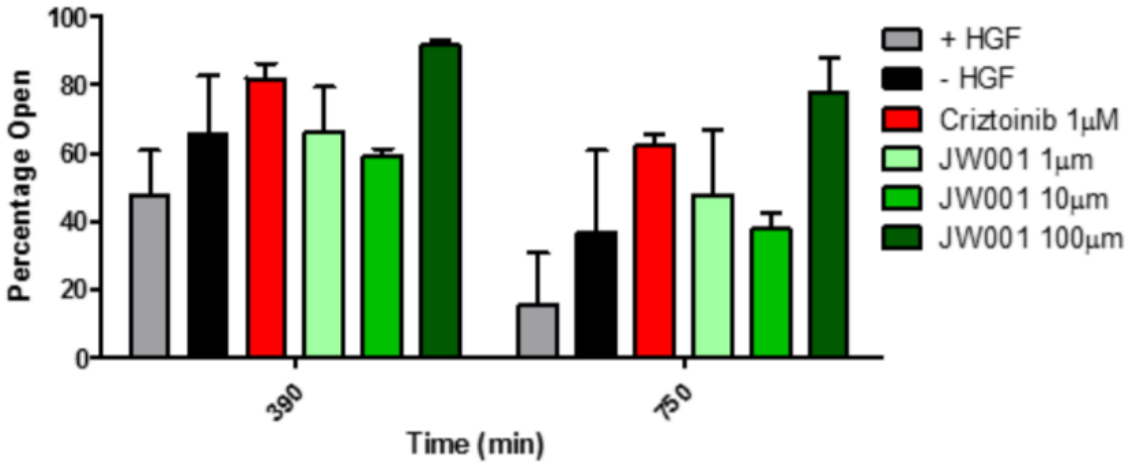

***Figure 54.* Graph showing the effects of HGF, crizotinib and (*S*)-3-(2,3-bis(sulfooxy)propoxy)benzonitrile sodium salt against wound size percent at 6- and 12-hour intervals.**

In the (*S*)-enantiomer, HGF stimulated, unstimulated and crizotinib treated cells have near identical results to the (*R*)-enantiomer, as expected. However, the (*S*)-enantiomer, has a much lesser effect at 1 and 10 µM concentrations, with a much higher effect at 100 µM keeping the wound near fully open, improving on that of crizotinib. This compound shows very good activity at high concentration, and with optimisation could potentially be improved to show efficacy at lower concentrations and should be further investigated.

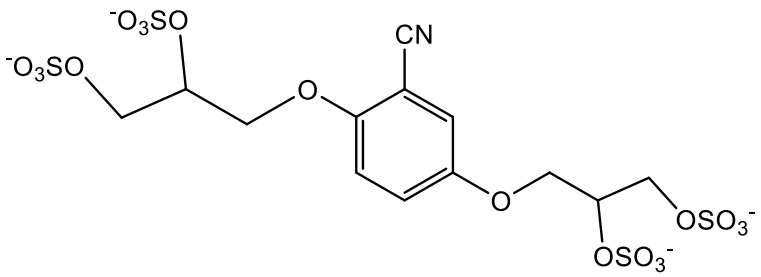

8

Figure 55. **Structure of 2,5-bis-(2,3-bis(sulfooxy)propoxy)benzonitrile.**

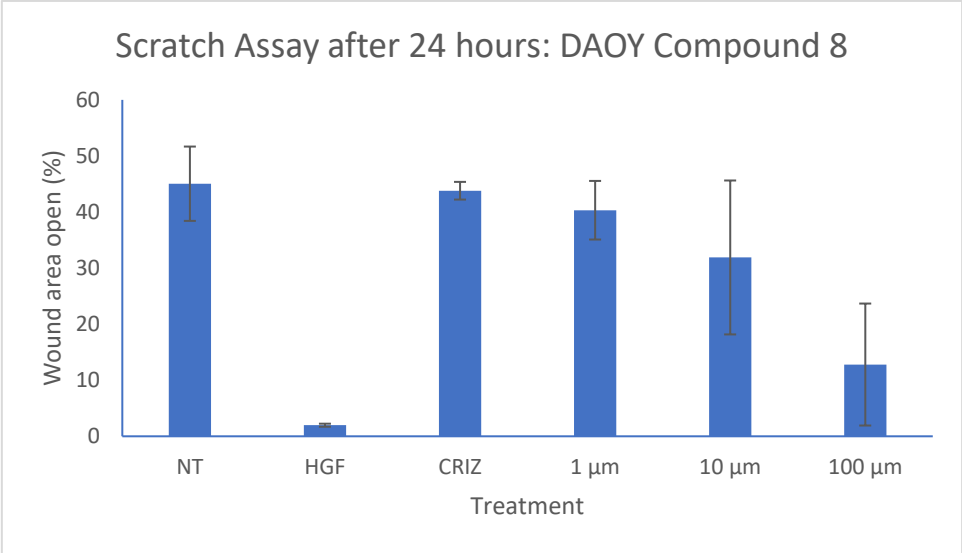

Figure 56. **Graph showing the effects of HGF, crizotinib and 2,5-bis-(2,3-bis(sulfooxy)propoxy)benzonitrile against wound size percent after 24 hours.**

Following a 24-hour period, HGF stimulated cells have closed the wound 98% of the way. Cells treated with 2,5-bis-(2,3-bis(sulfooxy)propoxy)benzonitrile **8** show slightly accelerated wound closure at 1 µM, increasing at both 10 and 100 µM, signified by faster wound closure than the untreated cells. It is however, decelerated compared to the HGF stimulated cells. Stimulation of cell motility is sometimes seen in these compounds, which may allow them to be used as a "dual purpose" drug, with some compounds showing inhibition of motility and some showing promotion, potentially allowing usage in both cancer and wound healing applications.

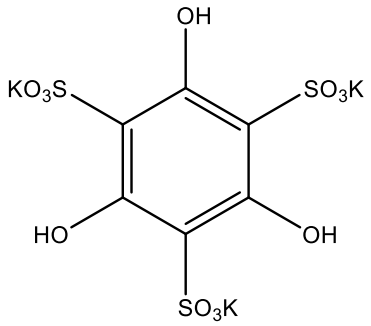

26

Figure 57. **Structure of 1,3,5-trihydroxy-2,4,6-benzenetrisulfonic acid potassium salt.**

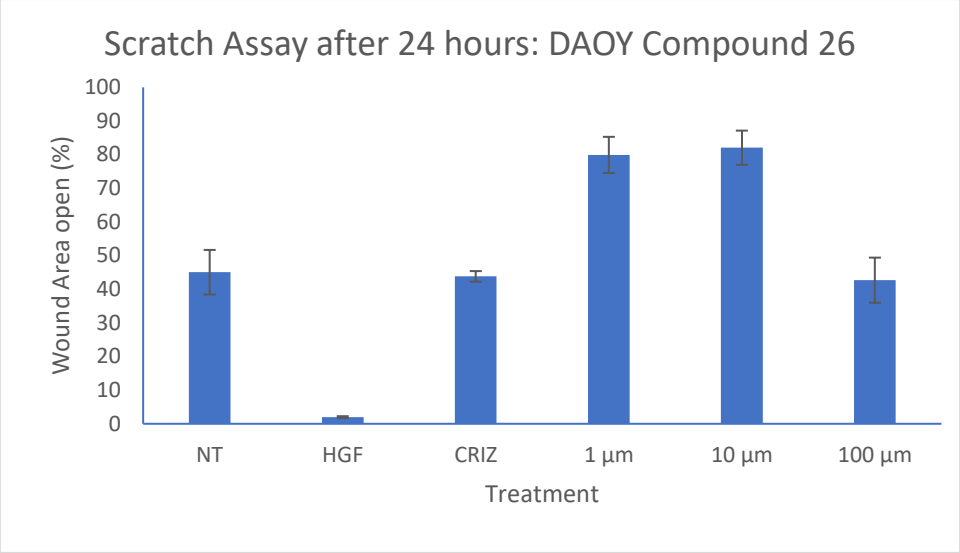

Figure 58. **Graph showing the effects of HGF, crizotinib and 1,3,5-trihydroxy-2,4,6-benzenetrisulfonic acid potassium salt against wound size percent after 24 hours.**

1,3,5-Trihydroxy-2,4,6-benzenetrisulfonic acid potassium salt **26**, however showed extremely strong activity at only 1 µM, slightly improving at 10 µM, with the efficacy falling to that of Crizotinib at 100 µM. Efficacy at 1 and 10 µM is around twice that of crizotinib. This compound has shown the best inhibition of cell motility tested so far and should be thoroughly investigated as a potential lead.

Testing on DAOY cells was performed by Sonia Morlando at the University of Salford.

2) MTT Cell Viability Assay:

In this assay, the toxicity of the drug against the cells is investigated in order to determine whether the drug is cytotoxic, which in our case would be undesirable, as these compounds are designed to have no cytotoxic activity.

For the short-term proliferation assay, cells were seeded in a 96 well plate at density of 2000 cells/well for DAOY, ONS76 and MB03. After 24 h of incubation at 37° with 5% CO2 cells were treated with scalar concentration (fold dilution 1:10) of drugs starting at 100 mM

(GAGs mimics) and 10 mM (Tivantinib). MTT assay was performed after 72 h of treatment adding 50 mL of thiazolyl blue tetrazolium bromide 3 mg/ml (Alfa Aesar) in each well. Following 3 h of incubation, MTT solution was dissolved in DMSO and the optical density was measured at 540 nM by using a microplate reader (FLUOstar Omega). All the results were normalized to controls and analysed using GraphPad Prism 5 software. In order to evaluate how DAOY and MB03 cells respond to tivantinib long treatment (9 days) we seeded cells at density of 200 per well in a 96 well plate. After 24 h of incubation, we treated cells three times within intervals of three days. Tivantinib treatment was performed in quadruplicates with drug at eight different concentration with dilution 1:10 starting at 10 µM. After 9 days, cells were stained with 0.5% Crystal Violet to assess cell viability. Plate was washed with normal water and stain was dissolved by adding 100 µL of methanol. Absorbance was measured at 540 nM and analysis was performed with GraphPad Prism 5 software.

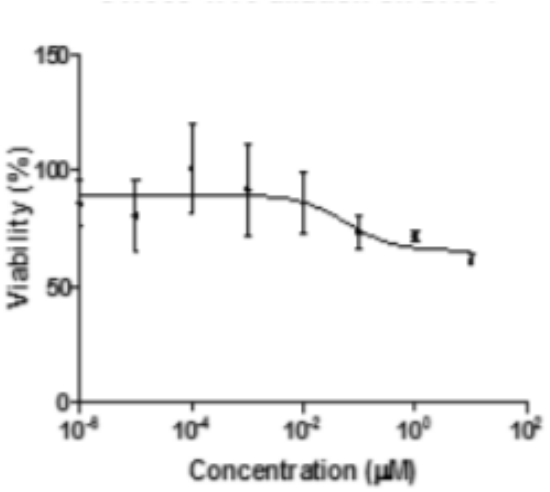

Cell viability stayed at its highest level until reaching a concentration of 10^{-2} µM, suggesting that this compound is not extremely cytotoxic, as it only starts to have effects on cells at high concentration of drug.

Figure 59. **Graph showing the effect of (*R*)-3-(2,3-bis(sulfooxy)propoxy)benzonitrile sodium salt on DAOY cell viability at varying concentrations.**

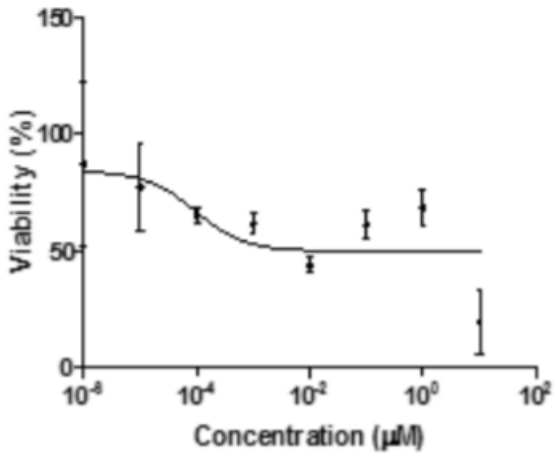

Here, cell viability decreased at only a concentration of 10^{-6} µM, therefore this compound is more cytotoxic than its enantiomer, possibly due to impurities having a cytotoxic effect, as its similar structure should not cause such a large discrepancy in cell toxicity.

Figure 60. **Graph showing the effect of (*S*)-3-(2,3-bis(sulfooxy)propoxy)benzonitrile sodium salt on DAOY cell viability at varying concentrations.**

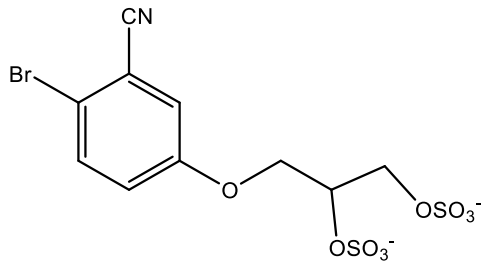
CN
Br
O
OSO_3^-
OSO_3^-

6

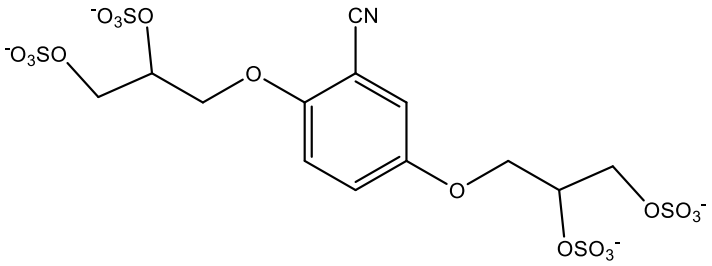
^-O_3SO
^-O_3SO
CN
O
O
OSO_3^-
OSO_3^-

8

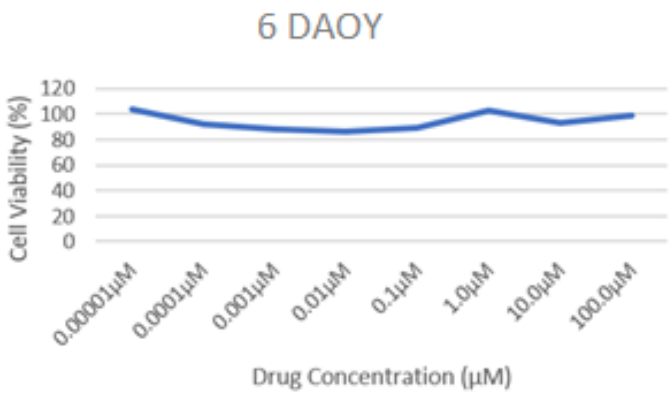
6 DAOY
Cell Viability (%)
120
100
80
60
40
20
0
0.00001µM
0.0001µM
0.001µM
0.01µM
0.1µM
1.0µM
10.0µM
100.0µM
Drug Concentration (µM)

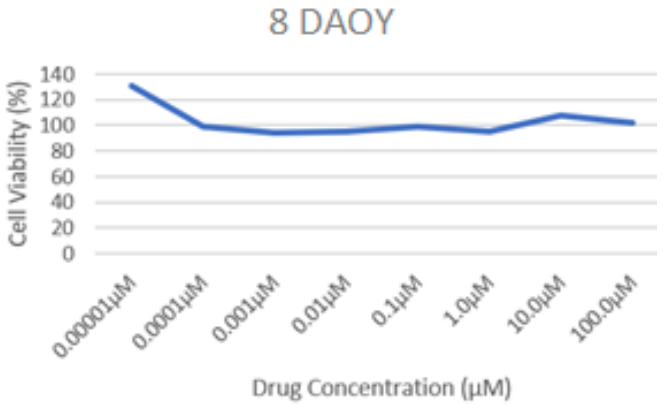
8 DAOY
Cell Viability (%)
140
120
100
80
60
40
20
0
0.00001µM
0.0001µM
0.001µM
0.01µM
0.1µM
1.0µM
10.0µM
100.0µM
Drug Concentration (µM)

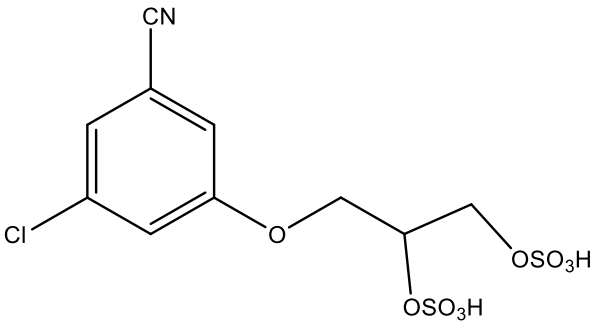
CN
Cl
O
OSO_3H
OSO_3H

17

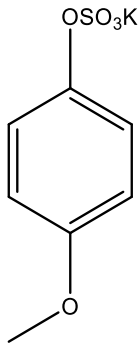
OSO_3K
O

24

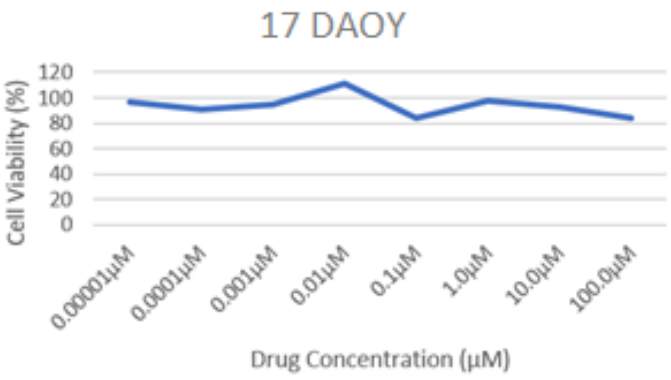
17 DAOY
Cell Viability (%)
120
100
80
60
40
20
0
0.00001µM
0.0001µM
0.001µM
0.01µM
0.1µM
1.0µM
10.0µM
100.0µM
Drug Concentration (µM)

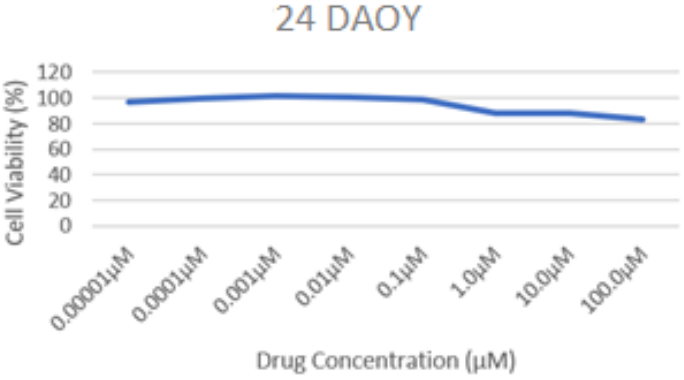
24 DAOY
Cell Viability (%)
120
100
80
60
40
20
0
0.00001µM
0.0001µM
0.001µM
0.01µM
0.1µM
1.0µM
10.0µM
100.0µM
Drug Concentration (µM)

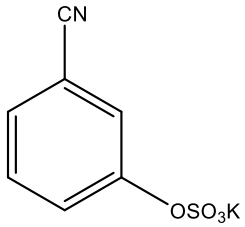

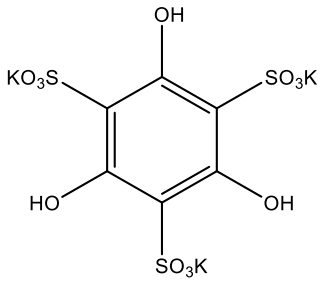

25 **26**

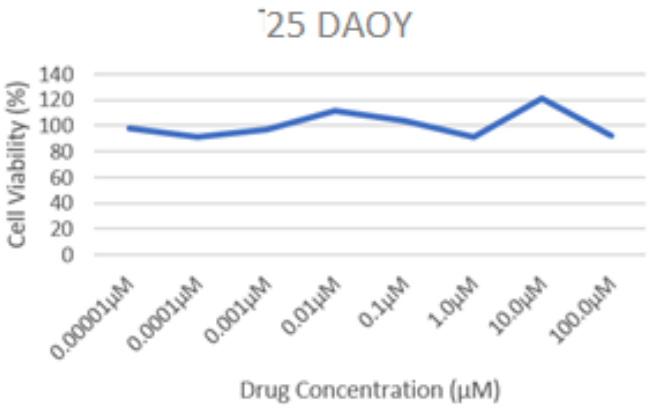

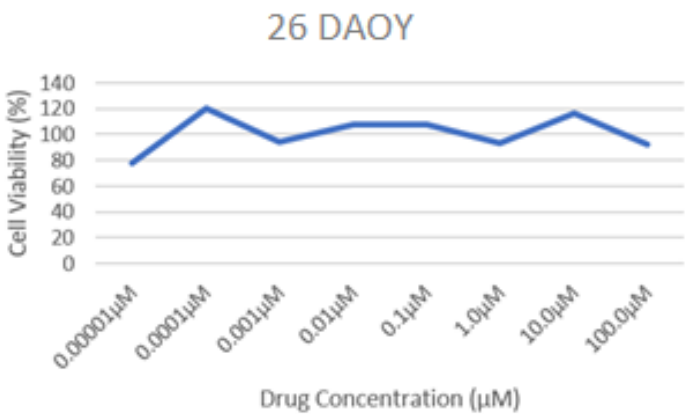

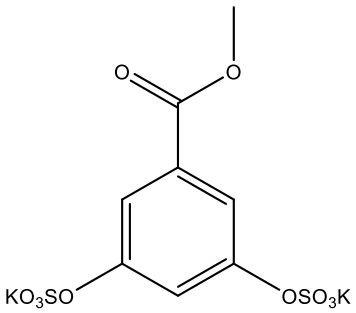

27

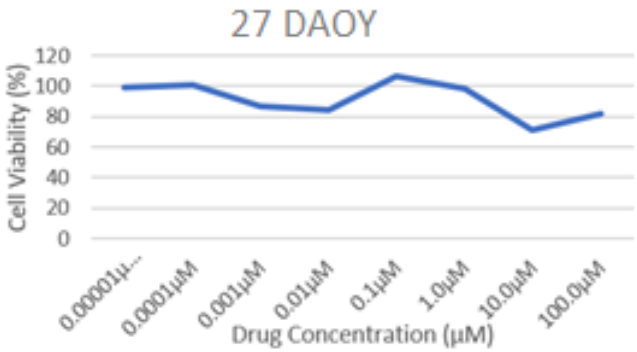

Figure 61. **Graphs showing the structures and effects of compounds 6, 8, 17, 24 25, 26 and 27 on DAOY cell viability at varying concentrations.**

As shown in the group of graphs in Figure **61**, as compounds **6**, **8**, **17**, **24, 25**, **26** and **27** all have a negligible effect on cell viability at all concentrations, as expected due to the compounds synthesised having little to no cytotoxic activity.

3. Experimental:

3.1. General Experimental:

Unless otherwise stated, all materials were obtained from Sigma Aldrich, Fluorochem, Alfa Aesar or Fischer Scientific and used as-is without further purification.

Analytical TLC was performed using Fischer Scientific aluminium backed silica gel 60 Å F_{254} sheets (0.25 mm thickness) and analysed using a 254 nm UV lamp.

Purifications were carried out by Flash Column Chromatography using Fischer Scientific silica gel 60 Å (200-400 mesh) and commercial laboratory-grade solvents obtained from Fischer Scientific.

All ^{1}H and ^{13}C NMR spectroscopy was performed by myself at Salford University on a Bruker Ultrashield 400 MHz spectrometer at ambient temperature and edited using Bruker Topspin software.

Testing of compounds on cells was performed by Sonia Morlando at Salford University on DAOY cell lines.

Mass Spectrometry was performed by Lee Harman at Manchester Metropolitan University on an Agilent 6540 LC-Q-ToF spectrometer at ambient temperature.

All NMR solvents were purchased from Cambridge Isotope Laboratories and used as-is.

FTIR spectra were recorded at Salford University by myself as a thin film using a Varian FTIR spectrometer at ambient temperature and edited using Thermo Fisher OMNIC software.

Anhydrous solvents were obtained from Sigma Aldrich in individual 100 mL SureSeal ™ bottles and backfilled with argon following each use. Dry reaction conditions were achieved by oven drying glassware at 200 °C and working under a dry argon atmosphere.

3.2. Materials and Methods:

3.2.1. Synthesis of 2-bromo-5-hydroxybenzonitrile:

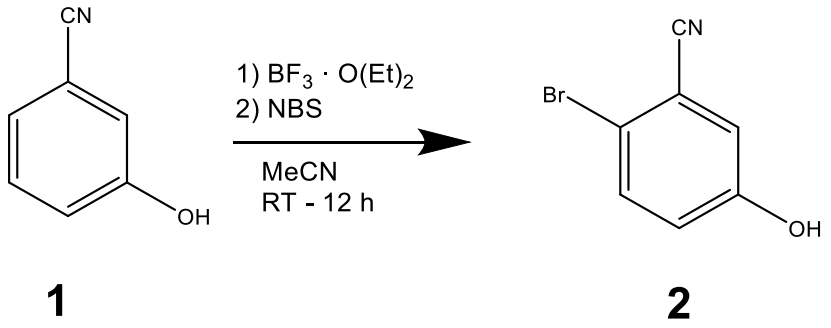

1 **2**

3-Cyanophenol (1.5 g, 12.6 mmol) was dissolved in acetonitrile (15 mL). Boron trifluoride diethyl etherate (1.55 mL, 12.6 mmol) was added dropwise, followed by *n*-bromosuccinimide (2.24 g, 12.6 mmol) and allowed to stir for 12 h at room temperature. The reaction was then quenched through the addition of saturated aqueous ammonium chloride (5 mL) and the mixture extracted with ethyl acetate (2 x 25 mL). The combined organic extracts were washed with water (2 x 25 mL), brine (15 mL), dried over magnesium sulfate and concentrated *in vacuo* to afford an off-white powder which was subjected to column chromatography (3 : 1 ethyl acetate : hexanes) to give 2-bromo-5-hydroxybenzonitrile as a white powder (2.3 g, 91.8%).

Spectral data corresponded to that found in literature (Oberhauser, 1997).

3.2.2. Synthesis of 2-bromo-5-allyloxybenzonitrile:

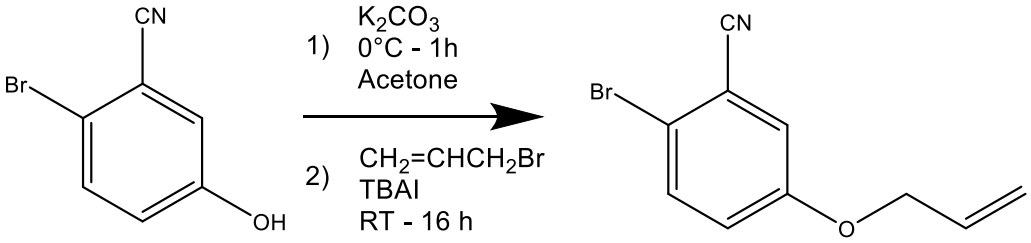

2 **9**

2-Bromo-5-hydroxybenzonitrile (0.5 g, 2.52 mmol) was dissolved in anhydrous acetone (20 mL) and added to a flask containing potassium carbonate (700 mg, 5 mmol) in anhydrous acetone (2 mL) at 0°C. Following 1 h stirring at 0°C, allyl bromide (0.3 mL, 3.7 mmol) and tetrabutylammonium iodide (185 mg, 0.5 mmol) were added and the reaction allowed to stir for 16 h at room temperature. Acetone was then evaporated *in vacuo* and the mixture diluted with ethyl acetate (20 mL), the organics washed with water (3 x 20 mL), brine (20 mL), dried over magnesium sulfate and concentrated *in vacuo* to afford 2-bromo-5-allyloxybenzonitrile as a yellow oil (0.498 g, 83%).

^{1}H NMR ($CDCl_3$, 400 MHz): δ 7.54 (d, *J* = 8.96 Hz, 1H), 7.16 (d, *J* = 3.00 Hz, 1H), 7.03 (dd, *J* = 8.96, 3.00 Hz, 1H), 6.02 (m, 1H), 5.42, (dd, *J* = 17.27, 1.37 Hz, 1H) 5.34, (dd, *J* = 10.53, 1.37 Hz, 1H) 4.55 (dt, 5.24, 1.43 Hz, 2H).

^{13}C NMR ($CDCl_3$, 400 MHz): δ 157.63, 134.00, 131.84, 121.52, 119.78, 118.69, 118.46, 117.28, 116.18, 69.41.

High-resolution mass spectroscopy (ESI+): (M+H)+: calculated for $C_{10}H_8BrNO$, 237.9868; found 237.9862.

IR: 2233, 1672, 1240, 582, cm-1.

3.2.3. Synthesis of 2-bromo-5-[(2,2-dimethyl-1,3-dioxolan-4-yl)methoxy]benzonitrile:

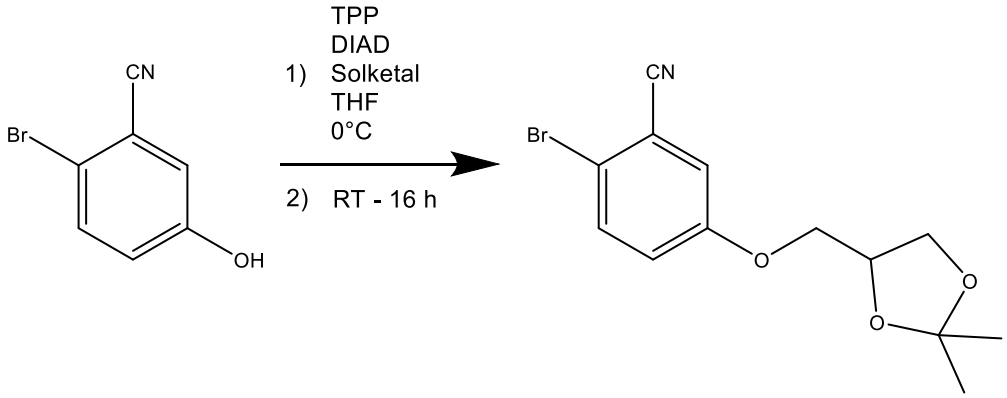

2 **3**

Under argon at 0°C, diisopropyl azodicarboxylate (0.63 mL, 3.24 mmol) was added dropwise to a solution 2-bromo-5-hydroxybenzonitrile (367.3 mg, 1.845 mmol), solketal (0.405 mL, 2.24 mmol) and triphenylphosphine (849 mg, 3.24 mmol) in dry tetrahydrofuran (3.5 mL), and the reaction allowed to stir for 16 h at room temperature. Solvents were then removed *in vacuo* to give a dark yellow oil that was subjected to column chromatography (3 : 1 petroleum ether 40-60 : ethyl acetate) to give 2-bromo-5-[(2,2-dimethyl-1,3-dioxolan-4-yl)methoxy]benzonitrile as a yellow oil (250 mg, 43.5%).

^{1}H NMR ($CDCl_3$, 400 MHz): δ 7.48 (d, *J* = 8.96 Hz, 1H), 7.11 (d, *J* = 3.01 Hz, 1H), 6.97 (dd, *J* = 8.96, 3.01 Hz, 1H), 4.36 - 4.40 (m, 1H), 4.10, (dd, *J* = 8.57, 6.50 Hz, 1H) 3.86 – 4.00, (m, 2H) 3.81 (dd, 8.57, 5.73 Hz, 1H), 1.38 (s, 3H), 1.33 (s, 3H).

^{13}C NMR ($CDCl_3$, 400 MHz): δ 157.68, 134.05, 121.31, 119.60, 116.96, 116.25, 116.15, 110.10, 73.66, 69.42, 66.41, 26.75, 25.26.

High-resolution mass spectroscopy (ESI+): (M+H)+: calculated for $C_{13}H_{14}BrNO_3$, 312.0235; found 312.0233.

IR: 2242, 1277, 1142, 11335, 585 cm-1.

3.2.4. Synthesis of 2-bromo-5-(2,3-dihydroxypropoxy)benzonitrile:

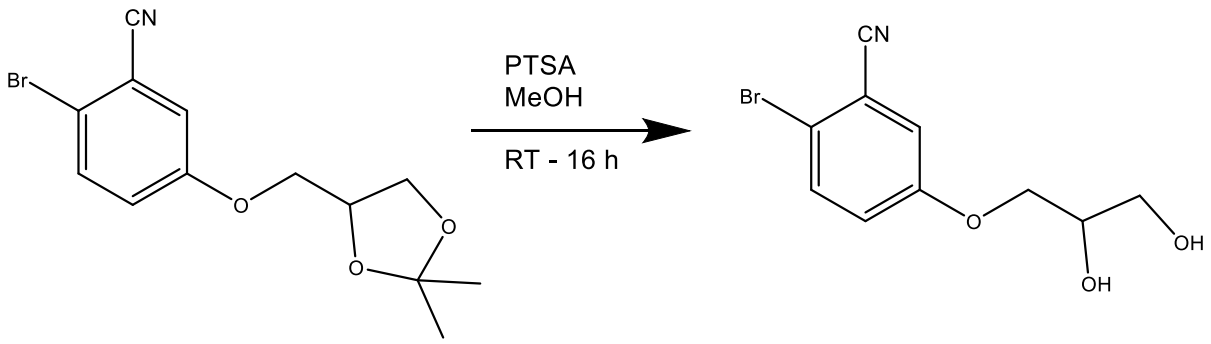

3 **4**

p-Toluenesulfonic acid (4 mg, 0.02 mmol) was added to a solution of 2-bromo-5-[(2,2-dimethyl-1,3-dioxolan-4-yl)methoxy]benzonitrile (60 mg, 0.2 mmol) in methanol (1 mL) and allowed to stir for 16 h. The solution was then diluted with dichloromethane (20 mL), washed with saturated aqueous sodium bicarbonate solution (15 mL), water (3 x 10 mL), brine (10 mL), dried over magnesium sulfate and concentrated *in vacuo* to afford 2-bromo-5-(2,3-dihydroxypropoxy)benzonitrile as a thick yellow oil (27 mg, 49.6%).

^{1}H NMR ($CDCl_3$, 400 MHz): δ 7.58 (d, *J* = 8.96 Hz, 1H), 7.21 (d, *J* = 3.00 Hz, 1H), 7.05 (dd, *J* = , 8.96, 3.00 Hz, 1H), 4.12 – 4.2 (m, 1H), 4.08 (d, *J* = 0.83 Hz, 1H), 3.73 – 3.93 (m, 2H), 2.54 (d, *J* = 4.64 Hz, 1H).

^{13}C NMR ($CDCl_3$, 400 MHz): δ 157.56, 134.21, 121.16, 119.79, 116.97, 116.34, 116.03, 70.06, 69.85, 63.45.

High-resolution mass spectroscopy (ESI+): (M+H)+: calculated for $C_{10}H_{10}BrNO_3$, 271.9922; found 271.9919.

IR: 3419, 2932, 2234, 1242, 586 cm-1.

3.2.5. Synthesis of 2,5-bis-[(2,2-dimethyl-1,3-dioxolan-4-yl)methoxy]benzonitrile:

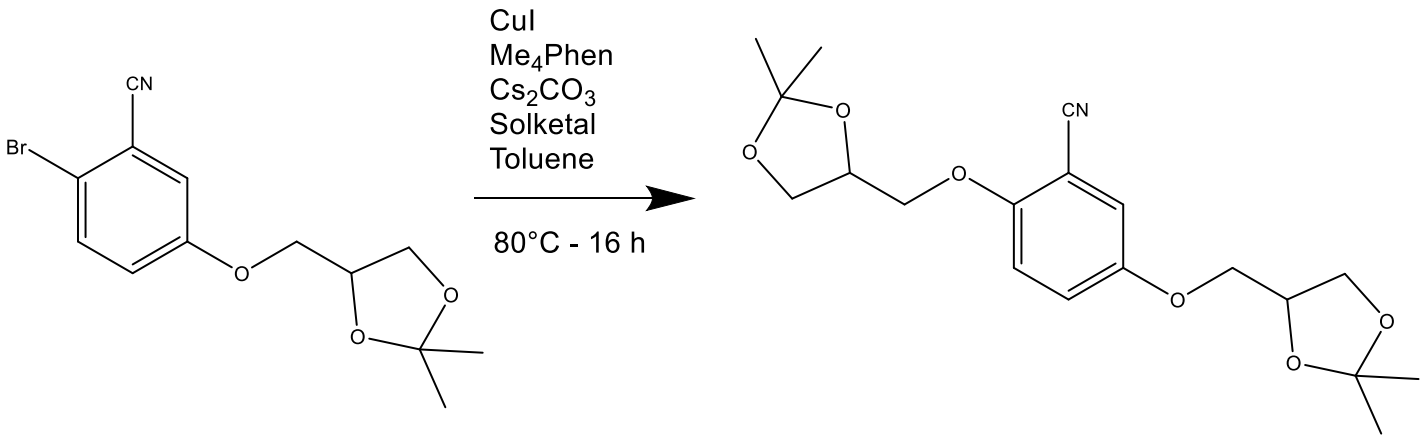

3 **5**

To an oven-dried screw cap vial was added copper (I) iodide (3.05 mg, 0.016 mmol), 3,4,7,8-tetramethyl-1,10-phenanthroline (7.56 mg, 0.032 mmol), caesium carbonate (208.5 mg, 0.04 mmol) and solketal (79 µL, 0.064 mmol) under argon atmosphere. 2-bromo-5-[(2,2-dimethyl-1,3-dioxolan-4-yl)methoxy]benzonitrile (100 mg, 0.32 mmol) in dry toluene (0.5 mL) was added to the vial by syringe. The reaction was then capped, heated to 80°C in an oil bath and stirred vigorously for 16 h. The mixture was then cooled to room temperature, diluted with ethyl acetate (20 mL) and washed with water (3 x 15 mL), brine (15 mL), dried over magnesium sulfate and concentrated *in vacuo* to give 2,5-bis-[(2,2-dimethyl-1,3-dioxolan-4-yl)methoxy]benzonitrile as a dark brown oil (58 mg, 95%).

^{1}H NMR ($CDCl_3$, 400 MHz): δ 7.55 (d, *J* = 8.95 Hz, 1H), 7.19 (d, *J* = 3.00 Hz, 1H), 7.04 (dd, *J* = , 8.95, 3.00 Hz, 1H), 4.51 – 4.44 (m, 1H), 4.28 – 4.21 (m, 1H), 4.17 (dd, *J* = 8.28, 1.74 Hz, 1H), 4.14 – 4.09 (m, 1H), 4.07 – 3.94 (m, 2H), 3.89 (dd, *J* = 8.57, 5.76 Hz, 1H), 3.80 (dd, *J* = 8.21,

6.52 Hz, 1H), 3.73 (d, *J* = 3.73 Hz, 1H), 3.62 (d, *J* = 5.10 Hz, 1H), 1.46 (s, 3H), 1.45 (s, 3H), 1,40 (s, 3H), 1.38 (s, 3H).

^{13}C NMR ($CDCl_3$, 400 MHz): δ 157.67, 134.06, 121.29, 119.58, 116.95, 116.29, 116.17, 110.09, 109.41, 73.65, 69.41, 66.42, 65.66, 62.99, 26.71, 25.26.

High-resolution mass spectroscopy (ESI+): (M+H)+: calculated for $C_{19}H_{25}NO_6$, 364.1760; found 364.1758.

IR: 2237, 1279, 1253, 1165, 1148, 1130, 1080 cm-1.

3.2.6. Synthesis of 2,5-bis-(2,3-dihydroxypropoxy)benzonitrile:

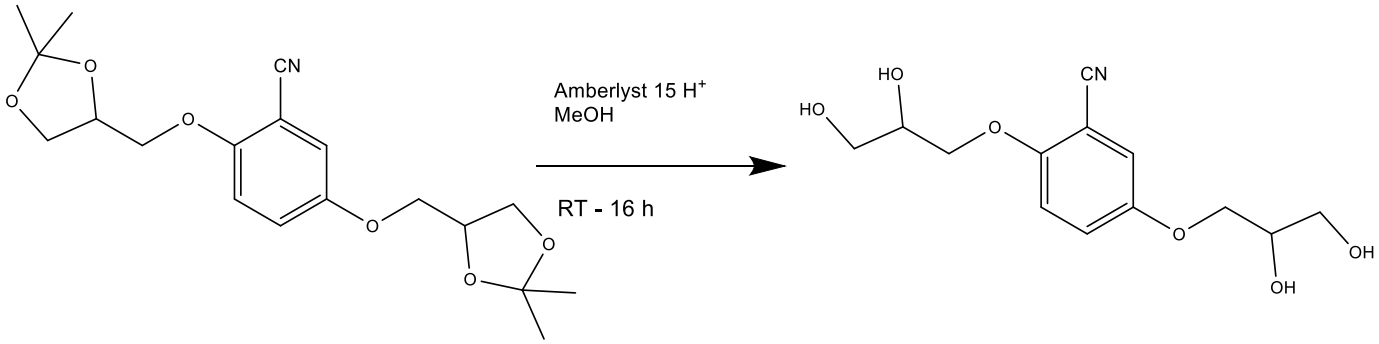

5 **7**

Amberlyst 15 H^+ (60mg) was added to a solution of bis-2,5-[(2,2-dimethyl-1,3-dioxolan-4-yl)methoxy]benzonitrile (54 mg, 0.148 mmol) in methanol (3 mL) and allowed to stir for 16 h. The resulting solution was decanted off, and the resin washed with methanol (3 x 10 mL). The combined organics were evaporated *in vacuo* to afford 2,5-bis-(2,3-dihydroxypropoxy)benzonitrile as a brown oil (24 mg, 50%).

^{1}H NMR ($CDCl_3$, 400 MHz): δ 7.46 (d, *J* = 8.96 Hz, 1H), 7.09 (d, *J* = 3.00 Hz, 1H), 6.94 (dd, *J* = 8.96, 3.00 Hz, 1H), 4.07 – 4.01 (m, 1H), 3.98 – 3.91 (m, 4H), 3.79 – 3.62 (m, 4H), 3.61 – 3.54 (m, 1H).

^{13}C NMR ($CDCl_3$, 400 MHz): δ 157.72, 134.09, 121.28, 119.77, 116.98, 116.18, 116.14, 70.17, 69.78, 64.03, 63.38.

High-resolution mass spectroscopy (ESI+): (M+H)+: calculated for $C_{13}H_{17}NO_6$, 284.1134; found 284.1130.

IR: 3404, 2232, 1251, 1216 cm-1.

3.2.7. Synthesis of 2-bromo-5-(2,3-bis(sulfooxy)propoxy)benzonitrile:

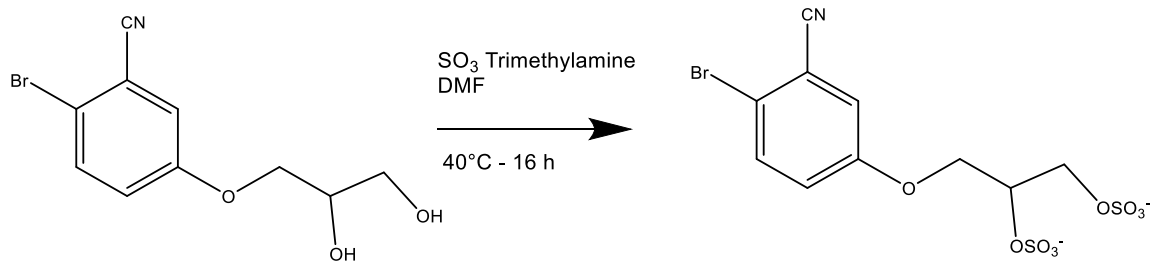

4 **6**

To a solution of 2-bromo-5-(2,3-dihydroxypropoxy)benzonitrile (27 mg, 0.1 mmol) in dry N,N-dimethylformamide (1 mL) was added sulfur trioxide trimethylamine complex (55.6 mg, 0.4 mmol) and the reaction heated to 40°C and allowed to stir for 16 h. Solvents were then removed *in vacuo* by azeotropic distillation using toluene/xylenes. Any remaining solvent residue was removed under high-vacuum to give a thick, dark yellow oil which was subjected to column chromatography (4 : 1 methanol : dichloromethane) to give 2-bromo-5-(2,3-bis(sulfooxy)propoxy)benzonitrile as a thick yellow oil (36 mg, 90.6%).

^{1}H NMR (MeOD, 400 MHz): δ 6.21 (dd, *J* = 8.90, 1.09 Hz, 1H), 5.90 (dd, *J* = 13.31, 3.02 Hz, 1H), 5.74 – 5.67 (m, 1H), 2.86 – 2.74 (m, 2H), 2.69 – 2.56 (m, 2H), 2.56– 2.41 (m, 1H).

^{13}C NMR (MeOD, 400 MHz): δ 159.95, 135.33, 122.93, 121.21, 117.99, 117.03, 116.21, 71.55, 69.35, 63.90.

High-resolution mass spectroscopy (ESI+): (M+H)+: calculated for $C_{10}H_8BrNO_9S_2$, 429.8902; found 429.8897.

IR: 2234, 1395, 1264, 1165, 1122, 571 cm-1.

3.2.8. Synthesis of 2,5-bis-(2,3-bis(sulfooxy)propoxy)benzonitrile:

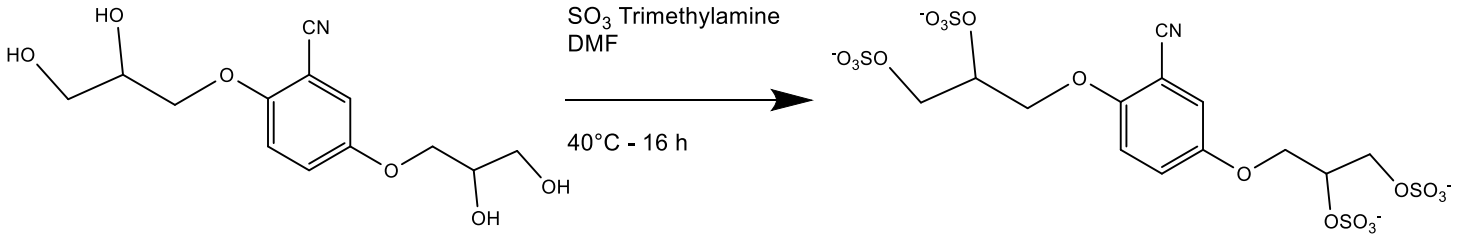

7 **8**

To a solution of 2,5-bis-(2,3-dihydroxypropoxy)benzonitrile (25 mg, 0.088 mmol) in dry N,N-dimethylformamide (1 mL) was added sulfur trioxide trimethylamine complex (53 mg, 0.38 mmol) and the reaction heated to 40°C and allowed to stir for 16 h. Solvents were then removed *in vacuo* by azeotropic distillation using toluene/xylenes. Any remaining solvent residue was removed under high-vacuum to give a thick, dark yellow oil which was subjected to column chromatography (methanol) to give 2,5-bis-(2,3-bis(sulfooxy)propoxy)benzonitrile as a thick yellow oil (30 mg, 83.3%).

^{1}H NMR (MeOD, 400 MHz): δ 7.69 (d, *J* = 8.99 Hz, 1H), 7.44 (dd, *J* = 8.62, 3.00 Hz, 1H), 7.28 – 7.22 (m, 1H), 4.30 (dd, *J* = 15.56, 4.99 Hz, 1H), 4.19 (dd, J = 10.00, 3.05 Hz, 1H), 4.12 – 4.06 (m, 4H), 4.04 (d, *J* = 5.89 Hz, 1H), 3.71 – 3.66 (m, 1H), 3.64 (d, *J* = 5.00 Hz, 1H), 3.60 (d, *J* = 5.80 Hz, 1H)

^{13}C NMR (D_2O, 400 MHz): δ 155.23, 130.29, 120.18, 119.27, 114.32, 114.03, 113.98, 68.58, 63.14, 62.27.

High-resolution mass spectroscopy (ESI+): (M+H)+: calculated for $C_{13}H_{13}NO_{18}S_4$, 599.9094; found 599.9089.

IR: 2236, 1410, 1395, 1245, 1219, 1133, 1082 cm-1.

3.2.9. Synthesis of 3-chloro-5-([2,2-dimethyl-1,3-dioxolan-4-yl]methoxy)benzonitrile:

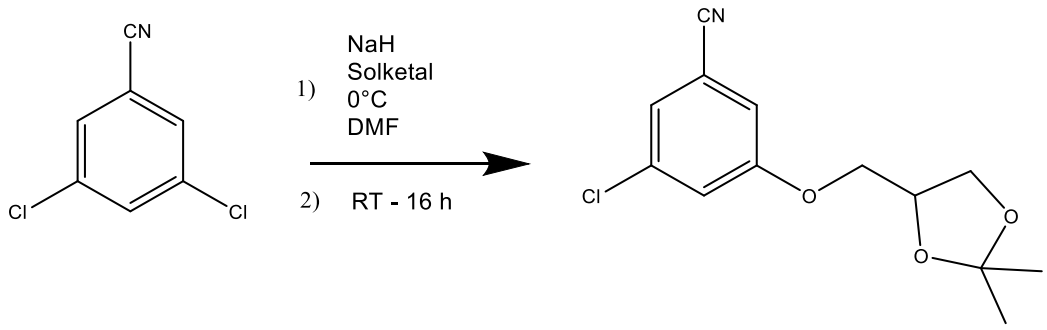

14 **15**

Sodium hydride (60% dispersion in mineral oil) (75.9 mg, 2.26 mmol) was added to a pre-dried round bottomed flask under argon atmosphere and washed with petroleum ether 40-60°C to remove any trace mineral oils. To the flask was then added dry N,N-dimethylformamide (3 mL) and cooled to 0°C. Solketal (0.27 mL, 1.914 mmol) was then added dropwise over 2 minutes, then allowed to stir at 0°C until any gas evolution ceased. 3,5-dichlorobenzonitrile (0.3g, 1.74 mmol) in dry N,N-dimethylformamide (2 mL) was then added slowly over 2 minutes and the reaction allowed to warm to room temperature and stir for 16 h. Following this, the mixture was poured into ice-cold 10% v/v HCl solution, extracted with ethyl acetate (2 x 30 mL), washed with water (3 x 15 mL), brine (15 mL), dried over magnesium sulfate and concentrated *in vacuo* to afford 3-chloro-5-([2,2-dimethyl-4-dioxolan-4-yl]methoxy)benzonitrile as a thick yellow oil (0.352 g, 75.6%).

^{1}H NMR ($CDCl_3$, 400 MHz): δ 7.26 (t, *J* = 1.53 Hz, 1H), 7.18 (t, *J* = 2.11 Hz, 1H), 7.11 – 7.09 (m, 1H), 4.53 – 4.45 (m, 1H), 4.19 (dd, J = 8.58, 6.49, 1H), 4.09 – 3.97 (m, 2H), 3.90 (dd, *J* = 8.58, 5.67 Hz, 1H), 1.47 (s, 3H), 1.42 (s, 3H).

^{13}C NMR ($CDCl_3$, 400 MHz): δ 159.32, 136.01, 124.52, 120.20, 117.40, 116.70, 114.20, 110.00, 73.80, 69.41, 66.43, 26.80, 25.22.

High-resolution mass spectroscopy (ESI+): (M+H)+: calculated for $C_{13}H_{14}ClNO_3$, 268.0741; found 268.0736.

IR: 2242, 1433, 1381, 1099, 670 cm-1.

3.2.10. Synthesis of 3-chloro-5-(2,3-dihydroxypropoxy)benzonitrile:

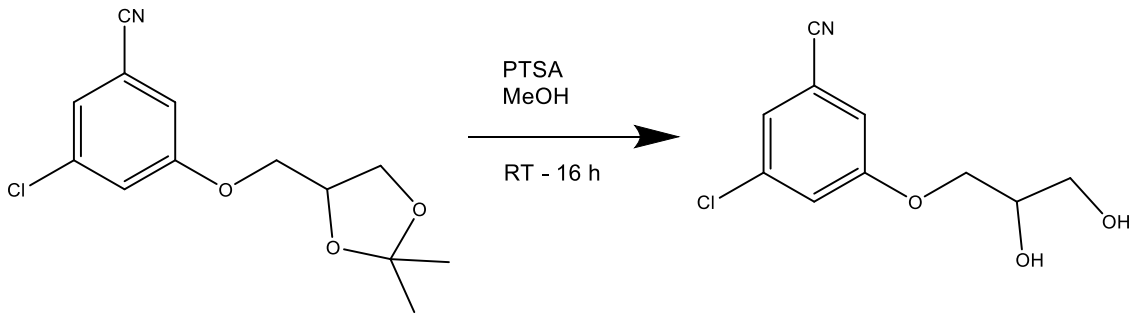

15 **16**

This synthesis was attempted using 2 different reactions.

<u>Reaction 1:</u>

To a stirred solution of 3-chloro-5-([2,2-dimethyl-4-dioxolan-4-yl]methoxy)benzonitrile (150 mg, 0.56 mmol) in methanol (2.5 mL) was added *para*-toluenesulfonic acid (13 mg, 0.068 mmol) in one portion and allowed to stir for 16 h at room temperature. Following this, the mixture was diluted with dichloromethane (40 mL), washed with saturated aqueous sodium bicarbonate solution (20 mL), water (2 x 20 mL), dried over magnesium sulfate and concentrated *in vacuo* to afford 3-chloro-5-(2,3-dihydroxypropoxy)benzonitrile as a thick dark yellow gel (50 mg, 39.6%).

^{1}H NMR ($CDCl_3$, 400 MHz): δ 7.26 (t, *J* = 1.45 Hz, 1H), 7.18 (t, *J* = 2.08 Hz, 1H), 7.11 – 7.09 (m, 1H), 4.18 – 4.10 (m, 1H), 4.10 – 4.02 (m, 2H), 3.87 – 3.71 (m, 2H).

^{13}C NMR ($CDCl_3$, 400 MHz): δ 159.36, 136.04, 124.48, 120.17, 117.44, 116.55, 114.02, 70.18, 69.73, 69.30.

High-resolution mass spectroscopy (ESI+): (M+H)+: calculated for $C_{10}H_{10}ClNO_3$, 228.0428; found 228.0422.

IR: 2234, 1433, 1381, 1099, 670 cm-1.

Reaction 2:

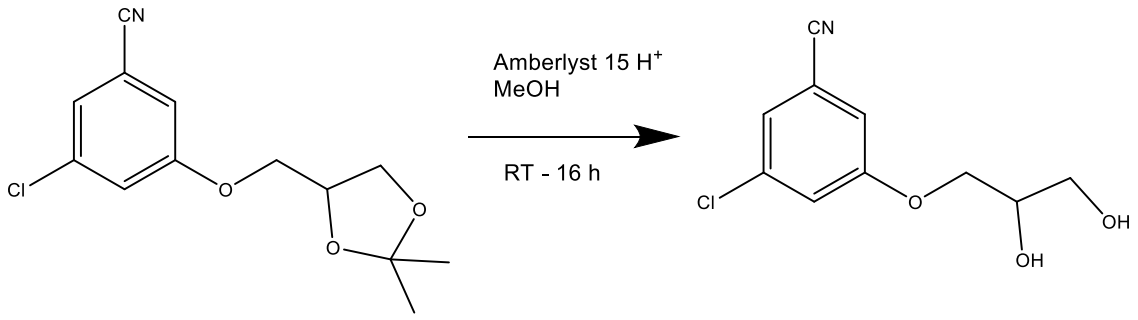

15 **16**

Amberlyst 15 H^+ (200 mg) was added to a solution of 3-chloro-5-([2,2-dimethyl-4-dioxolan-4-yl]methoxy)benzonitrile (54 mg, 0.148 mmol) in methanol (10 mL) and allowed to stir for 16 h. The resulting solution was decanted off, and the resin washed with methanol (3 x 10 mL). The combined organics were evaporated *in vacuo* to afford 3-chloro-5-(2,3-dihydroxypropoxy)benzonitrile as a thick dark yellow oil (0.166 g, 93%).

^{1}H NMR ($CDCl_3$, 400 MHz): δ 7.26 (t, *J* = 1.45 Hz, 1H), 7.18 (t, *J* = 2.08 Hz, 1H), 7.11 – 7.09 (m, 1H), 4.18 – 4.10 (m, 1H), 4.10 – 4.02 (m, 2H), 3.87 – 3.71 (m, 2H),

^{13}C NMR ($CDCl_3$, 400 MHz): δ 159.36, 136.04, 124.48, 120.17, 117.44, 116.55, 114.02, 70.18, 69.73, 69.30

High-resolution mass spectroscopy (ESI+): (M+H)+: calculated for $C_{10}H_{10}ClNO_3$, 228.0428; found 228.0423.

IR: 2234, 1433, 1381, 1099, 670 cm-1.

3.2.11. Synthesis of (*R*)-3-(2,3-dihydroxypropoxy)benzene:

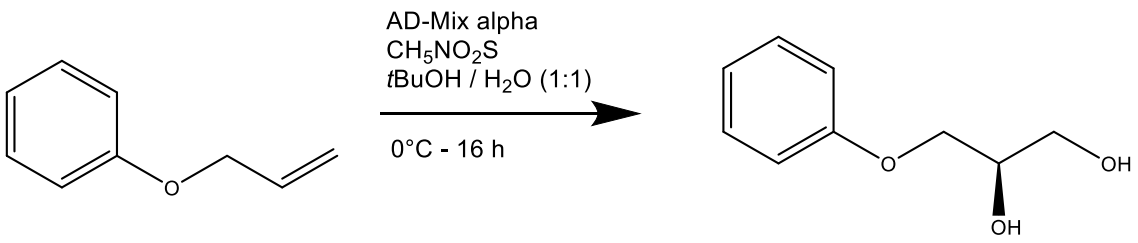

31 **32**

AD-mix α (5.5 g) was added to a round bottomed flask and dissolved in equal volumes tert-butanol and water totalling 60 mL and cooled to 0°C. Allyl phenyl ether (0.5 g, 3.726 mmol) and methanesulfonamide (0.372 g, 3.912 mmol) were added in one portion to the reaction and the reaction allowed to stir at 0°C for 16 h. The reaction was then quenched through the addition of sodium sulfite (3.25 g, 25.7 mmol). Solvents were removed in vacuo and methanol (40 mL) was added to the resulting salt and heated at reflux for 1 h. Concentration of the filtrate in vacuo afforded (*R*)-3-(2,3-dihydroxypropoxy)benzene as a thick yellow oil (0.547 g, 87.5%).

Spectral data corresponded to that found in literature (Kitaori, Furukawa, Yoshimoto, & Otera, 1999).

3.2.12. Synthesis of 3-chloro-5-(2,3-bis(sulfooxy)propoxy)benzonitrile:

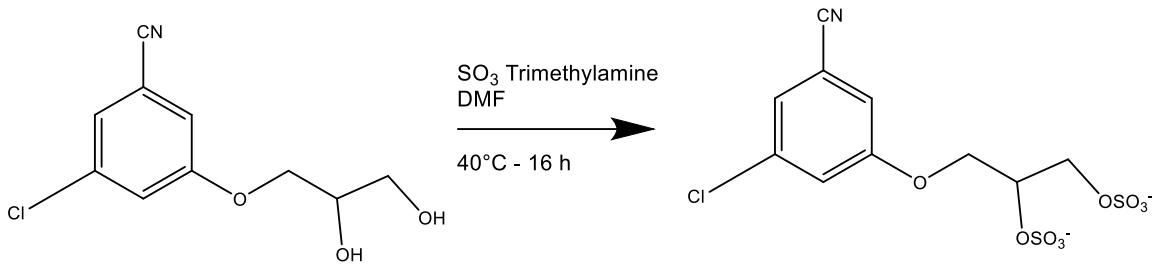

16 **17**

To a solution of 3-chloro-5-(2,3-dihydroxypropoxy)benzonitrile (158mg, 0.694 mmol) in anhydrous N,N-dimethylformamide (3.5 mL) was added sulfur trioxide trimethylamine complex (0.386 g, 2.77 mmol) and the reaction was allowed to stir at 40°C for 16 h. Solvent was removed *in vacuo* as an azeotrope with toluene. Any remaining solvents were removed under high vacuum. The crude product was dissolved in methanol and filtered through a cotton plug. Collection and concentration of the filtrate *in vacuo* gave 3-chloro-5-(2,3-bis(sulfooxy)propoxy)benzonitrile as a dark yellow gel (221 mg, 82.6%).

^{1}H NMR (MeOD, 400 MHz): δ 7.26 (t, *J* = 1.47 Hz, 1H), 7.18 (t, *J* = 2.09 Hz, 1H), 7.11 – 7.09 (m, 1H), 4.43 – 4.27 (m, 4H), 4.21 – 4.11 (m, 1H).

^{13}C NMR (MeOD, 400 MHz): δ 161.28, 137.17, 127.62, 125.46, 121.58, 118.08, 115.54, 75.52, 68.65, 55.41.

High-resolution mass spectroscopy (ESI+): (M+H)+: calculated for $C_{10}H_8ClNO_9S_2$, 385.9407; found 385.9402.

IR: 2236, 1376, 1291, 1141, 1120, 1058, 583

3.2.13. Synthesis of 2,2-dimethyl-4-(tosyloxy)methyl-1,3-dioxolane:

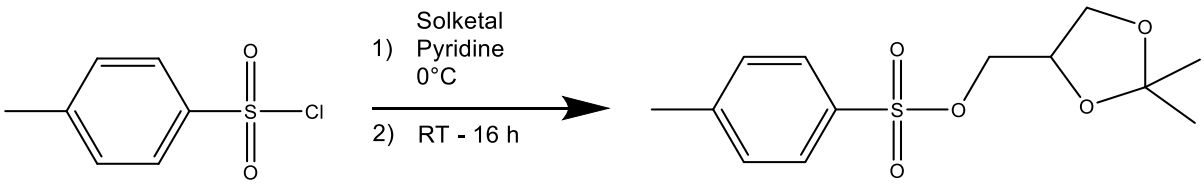

34 **35**

Para-toluenesulfonyl chloride was placed in a Soxhlet thimble and placed into the extractor. The collecting flask was filled with petroleum ether 40-60°C, insulated and the extraction process started. The extractor was allowed to function for 3 h, after which it was allowed to cool. Purified *para*-toluenesulfonyl chloride slowly crystallised out of the petroleum ether and was vacuum filtered to obtain the pure product. Remaining solids in the extraction thimble were discarded.

Freshly purified *para*-toluenesulfonyl chloride (4 g, 20.98 mmol) was added portionwise to a solution of solketal (2.5 g, 18.91 mmol) in pyridine (5 mL) at 0°C. The resulting mixture was slowly brought to room temperature and allowed to stir for 16 h. Pyridine is removed *in vacuo* and the residue diluted with ethyl acetate (25 mL), washed with cold 1M HCl solution (40 mL), saturated aqueous sodium bicarbonate solution (25 mL), brine (25 mL), dried over magnesium sulfate and concentrated *in vacuo* to afford 2,2-dimethyl-4-(tosyloxy)methyl-1,3-dioxolane as white crystals (4.84 g, 89.46%).

Spectral data corresponded to that found in literature (Krupa, Chodyński, Ostaszewska, Cmoch, & Dams, 2017).

3.2.14. Synthesis of 2,2-dimethyl-4-(phenoxy)methyl-1,3-dioxolane:

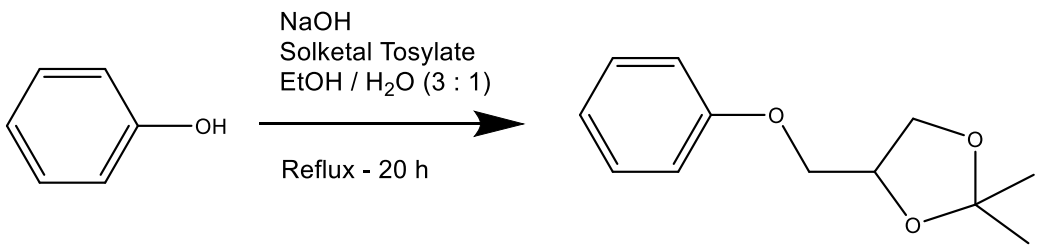

36 **37**

Sodium hydroxide (0.44 g, 11 mmol) was added portionwise to a stirred solution of phenol (1g, 11 mmol) in ethanol/water (3:1, 4 mL). Following stirring for 10 min, a solution of 2,2-Dimethyl-1,3-dioxolane-4-methanol *p*-toluenesulfonate (2.1 g, 7.34 mmol) in ethanol (2.5 mL) was added dropwise to the reaction over 1 minute. The reaction was then heated at reflux for 20 h. Following this, solvents were removed *in vacuo*, and the residue treated with 10% w/v sodium hydroxide solution (5 mL). The treated residue was then extracted with dichloromethane (3 x 10 mL), the combined organics washed with water (3 x 10 mL), brine (10 mL), dried over magnesium sulfate and concentrated *in vacuo* to give 2,2-dimethyl-4-(phenoxy)methyl-1,3-dioxolane as an off-white powder. (1.1 g, 48.08%).

Spectral data corresponded to that found in literature (Sugata et al., 2017).

3.2.15: Synthesis of 2,2-dimethyl-4-(2-deuterophenoxy)methyl-1,3-dioxolane:

General procedure for preparation of 2,2-dimethyl-4-(2-deuterophenoxy)methyl-1,3-dioxolane:

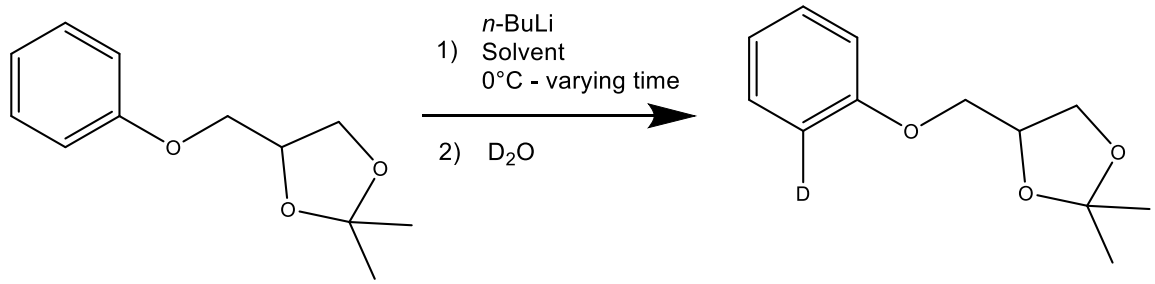

37 **38**

2,2-Dimethyl-4-(phenoxy)methyl-1,3-dioxolane (50mg, 0.236 mmol) was added to a pre-dried 2-necked round bottomed flask under argon atmosphere and dissolved in anhydrous solvent (5 mL). After cooling to 0°C, *n*-butyllithium 1.6M in hexanes (1.1 – 2.2 equivalents) were added dropwise over 2 minutes. Following stirring at 0°C for 2 hours, the reaction was quenched through addition of D_2O (0.5 mL). The mixture was then diluted with ether (20 mL), dried over magnesium sulfate, filtered and concentration of the filtrate *in vacuo* afforded the deuterated product.

^{1}H NMR (400 MHz, $CDCl_3$) δ = 7.28 (dd, *J* = 9.0, 7.2 Hz, 2H), 6.91 (d, *J* = 9.0 Hz, 2H), 4.48 (m, 1H), 4.17 (dd, *J* = 8.4, 6.6 Hz, 1H), 4.07 (dd, *J* = 9.6, 5.4 Hz, 1H), 3.94 (dd, *J* = 9.6, 6.0 Hz, 1H), 3.91 (dd, *J* = 8.4, 6.0 Hz, 1H), 1.47 (s, 3H), 1.41 (s, 3H).

^{13}C NMR (400 MHz, $CDCl_3$) δ = 157.35, 130.25, 121.11, 116.52, 108.95, 74.63, 68.92, 67.32, 27.25, 25.04.

High-resolution mass spectroscopy (ESI+): (M+H)+: calculated for $C_{10}H_{15}DO_3$, 210.1241; found 210.1235.

IR: 1455, 1368, 1073 cm-1.

***Table 4*. Reaction parameters for determination of optimal reaction conditions.**

Reaction Number	**Solvent**	**Reaction Time and temperature**	**Equivalents of *n*-butyllithium and additives**
1	THF	0°C – 2 hours	1.1
2	THF	0°C – 2 hours	2.2
3	THF	0°C – 2 hours	2.2 + TMEDA
4	Ether	0°C – 2 hours	2.2
5	Ether	0°C – 4 hours	2.2
6	Ether	0°C – 3 hours	2.2 + TMEDA

3.2.16. General procedure for aryl sulfate preparation:

Sulfur trioxide pyridine complex (1 equivalent per OH group) was added to a stirred solution of substituted phenol (8.4 mmol) in toluene (15 mL) and allowed to stir at reflux for 16 h. Following this the toluene was decanted off and the residue dissolved in distilled water (5 mL). 0.2M KOH solution was added to the crude mixture until it indicated basic on pH paper, followed by washing with ethyl acetate (3 x 20 mL). The basic solution was then acidified through addition of glacial acetic acid, washed with ethyl acetate (3 x 20 mL) and re-basified through addition of 0.2M KOH. The remaining solvent was removed *in vacuo* to give the corresponding aryl sulfate as potassium salt.

Synthesis of potassium 4-methoxyphenyl sulfate:

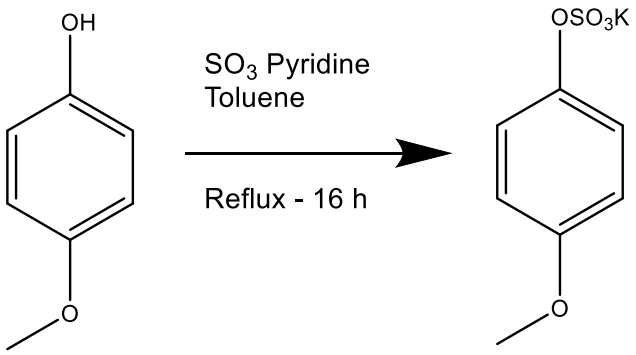

18 **24**

The reaction yielded potassium 4-methoxyphenyl sulfate as a white powder (1.4 g, 76.43%)

Spectral data corresponded to that found in literature (Denehy et al., 2006).

Synthesis of potassium 3-cyanophenyl sulfate:

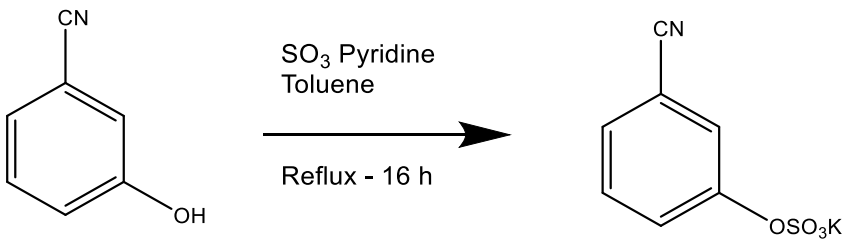

19 **25**

The reaction yielded potassium 3-cyanophenyl sulfate as an off-white powder (1.31 g, 73.03%)

Spectral data corresponded to that found in literature (Montero Bastidas, Oleskey, Miller, Smith, & Maleczka, 2019).

Synthesis of 1,3,5-trihydroxy-2,4,6-benzenetrisulfonic acid potassium salt:

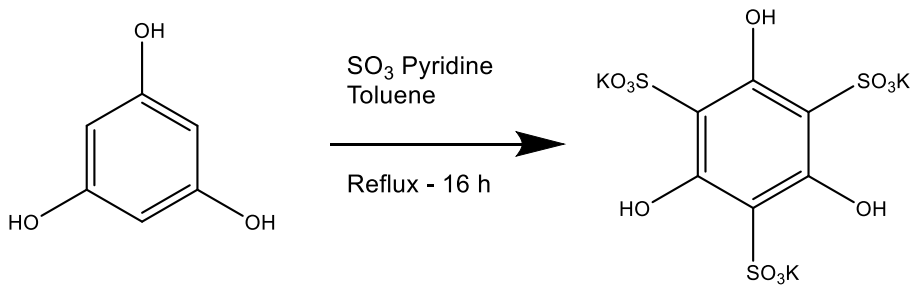

20 **26**

The reaction yielded 1,3,5-trihydroxy-2,4,6-benzenetrisulfonic acid potassium salt as a brown solid (2.2 g, 60.56%)

^{1}H NMR (400 MHz, D_2O) - No shifts observed.

^{13}C NMR (400 MHz, D_2O) δ = 181.50

High-resolution mass spectroscopy (ESI+): (M+3K)3+: calculated for $C_6H_3K_3O_{12}S_3$, 479.7698; found 479.7692.

IR: 3523, 1649, 1362, 1357, 1333, cm-1.

Synthesis of 3,5-bis(sulfooxy)benzoate potassium salt:

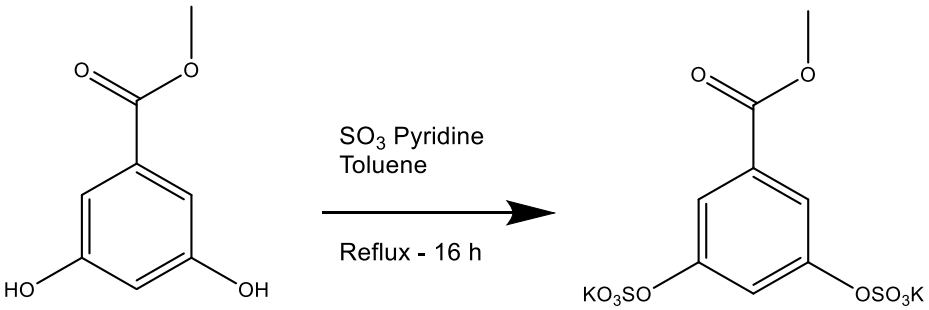

21 **27**

The reaction yielded methyl 3,5-bis(sulfooxy)benzoate potassium salt as a light brown solid (2.11 g, 69.01%)

^{1}H NMR (400 MHz, D_2O) δ = 7.56 (d, *J* = 2.26 Hz, 1H), 7.31 (t, *J* = 2.24 Hz, 1H), 6.66 (t, *J* = 2.30, 1H), 1.82 (3H, s).

^{13}C NMR (400 MHz, D_2O) δ = 151.36, 139.31, 119.56, 117.69, 110.20, 107.46, 58.63.

High-resolution mass spectroscopy (ESI+): (M+2K)2+: calculated for $C_8H_6K_2O_{10}S_2$, 403.8677; found 403.8672.

IR: 1710, 1403, 1382, 1133, 1073, 1052 cm-1.

Synthesis of methyl-3,5-bis(sulfooxy)benzene potassium salt:

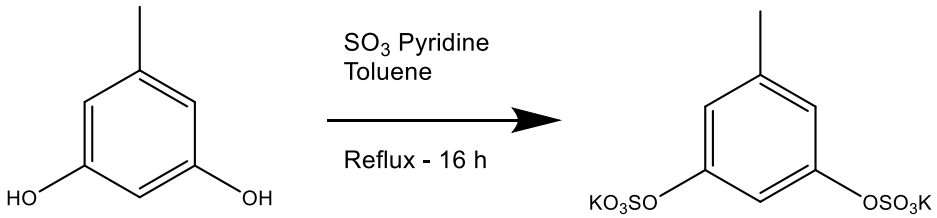

22 **28**

The reaction yielded methyl-3,5-bis(sulfooxy)benzene potassium salt as a light brown solid (2.01 g, 73.76%)

^{1}H NMR (400 MHz, D_2O) δ = 6.32 (d, *J* = 6.97 Hz, 2H), 6.25 (t, *J* = 2.11 Hz, 1H), 1.82 (s, 3H).

^{13}C NMR (400 MHz, D_2O) δ = 155.02, 153.33, 115.40, 113.18, 21.53.

High-resolution mass spectroscopy (ESI+): (M+2K)2+: calculated for $C_7H_6K_2O_8S_2$, 359.8778; found 359.8773.

IR: 1450, 1412, 1382, 1242, 1218. cm-1

Synthesis of 2,5-bis(sulfooxy)benzoic acid:

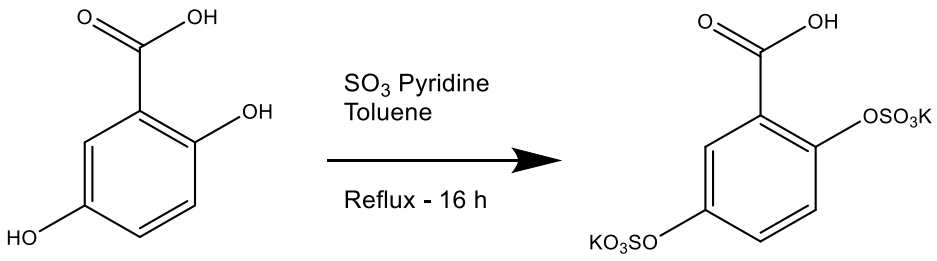

23 **29**

The reaction yielded 2,5-bis(sulfooxy)benzoic acid potassium salt as a light brown solid (1.9 g, 64.37%)

^{1}H NMR (400 MHz, D_2O) δ = 7.77 (d, *J* = 3.05 Hz, 1H), 7.68 (d, *J* = 3.02 Hz, 1H), 7.58 (d, *J* = 2.99 Hz, 1H)

^{13}C NMR (400 MHz, D_2O) δ = 174.52, 157.81, 143.17, 127.32, 125.53, 123.15, 117.20.

High-resolution mass spectroscopy (ESI+): (M+2K)2+: calculated for $C_7H_4K_2O_{10}S_2$, 389.8520; found 389.8517.

IR: 3523, 1637, 1483, 1441, 1242, 1220 cm-1

3.8.17. Synthesis of phloroglucinol trisulfate:

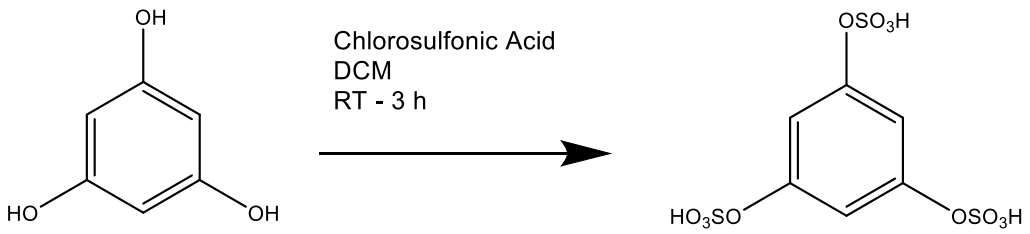

20 **30**

To a flask containing phloroglucinol (0.525 g, 4.16 mmol) was added a solution of chlorosulfonic acid (1.46 g, 12.5 mmol) in DCM (5 mL) over a period of 1 h at room temperature. Following addition of the acid solution, the mixture was stirred for 3 h at room temperature, followed by removal of the solvent *in vacuo*. The resulting solid was washed with *n*-hexanes (5 mL), filtered and dried to give phloroglucinol trisulfate as a light brown solid. (1.33 g, 66.27%)

^{1}H NMR (400 MHz, D_2O) δ = 5.92 (s, 1H), 5.86 (s, 1H), 5.83 (s, 1H).

^{13}C NMR (400 MHz, D_2O) δ = 155.81, 106.05.

High-resolution mass spectroscopy (ESI+): (M+H)+: calculated for $C_6H_6O_{12}S_3$, 366.9100; found 366.9093

IR: 1412, 1397, 1383, 1183, 1157, 1111 cm-1

3.2.18. Synthesis of 3-allyloxybenzonitrile:

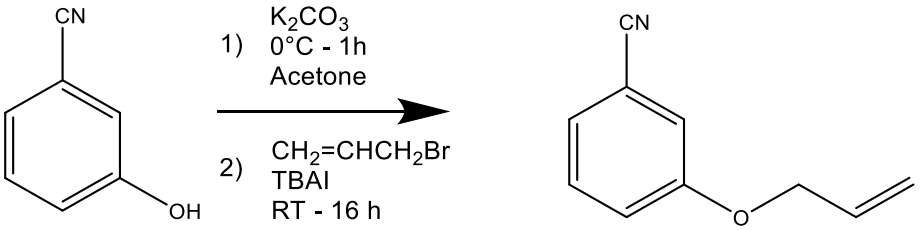

1 **9**

3-cyanophenol (2 g, 23.2 mmol) was dissolved in anhydrous acetone (50 mL) and added to a flask containing potassium carbonate (4.64 g, 33.6 mmol) in anhydrous acetone (5 mL) at 0°C. Following 1 h stirring at 0°C, allyl bromide (1.7 mL, 23.2 mmol) and tetrabutylammonium iodide (1.22 g, 3.3 mmol) were added and the reaction allowed to stir for 16 h at room temperature. Acetone was then evaporated *in vacuo* and the mixture diluted with ethyl acetate (60 mL), the organics washed with water (3 x 40 mL), brine (40 mL), dried over magnesium sulfate and concentrated *in vacuo* to afford 3-allyloxybenzonitrile as a yellow oil (2.54 g, 94.46%)

Spectral data corresponded to that found in literature (Pincock, Pincock, & Stefanova, 2002).

3.2.19. Synthesis of (*R*)-3-(2,3-dihydroxypropoxy)benzonitrile:

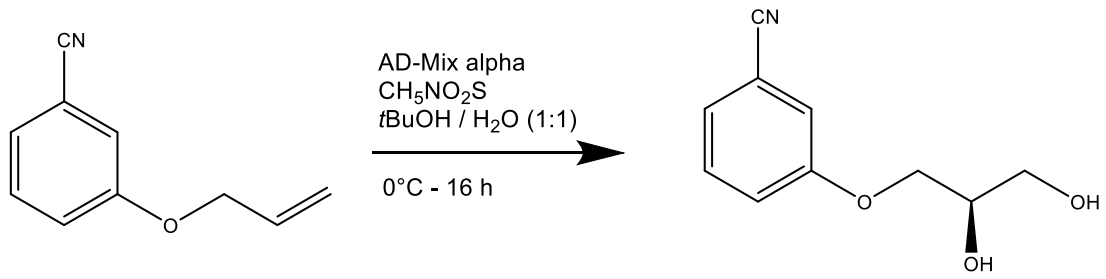

9 **10**

AD-mix α (5 g) was added to a round bottomed flask and dissolved in equal volumes tert-butanol and water totalling 40 mL and cooled to 0°C. 3-allyloxy benzonitrile (0.3 g, 1.886 mmol) and methanesulfonamide (0.224 g, 2.338 mmol) were added in one portion to the reaction and the reaction allowed to stir at 0°C for 16 h. The reaction was then quenched through the addition of sodium sulfite (3 g, 23.8 mmol). Solvents were removed *in vacuo* and methanol (30 mL) was added to the resulting salt and heated at reflux for 1 h. Concentration of the filtrate *in vacuo* afforded (*R*)-3-(2,3-dihydroxypropoxy)benzonitrile as a thick yellow oil (0.364 g, 81.87%)

Spectral data corresponded to that found in literature (Bredikhin, Bredikhina, Akhatova, Zakharychev, & Polyakova, 2009).

3.2.20. Synthesis of (*S*)-3-(2,3-dihydroxypropoxy)benzonitrile:

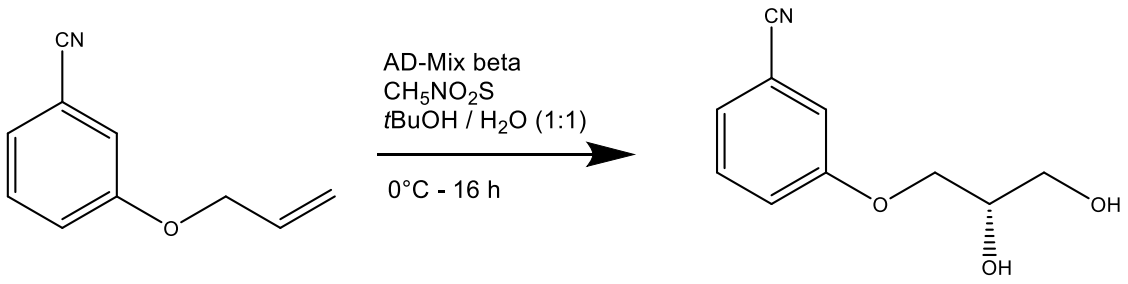

9 **11**

AD-mix ß (5 g) was added to a round bottomed flask and dissolved in equal volumes tert-butanol and water totalling 40 mL and cooled to 0°C. 3-allyloxy benzonitrile (0.3 g, 1.886 mmol) and methanesulfonamide (0.224 g, 2.338 mmol) were added in one portion to the reaction and the reaction allowed to stir at 0°C for 16 h. The reaction was then quenched through the addition of sodium sulfite (3 g, 23.8 mmol). Solvents were removed *in vacuo* and methanol (30 mL) was added to the resulting salt and heated at reflux for 1 h. Concentration of the filtrate *in vacuo* afforded (*S*)-3-(2,3-dihydroxypropoxy)benzonitrile as a thick yellow oil (0.317 g, 87.09%)

Spectral data corresponded to that found in literature (Bredikhin et al., 2009).

3.2.21. Synthesis of sulfur trioxide tributylamine complex:

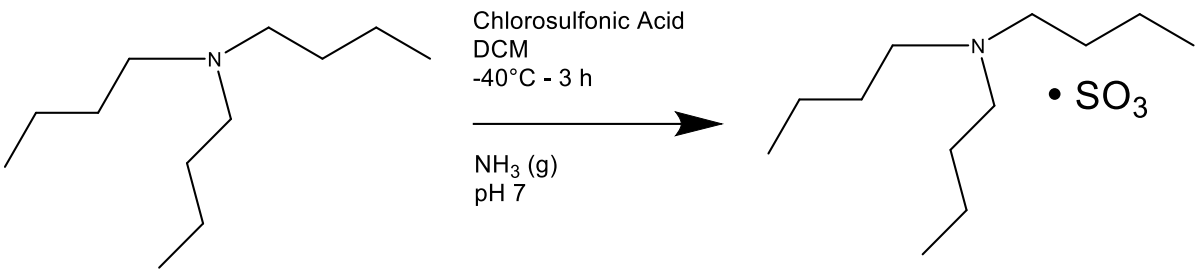

41 **42**

To a pre-dried 3-necked round-bottomed flask under argon atmosphere was added anhydrous dichloromethane (200 mL) and tributylamine (59.4 mL, 0.25 mol) under vigorous stirring and cooling to -40°C (MeCN / CO_2). To a pressure-equalising dropping funnel was then added a solution of chlorosulfonic acid (16.75 mL, 0.253 mol) in anhydrous dichloromethane (200 mL) and allowed to add slowly over 2 h ensuring the internal temperature did not exceed -30°C. Following addition of the acid solution, the reaction was allowed to stir for another 1 h at -40°C after which, gaseous ammonia was bubbled through the reaction mixture until pH 7 was achieved. The white solid was removed through vacuum filtration, washed with dichloromethane (100 mL) and the filtrate collected. Solvents were then removed *in vacuo* and the remaining crude product was treated with cold water (500 mL). The resulting precipitate was collected, washed with water (5 x 100 mL) and lyophilised to give sulfur trioxide tributylamine complex as a fine white powder. (57.4 g, 86.65%)

Spectral data corresponded to that found in literature (Gill et al., 2019).

3.2.22. Synthesis of (*S*)-3-(2,3-bis(sulfooxy)propoxy)benzonitrile sodium salt:

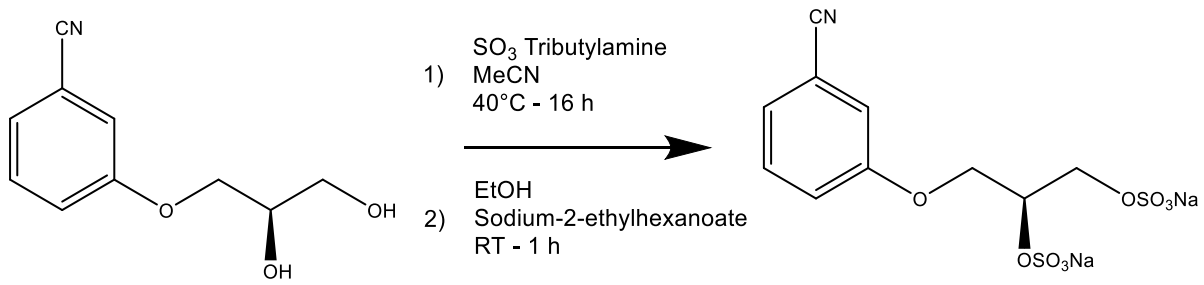

10 **12**

(*S*)-3-(2,3-dihydroxypropoxy)benzonitrile (0.3 g, 1.55 mmol) and sulfur trioxide tributylamine complex (1.24 g, 6.2 mmol) were added to a pre-dried round-bottomed flask under argon atmosphere and dissolved in anhydrous acetonitrile (8 mL), heated to 40°C and allowed to stir for 16 h. Following this, the reaction was cooled to room temperature, and solvents removed *in vacuo*. Water (30 mL) was added to the flask and the aqueous mixture was extracted with ethyl acetate (4 x 40 mL). Organic extracts were combined, dried over magnesium sulfate and filtered. The filtrate solvent was removed *in vacuo* to give the crude sulfate tributylammonium salt.

The tributylammonium salt was then dissolved in ethanol (50 mL) and to the solution was added sodium-2-ethylhexanoate (2.58 g, 15.5 mmol) and the mixture stirred vigorously for 1 h at room temperature. Solids were removed by filtration, collected and washed with ethanol (3 x 30 mL) and dried to give (*S*)-3-(2,3-bis(sulfooxy)propoxy)benzonitrile sodium salt as a white powder. (0.485g, 78.73%)

^{1}H NMR (400 MHz, D_2O) δ = 7.40 (t, *J* = 8.06 Hz, 1H), 7.36 – 7.30 (m, 2H), 7.29 – 7.24 (m, 1H), 4.85 – 4.74 (m, 1H), 4.39 - 4.20 (m, 4H).

^{13}C NMR (400 MHz, D_2O) δ = 157.88, 130.81, 125.70, 120.67, 119.46, 118.12, 111.85, 75.1, 66.6, 40.5.

High-resolution mass spectroscopy (ESI+): (M+2Na)2+: calculated for $C_{10}H_9NNa_2O_9S_2$, 396.9514; found 396.9510.

IR: 2234, 1440, 1375, 1223, 1124, 1077 cm-1.

3.2.23. Synthesis of (*R*)-3-(2,3-bis(sulfooxy)propoxy)benzonitrile sodium salt:

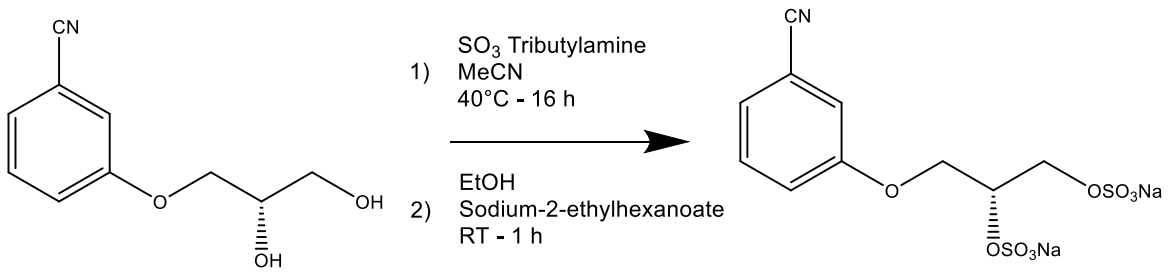

11 **13**

(*S*)-3-(2,3-dihydroxypropoxy)benzonitrile (0.225 g, 1.16 mmol) and sulfur trioxide tributylamine complex (1.24 g, 4.66 mmol) were added to a pre-dried round-bottomed flask under argon atmosphere and dissolved in anhydrous acetonitrile (6 mL), heated to 40°C and allowed to stir for 16 h. Following this, the reaction was cooled to room temperature, and solvents removed *in vacuo*. Water (30 mL) was added to the flask and the aqueous mixture was extracted with ethyl acetate (4 x 40 mL). Organic extracts were combined, dried over magnesium sulfate and filtered. The filtrate solvent was removed *in vacuo* to give the crude sulfate tributylammonium salt.

The tributylammonium salt was then dissolved in ethanol (50 mL) and to the solution was added sodium-2-ethylhexanoate (1.94 g, 11.7 mmol) and the mixture stirred vigorously for 1 h at room temperature. Solids were removed by filtration, collected and washed with ethanol (3 x 30 mL) and dried to give (*R*)-3-(2,3-bis(sulfooxy)propoxy)benzonitrile sodium salt as a white powder. (0.352 g, 76.32%)

^{1}H NMR (400 MHz, D_2O) δ = 7.40 (t, *J* = 8.07 Hz, 1H), 7.36 – 7.30 (m, 2H), 7.29 – 7.24 (m, 1H), 4.86 - 4.77 (m, 1H), 4.41 - 4.19 (m, 4H).

^{13}C NMR (400 MHz, D_2O) δ = 157.88, 130.81, 125.70, 120.67, 119.46, 118.12, 111.85, 75.1, 66.6, 40.5.

High-resolution mass spectroscopy (ESI+): (M+2Na)2+: calculated for $C_{10}H_9NNa_2O_9S_2$, 396.9514; found 396.9510.

IR: 2234, 1440, 1375, 1219, 1134, 1077 cm-1.

3.2.24. General procedure for *ortho* lithiation:

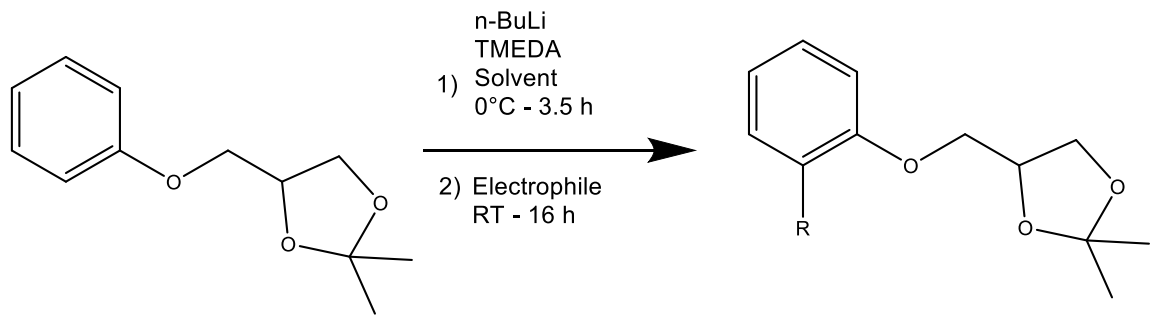

37 **43**

A solution of 2,2-dimethyl-4-(phenoxy)methyl-1,3-dioxolane (50 mg, 0.26 mmol) and a chosen quantity of freshly distilled anhydrous TMEDA in anhydrous solvent (5 mL) was added to a pre-dried round-bottomed flask under argon atmosphere and allowed to cool to 0°C. A chosen quantity of *n*-butyllithium 1.6M in hexanes was added dropwise over 5 minutes, then allowed to stir at 0°C for 3.5 h. Following this, the electrophile was added, and the reaction allowed to warm to room temperature and stir for 16 h. The reaction is then diluted through the addition of solvent (20 mL) and washed with water (3 x 15 mL), brine (15 mL), dried over magnesium sulfate, filtered, and the filtrate concentrated *in vacuo* to give the desired *ortho* substituted product.

Table 6. **Reactants and reaction conditions for syntheses MR18 - 25.**

Compound	Electrophile	Equivalents of n-butyllithium and additives	Reaction time + Temperature	Yield
MR18	MeI	2.2 + TMEDA	3.5 h - 0°C	15%
MR19	Allyl bromide	2.2 + TMEDA	3 h - 0°C	30%
MR20	Allyl bromide	4 + TMEDA - TBME	2 h - 0°C	5%
MR21	Allyl bromide	7 + TMEDA	2 h - 0°C	40%
MR22	Benzyl bromide	2.2 + TMEDA	2 h - 0 °C	24%
MR23	TMS-Cl	2.2 + TMEDA	2 h - 0°C	Complex Mixture
MR24	TMS-Cl	7 + TMEDA	2 h - 0°C	Complex Mixture
MR25	Benzaldehyde	2.2 + TMEDA	2 h - 0°C	13%

3.2.25. Synthesis of 3-(2,3-dimethoxyphenylmethyl)benzonitrile:

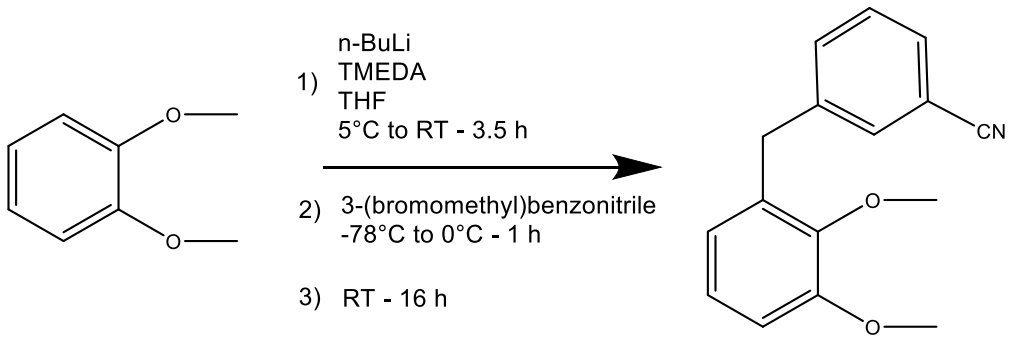

39 **40**

A solution of 1,2-dimethoxy benzene (1.1 mL, 8.63 mmol) and freshly distilled anhydrous TMEDA (1.82 mL, 12.1 mmol) in anhydrous THF (25 mL) was added to a pre-dried round-bottomed flask under argon atmosphere and allowed to cool to 5°C. *n*-Butyllithium 1.6M in hexanes (6.47 mL, 10.4 mmol) was added dropwise over 5 minutes, then allowed to stir at room temperature for 3.5 h. Following this, the reaction was cooled to -78°C (CO_2 / acetone) and a solution of 3-(bromomethyl) benzonitrile (2 g, 10.4 mmol) in anhydrous THF (5 mL) was added over 1 minute, the reaction allowed to warm to 0°C and stir for 1 h, followed by room temperature for 16 h. The suspension was then cooled to 10°C, quenched through addition of saturated NH_4Cl solution (25 mL). The aqueous phase was separated, extracted with THF (3 x 40 mL), the organics combined, dried over magnesium sulfate, filtered, and the filtrate concentrated *in vacuo* to give 3-(2,3-dimethoxyphenylmethyl)benzonitrile as an off-white solid (1.37 g, 62.84%)

^{1}H NMR (400 MHz, $CDCl_3$) δ = 7.51 – 7.45 (m, 1H), 7.43 – 7.38 (m, 1H), 7.36 – 7.33 (m, 2H), 7.11 (dd, J = 8.00, 1.45 Hz, 1H), 6.92 – 6.89 (m, 1H), 6.85 (dd, *J* = 8.28, 1.47 Hz, 1H), 3.87 (s, 2H), 3.854 (s, 3H), 3.85 (s, 3H).

^{13}C NMR (400 MHz, $CDCl_3$) δ = 153.99, 148.90, 146.55, 141.96, 133.04, 131.99, 130.13, 129.38, 125.06, 124.80, 120.93, 111.70, 111.42, 60.56, 55.83, 36.77.

High-resolution mass spectroscopy (ESI+): (M+H)+: calculated for 254.1181; found 254.1175.

IR: 2231, 1432, 1448, 1121, 1104 cm-1.

Conclusion:

Throughout this project, several improvements in order to streamline the synthesis of these inhibitors have been made. Firstly, the development of a one-pot procedure to synthesise both aryl sulfates and sulfonates allows us to quickly and effectively convert both commercially available substituted phenols and more complex, lab-synthesised phenols into potential HGF-Met inhibitors, which are then able to be tested for efficacy in inhibiting cell mobility. Unfortunately, the synthesis of these compounds generally results in moderate yields. Development of a better synthetic route which increases both yield and purity would be advantageous and should be considered in future research.

Secondly, major improvements in the synthesis of these glycomimetic compounds have been recently developed which have allowed us to easily synthesise, then purify target compounds in a small amount of time and steps through the use of novel reagents and techniques. Usage of SO_3 tributylamine complex has allowed us to exchange the use of complex, highly polar and difficult separations by column chromatography with common solvent-based workups followed by facile ion exchange procedures, not previously available in the synthesis and purification of these glycomimetics.

Testing of our compounds showed some positive results in terms of inhibiting cell motility in wound healing assays at moderate to low molar concentrations. With improvements to the SAR of these compounds, it may be possible to make these inhibitors more effective at lower concentrations through implementation of different, more effective sidechains or substitution of different aryl-bonded groups with a higher efficacy.

Unfortunately, due to time limitations, it was not possible to synthesise a diarylmethane derived series of compounds, however given further time and resources it would be

possible to produce a number of various substituted diarylmethanes and investigate their activities against cell motility.

Additionally, further investigation into different sulfation types such as N-sulfation have not been trialled in the production and testing of HGF-Met inhibitors as of yet and warrants investigation. Synthesis of more aryl sulfate and sulfonate compounds is also necessary as there is little data on their effectiveness as HGF-Met inhibitors and testing a wider range of compounds would allow us to create a set of data on the efficacy of these compounds.

Overall, we have demonstrated that synthesis of several small molecule HGF-Met inhibitors can be achieved at high yield through a relatively short and effective synthesis, with some compounds showing good activity against cell motility at relatively low molar concentrations, with little effects on cell viability. Further research into development of these compounds should be considered as a better SAR may be derived and used to further improve these HGF-Met inhibitors allowing higher efficacy at lower molar concentrations.

Future Work:

The research presented in this thesis begins to address the use of polysulfated glycosaminoglycans as HGF-Met inhibitors as a way to reduce metastasis through reducing cell motility. While some success in preventing cell motility was achieved with the structures depicted in section 2.6, there are many more structures to be investigated which may potentially have higher efficacy than the ones synthesised during this research project.

Firstly, it is not completely certain yet what exactly drives the SAR of these molecules. Further work would involve modifying structures with known efficacy and determining

which moieties are responsible for increasing efficacy and specificity, while lowering cytotoxicity. Research should also be conducted into whether enantiomers do in fact play a critical part in providing any higher or lower activity of the synthesised compound.

As discussed in the conclusion, N-Sulfation is one direction that has not been investigated yet in the synthesis and testing of HGF-Met inhibitors and could potentially hold some valuable results as to date, our research has only focused on O- sulfation. Therefore, investigation of this class of molecule is well worth the time, as it is possible that N- sulfated compounds have a much better efficacy when compared to O- sulfated compounds.

Another area that should be investigated is further methods which may allow us to streamline our syntheses. At present our current syntheses are relatively short and easy to obtain the final compound in few steps, with facile solvent-based workups. This however generally results in moderate yields. Investigation into development of a synthetic pathway/workup which does not result in a large loss of yield would be advantageous and should be considered in future to allow simpler purifications and larger amounts of material, which in turn will make potential longer syntheses much more attainable.

Further research should also be considered into larger molecules, such as the diarylmethane-based compounds which we did not have sufficient time to look into, as discussed above, could have the potential to have a very good SAR and be better candidates for inhibition when compared to the current compounds we have investigated.

Addressing these future areas could allow us to improve the SAR of our compounds, and bring us closer to having a definite hit compound which we can then develop further.

References:

Afratis, N., Gialeli, C., Nikitovic, D., Tsegenidis, T., Karousou, E., Theocharis, A. D., … Karamanos, N. K. (2012). Glycosaminoglycans: Key players in cancer cell biology and treatment. *FEBS Journal*, *279*(7), 1177–1197. https://doi.org/10.1111/j.1742-4658.2012.08529.x

Altman, R. A., Shafir, A., Choi, A., Lichtor, P. A., & Buchwald, S. L. (2008). An Improved Cu-Based Catalyst System for the Reactions of Alcohols with Aryl Halides. *The Journal of Organic Chemistry*, *73*(1), 284–286. https://doi.org/10.1021/jo702024p

Aquino, C. J., Dickson, H., & Peat, A. J. (2008). *WO 2008/157273 A1*. Retrieved from https://www.lens.org/lens/patent/126-627-864-590-043

Batesky, D. C., Goldfogel, M. J., & Weix, D. J. (2017). Removal of Triphenylphosphine Oxide by Precipitation with Zinc Chloride in Polar Solvents. *The Journal of Organic Chemistry*, *82*(19), 9931–9936. https://doi.org/10.1021/acs.joc.7b00459

Beddoe, R. H., Andrews, K. G., Magné, V., Cuthbertson, J. D., Saska, J., Shannon-Little, A. L., … Denton, R. M. (2019). Redox-neutral organocatalytic Mitsunobu reactions. *Science*, *365*(6456), 910–914. https://doi.org/10.1126/science.aax3353

Belting, M. (2014). Glycosaminoglycans in cancer treatment. *Thrombosis Research*, *133 Suppl 2*, S95-101. https://doi.org/10.1016/S0049-3848(14)50016-3

Birchmeier, C., Birchmeier, W., Gherardi, E., & Vande Woude, G. F. (2003). Met, metastasis, motility and more. *Nature Reviews Molecular Cell Biology*, *4*(12), 915–925. https://doi.org/10.1038/nrm1261

Bredikhin, A. A., Bredikhina, Z. A., Akhatova, F. S., Zakharychev, D. V., & Polyakova, E. V. (2009). From racemic compounds through metastable to stable racemic conglomerates: crystallization features of chiral halogen and cyano monosubstituted phenyl glycerol ethers. *Tetrahedron Asymmetry*, *20*(18), 2130–2136. https://doi.org/10.1016/j.tetasy.2009.09.008

Buchstein, N., Hoffmann, D., Smola, H., Lang, S., Paulsson, M., Niemann, C., … Eming, S. A. (2009). Alternative proteolytic processing of hepatocyte growth factor during wound repair. *American Journal of Pathology*, *174*(6), 2116–2128. https://doi.org/10.2353/ajpath.2009.080597

Bunte, A. N. (2017). *Synthesis of potential inhibitors of HGF-Met interaction*. University of Salford.

Cavallaro, U., & Christofori, G. (2004). Multitasking in tumor progression: Signaling functions of cell adhesion molecules. *Annals of the New York Academy of Sciences*, *1014*, 58–66. https://doi.org/10.1196/annals.1294.006

Cecchi, F., Rabe, D. C., & Bottaro, D. P. (2012). Targeting the HGF/Met signaling pathway in cancer therapy. *Expert Opinion on Therapeutic Targets*, *16*(6), 553–572. https://doi.org/10.1517/14728222.2012.680957

Dally, J., Khan, J. S., Voisey, A., Charalambous, C., John, H. L., Woods, E. L., … Midgley, A. C. (2017). Hepatocyte growth factor mediates enhanced wound healing responses and resistance to transforming growth factor-β1-driven myofibroblast differentiation in oral mucosal fibroblasts. *International Journal of Molecular Sciences*, *18*(9). https://doi.org/10.3390/ijms18091843

Denehy, E., White, J. M., & Williams, S. J. (2006). Ground state structures of sulfate monoesters and sulfamates reveal similar reaction coordinates for sulfuryl and sulfamyl transfer. *Chemical Communications*, (3), 314–316. https://doi.org/10.1039/b513712h

Dua, R., Zhang, J., Parry, G., & Penuel, E. (2011). Detection of hepatocyte growth factor (HGF) ligand-c-MET receptor activation in formalin-fixed paraffin embedded specimens by a novel proximity assay. *PLoS ONE*, *6*(1). https://doi.org/10.1371/journal.pone.0015932

Elsevier. (2019). Asymmetric Dihydroxylation - an overview | ScienceDirect Topics. Retrieved November 18, 2019, from https://www.sciencedirect.com/topics/chemistry/asymmetric-dihydroxylation

Fafalios, A., Ma, J., Tan, X., Stoops, J., Luo, J., DeFrances, M. C., & Zarnegar, R. (2011). A hepatocyte growth factor receptor (Met)-insulin receptor hybrid governs hepatic glucose metabolism. *Nature Medicine*, *17*(12), 1577–1584. https://doi.org/10.1038/nm.2531

Falconer, R. A., Jablonkai, I., & Toth, I. (1999). Efficient synthesis of thioglycosides via a Mitsunobu condensation. *Tetrahedron Letters*, *40*(49), 8663–8666. https://doi.org/10.1016/S0040-4039(99)01834-1

Gill, D. M., Male, L., & Jones, A. M. (2019). Sulfation made simple: A strategy for synthesising sulfated molecules. *Chemical Communications*, *55*(30), 4319–4322. https://doi.org/10.1039/c9cc01057b

Hentges, S. G., & Sharpless, K. B. (1980). Asymmetric Induction in the Reaction of Osmium Tetroxide with Olefins. *Journal of the American Chemical Society*, *102*(12), 4263–4265.

https://doi.org/10.1021/ja00532a050

Jiang, J., Li, L., He, Y., & Zhao, M. (2013). Collective cell migration: Implications for wound healing and cancer invasion. *Burns & Trauma*, *1*(1), 21. https://doi.org/10.4103/2321-3868.113331

Jiang, W. G., Sanders, A. J., Katoh, M., Ungefroren, H., Gieseler, F., Prince, M., … Santini, D. (2015). Tissue invasion and metastasis: Molecular, biological and clinical perspectives. *Seminars in Cancer Biology*, *35*, S244–S275. https://doi.org/10.1016/j.semcancer.2015.03.008

Jumina, Nurmala, A., Fitria, A., Pranowo, D., Sholikhah, E. N., Kurniawan, Y. S., & Kuswandi, B. (2018). Monomyristin and monopalmitin derivatives: Synthesis and evaluation as potential antibacterial and antifungal agents. *Molecules*, *23*(12). https://doi.org/10.3390/molecules23123141

Kalluri, R., & Weinberg, R. A. (2009). The basics of epithelial-mesenchymal transition. *Journal of Clinical Investigation*, *119*(6), 1420–1428. https://doi.org/10.1172/JCI39104

Karimi-Jaberi, Z., Pooladian, B., Moradi, M., & Ghasemi, E. (2012). 1, 3, 5-tris(hydrogensulfato) benzene: A new and efficient catalyst for synthesis of 4, 4'-(arylmethylene) bis(1H-pyrazol-5-ol) derivatives. *Cuihua Xuebao/Chinese Journal of Catalysis*, *33*(12), 1945–1949. https://doi.org/10.1016/S1872-2067(11)60477-4

Kitaori, K., Furukawa, Y., Yoshimoto, H., & Otera, J. (1999). *CsF in Organic Synthesis. Regioselective Nucleophilic Reactions of Phenols with Oxiranes Leading to Enantiopure [~-Biockers*. *Tetrahedron* (Vol. 55).

Ko, K. R., Lee, J., Lee, D., Nho, B., & Kim, S. (2018). Hepatocyte Growth Factor (HGF)

Promotes Peripheral Nerve Regeneration by Activating Repair Schwann Cells. *Scientific Reports*, *8*(1), 8316. https://doi.org/10.1038/s41598-018-26704-x

Krupa, M., Chodyński, M., Ostaszewska, A., Cmoch, P., & Dams, I. (2017). A novel convergent synthesis of the potent antiglaucoma agent tafluprost. *Molecules*, *22*(2), 555. https://doi.org/10.3390/molecules22020217

Leber, M. F., & Efferth, T. (2009). Molecular principles of cancer invasion and metastasis (Review). *International Journal of Oncology*, *34*(4), 881–895. https://doi.org/10.3892/ijo_00000214

Lemmon, M. A., & Schlessinger, J. (2010). Cell signaling by receptor tyrosine kinases. *Cell*, *141*(7), 1117–1134. https://doi.org/10.1016/j.cell.2010.06.011

Lipshutz, B. H., Chung, D. W., Rich, B., & Corral, R. (2006). Simplification of the Mitsunobu reaction. Di-p-chlorobenzyl azodicarboxylate: A new azodicarboxylate. *Organic Letters*, *8*(22), 5069–5072. https://doi.org/10.1021/ol0618757

Ma, D., & Cai, Q. (2003). N,N-Dimethyl Glycine-Promoted Ullmann Coupling Reaction of Phenols and Aryl Halides. *Organic Letters*, *5*(21), 3799–3802. https://doi.org/10.1021/ol0350947

Maroun, C. R., & Rowlands, T. (2014). The Met receptor tyrosine kinase: A key player in oncogenesis and drug resistance. *Pharmacology and Therapeutics*, *142*(3), 316–338. https://doi.org/10.1016/j.pharmthera.2013.12.014

Matsumoto, K., & Nakamura, T. (1997). Hepatocyte growth factor (HGF) as a tissue organizer for organogenesis and regeneration. *Biochemical and Biophysical Research Communications*, *239*(3), 639–644. https://doi.org/10.1006/bbrc.1997.7517

Mehltretter, G. M., Dobler, C., Sundermeier, U., & Beller, M. (2000). An improved version of the Sharpless asymmetric dihydroxylation. *Tetrahedron Letters*, *41*(42), 8083–8087. https://doi.org/10.1016/S0040-4039(00)01396-4

Mitsunobu, O. (1981). The Use of Diethyl Azodicarboxylate and Triphenylphosphine in Synthesis and Transformation of Natural Products. *Synthesis*, *1981*(01), 1–28. https://doi.org/10.1055/s-1981-29317

Mizuno, S., & Nakamura, T. (2013). HGF-MET cascade, a key target for inhibiting cancer metastasis: The impact of NK4 discovery on cancer biology and therapeutics. *International Journal of Molecular Sciences*, *14*(1), 888–919. https://doi.org/10.3390/ijms14010888

Mo, H.-N., & Liu, P. (2017). Targeting MET in cancer therapy. *Chronic Diseases and Translational Medicine*, *3*(3), 148–153. https://doi.org/10.1016/j.cdtm.2017.06.002

Montero Bastidas, J. R., Oleskey, T. J., Miller, S. L., Smith, M. R., & Maleczka, R. E. (2019). Para-Selective, Iridium-Catalyzed C−H Borylations of Sulfated Phenols, Benzyl Alcohols, and Anilines Directed by Ion-Pair Electrostatic Interactions. *J. Am. Chem. Soc*, *141*, 9. https://doi.org/10.1021/jacs.9b08464

Munir, I., Zahoor, A. F., Rasool, N., Naqvi, S. A. R., Zia, K. M., & Ahmad, R. (2019, February 15). Synthetic applications and methodology development of Chan–Lam coupling: a review. *Molecular Diversity*. Springer International Publishing. https://doi.org/10.1007/s11030-018-9870-z

Nakamura, T., & Mizuno, S. (2010). The discovery of Hepatocyte Growth Factor (HGF) and its significance for cell biology, life sciences and clinical medicine. *Proceedings of the Japan*

Academy Series B: Physical and Biological Sciences, *86*(6), 588–610. https://doi.org/10.2183/pjab.86.588

Naldini, L., Vigna, E., Bardelli, A., Follenzi, A., Galimi, F., & Comoglio, P. M. (1995). Biological activation of pro-HGF (hepatocyte growth factor) by urokinase is controlled by a stoichiometric reaction. *Journal of Biological Chemistry*, *270*(2), 603–611. https://doi.org/10.1074/jbc.270.2.603

Oberhauser, T. (1997). A New Bromination Method for Phenols and Anisoles: NBS/HBF 4 ·Et 2 O in CH 3 CN . *The Journal of Organic Chemistry*, *62*(13), 4504–4506. https://doi.org/10.1021/jo9622993

Oliveira, A. G., Araújo, T. G., Carvalho, B. de M., Rocha, G. Z., Santos, A., & Saad, M. J. A. (2018). The role of Hepatocyte Growth Factor (HGF) in insulin resistance and diabetes. *Frontiers in Endocrinology*, *9*(AUG), 503. https://doi.org/10.3389/fendo.2018.00503

Organ, S. L., & Tsao, M. S. (2011). An overview of the c-MET signaling pathway. *Therapeutic Advances in Medical Oncology*, *3*(1), S7–S19. https://doi.org/10.1177/1758834011422556

Pincock, A. L., Pincock, J. A., & Stefanova, R. (2002). Substituent effects on the rate constants for the photo-claisen rearrangement of allyl aryl ethers. *Journal of the American Chemical Society*, *124*(33), 9768–9778. https://doi.org/10.1021/ja011981y

Raiber, E. A., Wilkinson, J. A., Manetti, F., Botta, M., Deakin, J., Gallagher, J., … Ducki, S. W. (2007). Novel heparin/heparan sulfate mimics as inhibitors of HGF/SF-induced MET activation. *Bioorganic and Medicinal Chemistry Letters*, *17*(22), 6321–6325. https://doi.org/10.1016/j.bmcl.2007.08.074

Ricci, G., Catizone, A., & Galdieri, M. (2002). Pleiotropic activity of hepatocyte growth factor during embryonic mouse testis development. *Mechanisms of Development*, *118*(1–2), 19–28. https://doi.org/10.1016/S0925-4773(02)00247-2

Sambiagio, C., Marsden, S. P., Blacker, A. J., & McGowan, P. C. (2014, May 21). Copper catalysed Ullmann type chemistry: From mechanistic aspects to modern development. *Chemical Society Reviews*. Royal Society of Chemistry. https://doi.org/10.1039/c3cs60289c

Scott, R. A., & Panitch, A. (2013). Glycosaminoglycans in biomedicine. *Wiley Interdisciplinary Reviews: Nanomedicine and Nanobiotechnology*, *5*(4), 388–398. https://doi.org/10.1002/wnan.1223

Sigma Aldrich. (2019). MSDS - 225541. Retrieved December 23, 2019, from https://www.sigmaaldrich.com/MSDS/MSDS/DisplayMSDSPage.do?country=GB&language=en&productNumber=225541&brand=ALDRICH&PageToGoToURL=https%25253A%25252F%25252Fwww.sigmaaldrich.com%25252Fcatalog%25252Fsearch%25253Fterm%25253Ddiad%252526interface%25253DAll%252526N%25253D0%252526mode%25

Stuelten, C. H., Parent, C. A., & Montell, D. J. (2018). Cell motility in cancer invasion and metastasis: Insights from simple model organisms. *Nature Reviews Cancer*, *18*(5), 296–312. https://doi.org/10.1038/nrc.2018.15

Sugata, H., Tsubogo, T., Kino, Y., & Uchiro, H. (2017). Ullmann C-O coupling of sterically hindered secondary alcohols using excess amount of strongly coordinating monodentate ligands. *Tetrahedron Letters*, *58*(10), 1015–1019. https://doi.org/10.1016/j.tetlet.2017.01.095

Tunoori, A. R., Dutta, D., & Georg, G. I. (1998). Polymer-bound triphenylphosphine as traceless reagent for Mitsunobu reactions in combinatorial chemistry: Synthesis of aryl ethers from phenols nad alcohols. *Tetrahedron Letters*, *39*(48), 8751–8754. https://doi.org/10.1016/S0040-4039(98)01988-1

Varasi, M., Walker, K. A. M., & Maddox, M. L. (1987). A revised mechanism for the Mitsunobu reaction. *The Journal of Organic Chemistry*, *52*(19), 4235–4238. https://doi.org/10.1021/jo00228a016

Volpi, N. (2006). Therapeutic applications of glycosaminoglycans. *Current Medicinal Chemistry*, *13*(15), 1799–1810. https://doi.org/10.2174/092986706777452470

Werle, S., Fey, T., Neudörfl, J. M., & Schmalz, H.-G. (2007). Enantioselective Synthesis of a *trans* -7,8-Dimethoxycalamenene. *Organic Letters*, *9*(18), 3555–3558. https://doi.org/10.1021/ol071228v

Yadav, M., Raghupathy, R., Saikam, V., Dara, S., Singh, P. P., Sawant, S. D., … Vishwakarma, R. A. (2014). Synthesis of non-hydrolysable mimics of glycosylphosphatidylinositol (GPI) anchors. *Organic and Biomolecular Chemistry*, *12*(7), 1163–1172. https://doi.org/10.1039/c3ob42116c

Yamada, S., Sugahara, K., & Özbek, S. (2011). Evolution of glycosaminoglycans: Comparative biochemical study. *Communicative and Integrative Biology*, *4*(2), 150–158. https://doi.org/10.4161/cib.4.2.14547

Yang, J., Dai, L., Wang, X., & Chen, Y. (2011). Di-p-nitrobenzyl azodicarboxylate (DNAD): An alternative azo-reagent for the Mitsunobu reaction. *Tetrahedron*, *67*(7), 1456–1462. https://doi.org/10.1016/j.tet.2010.12.036

Yano, K., Tsuda, E., Ueda, M., & Higashio, K. (1998). Natural hepatocyte growth factor (HGF) from human serum and a bound form of recombinant HGF with heparan sulfate are indistinguishable in their physicochemical properties. *International Journal of Biological Macromolecules*, *23*(3), 227–235. https://doi.org/10.1016/S0141-8130(98)00051-8

Yilmaz, M., & Christofori, G. (2010). Mechanisms of motility in metastasizing cells. *Molecular Cancer Research*, *8*(5), 629–642. https://doi.org/10.1158/1541-7786.MCR-10-0139

Yip, G. W., Smollich, M., & Götte, M. (2006). Therapeutic value of glycosaminoglycans in cancer. *Molecular Cancer Therapeutics*, *5*(9), 2139–2148. https://doi.org/10.1158/1535-7163.MCT-06-0082